ANALYTICAL-NUMERICAL METHODOLOGY TO MEASURE UNDAMAGED, FRACTURE AND HEALING PROPERTIES OF ASPHALT MIXTURES

A Dissertation

by

YASSER KOOHI

Submitted to the Office of Graduate Studies of
Texas A&M University
in partial fulfillment of the requirements for the degree of

DOCTOR OF PHILOSOPHY

Approved by:

Chair of Committee,	Robert Lytton
Committee Members,	Dallas Little
	Nasir Gharaibeh
	Anastasia Muliana
Head of Department	John Niedzwecki

December 2012

Major Subject: Civil Engineering

Copyright 2012 Yasser Koohi

ABSTRACT

Unlike in laboratory compacted asphalt mixtures, the distribution of viscoelastic properties in field layers is not uniform because of nonuniform air void distribution and aging. Therefore, characterization of field specimens is more challenging compared to that of laboratory compacted specimens. Formerly, characterization of field asphalt mixtures was based on binder tests which are useful but do not represent the properties of the asphalt mixtures because binder is only a component in the asphalt mixture. This study uses linear viscoelastic theory and numerical modeling to obtain the undamaged and damaged viscoelastic properties of both laboratory made and field compacted asphalt concrete. Additionally, it uses fracture mechanics principles to find the fracture and healing properties of aged asphalt specimens.

The analytical models presented in this research have been successfully verified by testing the actual field specimens of different ages. The model developed in this dissertation is suitable to track the viscoelastic, fracture and healing properties of the field specimen with time and depth. The test protocols and analytical models described in this study can be used for the development of reliable performance models for field-aged asphalt layers.

DEDICATION

This dissertation is dedicated to my parents, Ebrahim and Zomorrod, who did everything for me in life

ACKNOWLEDGEMENTS

I would like to thank my committee chair, Dr. Robert Lytton because without his help this dissertation could not have been written . I thank him, for teaching me to have initiative and to be creative. I will always try to be courageous in trying new ideas. I must thank him for his continuous support throughout my education.

I would like to thank my committee member Dr. Little who provided funding for my research and helped me throughout my years here. I also would like to thank Dr. Gharaibeh and Dr. Muliana, for their guidance and support throughout the course of this research.

Thanks also go to my friends and colleagues and the department faculty and staff for making my time at Texas A&M University a great experience namely, Dr. Masoud Darabi, Dr. Rong Luo, Denise Cunagin, Brandon Jamison for his wonderful editing skills and Jim Lawrence for providing me with his test data.

I also want to extend my gratitude to the Federal Highway Administration and the Texas Department of Transportation, which provided the survey instrument and funding. I gratefully acknowledge receiving aged sample data from the Texas Department of Transportation and Texas Transportation Institute project 0-6009.The data was provided by Dr. Charles J. Glover, Chemical Engineering Department and Dr. Amy Epps-Martin, Zachry Civil Engineering Department,

Finally, thanks to my parents, Ebrahim and Zomorrod, for their encouragement and to my stepmom Fereshte for her support.

TABLE OF CONTENTS

LIST OF FIGURES

Page

LIST OF TABLES

Page

CHAPTER I

INTRODUCTION

Asphalt concrete is a commonly used construction material in highway projects because of its durability and reparability. The performance of the asphalt layer can directly affect the life cycle cost of transportation infrastructures. Using a reliable performance model to predict the field performance and improved mixture design can significantly decrease future maintenance and rehabilitation costs.

Due to the high volumes of asphalt concrete in the roads, any improvement in the durability of the asphalt layer has a significant impact on the construction and rehabilitation costs of a project. However, without a good understanding of the mechanical behavior of the asphalt layers in the field , developing a reliable performance model is impossible. In the light of these facts there have been numerous research projects undertaken to predict and evaluate the performance of asphalt concrete using different empirical and mechanistic approaches. However, characterization of the asphalt layer is not an easy task, firstly because of the viscoelastic behavior of the binder as an adhesive agent in the mixture and secondly because of various loading and environmental factors.

Many test protocols have been developed to mimic the field performance of asphalt mixtures in the laboratory environment. These tests are designed to simulate different distresses such as fatigue, rutting and reflective cracking of the asphalt layer in the laboratory condition. However, the mixtures which are made in the laboratory are

different from those in the field; therefore, different methods such as oven aging and moisture conditioning are used to simulate the field environment in the laboratory (Kandhal and Cooley Jr, 2006, Khan, et al., 1998, Peterson, et al., 2003, Sigurjonsson and Ruth, 1990, Singh, et al., 2011).

The mechanical properties of laboratory compacted samples cannot be substituted for those of asphalt concrete (AC) a in the field. Unlike for laboratory compacted mixtures, the characterization of viscoelastic properties of field-aged asphalt mixtures is more challenging for pavement engineers because there are numerous issues that make it very difficult to tackle. Among these issues are the various loading scenarios, the different environmental conditions, several crack propagation systems, compaction problems, and binder aging. The solution for these problems cannot be obtained by relying on the empirical correlations which has become dominant in this field (Akisetty, et al., 2011, Brandes and Robinson, 2006, Hadley, et al., 1970, Jeong Ho, et al., 2012, Kim, et al., 2011, Selim and Ezz-Aldin, 1990, Yan, et al., 2009, Zhang, et al., 2008) .

Correlations may work in a particular case but they cannot be extended to more complicated cases. A fundamental approach which combines the chemical and mechanical characteristics of the actual field-aged mixture components like binder and aggregates is the most efficient approach. The beauty of the fundamental approach is that it is not limited to a specific material or boundary conditions and it can be applied to various materials in different scenarios. As mentioned before neither the asphalt mixture

nor the external forces acting on it follows simple mechanistic theories. Therefore, the mechanistic approach is still at the beginning of the journey.

As mentioned before there are significant differences between laboratory compacted asphalt mixtures and field layers. The two most important differences which are very difficult to simulate in the laboratory, are the air void distribution and aging phenomenon. Several methods have been developed to mimic the compaction of the asphalt layer and aging in the laboratory environment such as gyratory compaction and oven simulation of aging. The results of extensive research on laboratory and field aging indicate that the current laboratory aging methods cannot reproduce the field aging for intervals greater than 2 years(Anderson, 2002, Feipeng, et al., 2009, Glover, et al., 1989, Jia, et al., 2005, Juan and Xiaoning, 2005, Karakouzian, et al., 2003, Kevern, et al., 2009, Lee, et al., 2009, Li, et al., 2008, Peterson, et al., 2004, Romero and Roque, 1997, Singh, et al., 2011, Zhang, et al., 2011, Zou, et al., 2004).

The field compaction of the asphalt layers is not as consistent as the laboratory methods of compaction. X-ray analysis of field cores shows that the air void distribution in the field layers is a c-shaped curve and that the center of the layer has a lower air void ratio compared to the edges. Figure 1 shows the air void distribution of a field layer which has been analyzed using the x-ray computed tomography method; the high air void contents on the edges result in a c-shape air void distribution profile. The temperature of the asphalt mixture is very important in the compaction process; therefore, the center of the asphalt layer is compacted more than the edges. The research shows the air void distribution in the field specimen is also dependent on the

construction methods and the compaction energy that the layer receives(Abd El Halim and Haas, 1994, Beainy, et al., 2010, Kassem, et al., 2008, Khan, et al., 1998, Masad and Kassem, 2008).

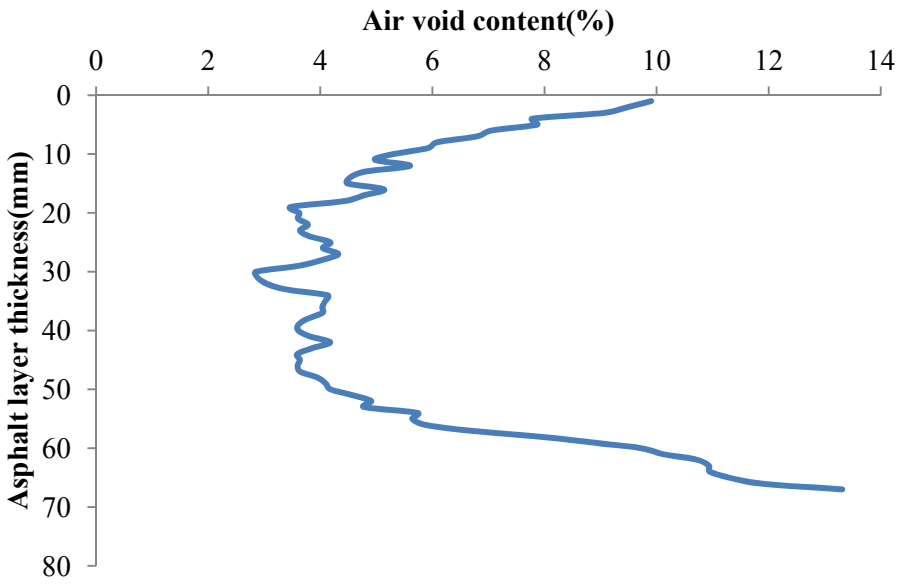

Figure 1.Air void distribution in field asphalt layers

Characterization of aging of the asphalt layers in the field is even more challenging than describing the air void distribution because it is a function of time and environmental conditions. Therefore, the viscoelastic properties of the asphalt layer in the field are changing with time as the binder ages. For many years pavement research has been focused on the binder characteristics and the characterization of other components such as aggregates. More importantly, asphalt concrete as a mixture has

been overlooked in several research studies. For many years researchers have viewed asphalt binder as glue that behaved viscoelastically, and studied the binder separately from the mixture to characterize processes such as aging (Doh, et al., 2010, Feng, et al., 2011, Kim, 2005, Radziszewski, et al., 1996, Renjie and Li, 2009, Zhong, et al., 2008).

This trend continues at the present time and it has resulted in less understanding about the mechanical properties of the asphalt mixtures which is usually different from those of the binder. Though binder is one of the basic components and is the adhesive agent in the asphalt mixture, it still is a component in the mixture and has to be studied together with all other components; the response of the asphalt concrete is the result of the interactions between all of the components in the mixture.

The focus of this research is on the quantification of the viscoelastic properties of asphalt concrete in the laboratory and in the field such as complex modulus, fracture and healing properties using the principles of fracture mechanics and based on linear viscoelasticity theory. Moreover, this study is aimed at tracking the change of these properties relative to time, depth and temperature of the asphalt layer.

The study is focused on developing new analysis methods applied to different cases to obtain more fundamental material properties using already available test methods. For example, the direct tension (DT) test is used to find the complex stiffness gradient of field-aged asphalt specimens with depth and time. Subsequently, the overlay tester (OT) results have been used to evaluate the fracture properties of field-aged asphalt layers.

Objectives

The objectives of this study are:

- Develop an efficient and reliable method to calculate the undamaged viscoelastic properties of the field-aged and laboratory mixtures
- Implement a model and test method to produce the profile of the viscoelastic properties of the field-aged layers as a function of thickness and time
- Design a methodology to find the fracture and healing properties of the field-aged and laboratory asphalt mixtures based on fracture mechanics principles
- Track the change in the viscoelastic properties of the field asphalt layers with time
- Modify the test and analysis procedure of the available test methods to obtain the maximum number of mechanical properties in the minimum time
- Develop a user defined material subroutine for functionally graded materials to be used in different finite element (FE) models to simulate the field tests.

In this study, the available test apparatus, an Electro-Hydraulic Servo machine was used to find the undamaged viscoelastic properties of both field and laboratory compacted mixtures such as complex modulus, Poisson's ratio and corresponding master curves in tension. The new testing protocol and analysis methods were established to obtain the viscoelastic properties as a function of time and depth of the layer. This study presents a novel method to calculate the complex stiffness gradient of a field aged specimen using a direct tension test. Since the field asphalt mixtures are not aged uniformly with pavement depth, there is a modulus gradient through the thickness of the

asphalt layer. The asphalt mixture is stiffer at the surface. As a result, rectangular specimens cut from field cores when tested in a direct tension test in Electro-Hydraulic servo machines with feedback frequency tend to oscillate. An analytical method has been developed to analyze the oscillating behavior of the specimen and to produce the stiffness gradient function as it varies with loading frequency and position relative to the pavement surface. Furthermore, a finite element simulation of the test is conducted to verify the validity and robustness of the proposed method. This method was successfully used to characterize aged viscoelastic properties of field cores obtained from different roads in Texas.

Asphalt layers under different repeated loading and rest periods experience both fatigue and healing processes. The tests are costly and time consuming and the results are highly variable. Current methods of evaluating these phenomena using the Overlay Tester (OT) rely on counting the number of load repetitions until the crack breaks through the sample.

This research provides a novel analysis method based on the viscoelastic fracture mechanics and Finite Element modeling to predict the actual crack growth rate in asphalt mixes both in the laboratory compacted and field samples using the Overlay Tester. Furthermore the new method uses viscoelastic fracture mechanics principles to find the fracture and healing properties of the asphalt mixes.

The resulting test is fast, less costly and more repeatable and than previous methods using the Overlay Tester. This test procedure and analysis methodology were

designed to get both fracture and healing properties of the asphalt specimens in the laboratory and field.

The precision of the test method was determined and improved by testing lab compacted specimens .The Coefficients of Variation of the laboratory compacted mixture undamaged properties are comparable with the test results.

The test outputs of the field specimens from these tests were often difficult to explain because of the complicated characteristics of the field-aged specimen. Therefore both tests were simulated using a FE code in Abaqus. The study of test simulations was the key to interpret the asphalt specimen responses under different loading scenarios specially in the case of aged specimen. The functionally graded material subroutine which has been developed in this study can be used for a variety of purposes for different simulations of the stiffness and Poisson's ratio gradients with depth.

Applications

Many models, especially the numerical simulation of the pavement structure, use either an average value for the complex modulus in the field layers or rely only on the binder rheology-based models. In fact, the viscoelastic properties are neither uniform nor constant with time in field-aged layers. The current uniform or average modulus assumptions create errors in the stress and strain calculations. Hence, a more accurate estimation of the stiffness properties as a function of time and location in the pavement

can be used in this model. This gradient function also can be monitored and tracked in different stages of the pavement life.

On the other hand, some of the tests such as the OT do not currently produce consistent results due not only to the test protocol but also to the analysis method. The results of this study can be used to analyze the data in a more mechanistic and accurate manner to obtain more material properties using the same outputs.

The results of this study can be used as a component for a comprehensive aging model or in any pavement performance model. Moreover the methodology in this study can be used to evaluate the current condition of the pavement for any Maintenance and Rehabilitation (M&R) purposes. The field test protocol presented here can be used to predict the life span of the asphalt layer based on the binder aging and the fracture characteristics of the field layer.

Binder testing in asphalt research has been well developed and is often used for different model developments, but these models have never been verified using another method. This study is purposing an accurate procedure to improve and verify the binder test results from an independent point of view.

As previously mentioned, the current aging models are largely based on binder rheology. A model to relate the binder properties to mixture properties and vice versa is required. The results of this study can be used in a previously developed self-consistent micromechanics model (Luo and Lytton, 2011) to back calculate the mixture properties for a given aggregate and binder as a function of asphalt layer age.

The FE model developed in this study can be used to modify the OT test to get more consistent results. Furthermore, the FGM-UMAT can be used together with any numerical simulation of laboratory tests of the field aged asphalt specimens or and material with stiffness profile.

Performed Tasks

Task 1. Literature review

A complete literature review was carried out in this research. The different methods to test the field specimens were surveyed to find an efficient and quick test method to find the viscoelastic properties. In addition different aging prediction models also were reviewed.. The rheological characteristics of the aged binders were reviewed to evaluate the effect of the binder aging on the stiffness gradient. Furthermore, the DT test methodology tension test of the laboratory specimen that had been developed previously by other researchers was reviewed. The backgrounds of the OT test such as its origin, current analysis methods and its modifications was studied as a part of this literature review.

In order to develop the analytical methods the valuable previous works of fracture mechanics and linear viscoelasticity was studied in this effort. The different aging prediction models also were reviewed. The correspondence principle and its applications to model the asphalt concrete was very helpful in this study.

The material used in this study includes technical papers, reports and also a number of class notes from Professor Lytton's lectures in different courses in Texas A&M University.

Task 2. Develop a model and test to find undamaged viscoelastic properties of the field specimens

The undamaged properties of the field-aged asphalt specimens has been obtained using both DT and OT tests. The tests are designed to be nondestructive and the specimen can be used for subsequent tests. The test is very quick and efficient .The procedure and methodology to find the undamaged average complex modulus and Poisson's ratio of the field specimen from DT and OT tests are described in chapters 3 and 5, respectively.

Task 3. Develop a model to calculate the stiffness gradient of the field aged asphalt specimens

The field specimens during the DT test are oscillating and the results of the numerical duplication of the test indicates that this oscillation happens because of the stiffness gradient in the field specimens.

The comprehensive test method and analysis to find the stiffness gradient of the field specimen using DT test based on linear viscoelastic theory and signal processing techniques has been presented in chapter 3.

Task 4. Design a new crack growth estimation model for the OT test

As mentioned formerly counting the number of load cycles to evaluate an asphalt mixture using the OT test is not reliable. Therefore a new methodology was developed in this study.

A new crack growth estimation methodology based on linear viscoelasticity and fracture mechanics principles using numerical tools has been presented in chapter 4 and 6 for laboratory and field specimens, respectively.

Task 5. Implement a new methodology to find the fracture and healing properties of field and laboratory samples

During each closing cycle in the OT test, a lot of healing occurs and the FE model confirms this observation.

The methodology to find the fracture and healing properties of the asphalt concrete specimens for both laboratory and field specimens are presented in chapters 4 and 5 respectively.

Task 6. The FGM-UMAT subroutine to model the stiffness profiles in numerical models

As previously mentioned, the UMAT subroutine to the Abaqus system can be used with any asphalt test simulation. The procedure to develop the UMAT subroutine and its results are presented in chapter 5 and appendix B.

CHAPTER II

LITERATURE REVIEW

Viscoelastic Properties of Aged Binder and Mixtures in Field

Characterization of asphalt layers in the field plays an important role in the study of the long term performance of asphalt concrete layers in roads. Asphalt concrete (AC) is a complex visco-elasto-plastic material whose properties depend on temperature and loading frequencies(Antes, et al., 2003, Chatti and Kim, 1999, Daniel and Kim, 1998, Songqing and Jinfei, 2010, Zhao, et al., 2010).

In recent years, the quantification of the mechanical properties of the field aged asphalt concrete has become the major focus of many research projects(Chatti, et al., 1995, Motola and Uzan, 2007, Solaimanian, 2008).Characterization of the properties of field asphalt layers is even more challenging than those of the laboratory compacted mixtures due to aging of the binder and various crack propagation mechanisms under different loading patterns in a layer. There have been several research studies conducted to measure the aging properties and crack susceptibility of asphalt concrete mixtures(Bayat and Knight, 2010, Lee, et al., 2009, Li, et al., 2011, Wu, et al., 2010).

The mechanical properties of laboratory compacted samples cannot be substituted for those of the asphalt concrete (AC) in the field (Mohammad, et al., 2007). Though several methods have been used to simulate the field conditions in the laboratory environment, none of them are able to perfectly mimic the true field performance of the

asphalt layer with sufficient accuracy (Huang, et al., 1996, Li, et al., 2008, 2008, Memon and Chollar, 1997, Mollenhauer, et al., 2010, Phromsorn and Kennedy, 1995).

The complex modulus of AC is a key fundamental property which is used in almost all design specifications and performance models. Many different factors such as binder type, mix volumetric parameters, construction method and air void distribution affect the complex modulus of the AC. Some semi-empirical models have been used to predict the AC modulus in the laboratory such as a simple version of the Hirsch model based on the law of mixtures (Christensen Jr, et al., 2003, Dongre, et al., 2005) and the Mechanistic Empirical Pavement Design Guide (MEPDG)'s empirical model (Bari, et al., 2006, Dongre, et al., 2005).

In contrast to a laboratory molded specimen, the field samples have a non uniform air void distribution. The field compactibility depends on different factors such as lift thickness, temperature of the mixture during compaction and the energy applied during compaction (Leiva and West, 2008). Moreover, the field layer stiffness changes with time due to the aging process. The aging of the binder increases its stiffness and makes it more brittle and susceptible to fatigue and low temperature cracking (Huang and Grimes, 2010, Li and Li, 2007, Molenaar, et al., 2010, Raad, et al., 2001, Tian, et al., 2004, Woo, et al., 2008, 2008).

It is well-known that the complex modulus in the field is not uniformly distributed throughout the depth. Different factors such as temperature gradient, air void distribution and the aging process change the stiffness gradient function. Sometimes these factors act simultaneously, for example, the aging depends on the interconnected

air void distribution(Woo, et al., 2008). Recent studies show that along with the average temperature of the asphalt layer, the temperature gradient also changes the complex modulus (Nazarian and Alvarado, 2006).

The most recent attempts to calculate the stiffness gradient are generally based on binder extraction with a chemical solvent from different depths. The extracted binder is tested using the Dynamic Shear Rheometer (DSR) to determine the complex shear modulus and phase angle of the aged binder (Farrar, et al., 2006, Huang and Grimes, 2010, Molenaar, et al., 2010, Soon-Jae, et al., 2009, Soon-Jae, et al., 2008, Tian, et al., 2004). However, this method has been criticized for various reasons, e.g., the extraction process may change the binder characteristics, binder ages non-uniformly in the field and the air void distribution is not consistent in the field samples (Hanson, et al., 2009).

Many researchers have assumed that the key element in aging is only binder; therefore, they tried to correlate binder performance tests to the stiffness of the mixture in the field (Bari and Witczak, 2007, Bari, et al., 2006, Christensen Jr, et al., 2003, Fonseca and Witczak, 1996, Mirza and Witczak, 1996, Pellinen, et al., 2007, Witczak and Fonseca, 1996).

There is a semi-empirical model which has been calibrated using extensive field data called the Global Aging System (GAS) to consider the stiffness gradient effect. This model has been used in the MEPDG, and it assumes that there is a severe aging gradient in the top 0.5 inches of the asphalt layer. The design guide only accounts for the aging of this surface layer in its modulus calculations(NCHRP, 2004), but new research in this

area indicates that the binder ages in depths well below the surface due to oxygen permeation through interconnected air voids (Woo, et al., 2008).

There are different models which can be used to estimate the asphalt mixture stiffness using the viscoelastic properties of binders and mastics. Three famous available models are the Di Benedito model, the Hirsch model and the Witczak model (Bari and Witczak, 2007, Christensen Jr, et al., 2003, Delaporte, et al., 2007, Olard, et al., 2005).

The Hirsch model uses law of mixtures to predict the dynamic modulus of asphalt mixtures according to the binder modulus and volumetric components. There are different versions of Hirsch model such as the simple version, the version which uses mastic properties and also the version which incorporates the effect of film thickness. The simplest version seemed to be more accurate than others. In this model the dynamic modulus of asphalt was directly measured from the binder modulus, Voids in the Mineral Aggregates(VMA) and Voids Filled with Asphalt(VFA) (Christensen Jr, et al., 2003).

The Di Benedito model suggests a very comprehensive correlation between binder and mastics. It was found that the mixture property is controlled by mastics more than binders. The filler added to binder has been found to change the rheological master curves shape and increase the failure stress at different temperatures and loading frequencies, and the filler has a significant impact on rutting resistance and stress controlled fatigue(Anderson, et al., 1992, Delaporte, et al., 2007, Hanzik and Luxemburk, 1978, Wang, et al., 2011, Yong, et al., 2009, Zhan, et al., 2009).

The earlier versions of Witczak dynamic stiffness model were only good for the laboratory made samples .The modulus in this model was a function of temperature and it also was not very accurate at very high and low temperatures. In the revised version of the model the temperature was replaced by actual binder viscosity .The revised Witczak model uses the binder viscosity as a variable to predict the dynamic modulus of the mixtures in different ages. The sensitivity studies showed that this model can reasonably predict the dynamic modulus in the field. The GAS is the model which is used in the MEPDG which incorporates aging in the modulus prediction with time. The predictive model was developed using curve fitting and statistical regression analysis. The predictive equations were established by the assumption that there is a linear correlation between log viscosity and log temperature for asphalt binders. This method has been developed for original unmodified binder. The model was verified with data from 40 field projects (Fonseca and Witczak, 1996, Mirza and Witczak, 1996).

The latest version of the Witczak dynamic modulus predictive model was created using an extensive database containing 7400 data points from 346 different mixtures. This model predicts the dynamic modulus of the asphalt mixtures as a function of volumetric properties, material characteristics, temperatures and the loading frequencies. The model was shown to be statistically reliable in predicting the asphalt dynamic modulus. (Bari and Witczak, 2007, Bari, et al., 2006).

It should be noted here the MEPDG guide has three different input levels. The level one gets actual test results as input. The second level uses the latest version of Witczak model to predict the dynamic modulus. The third level is the simplest level

which gets the binder PG grading results as inputs. As previously discussed, this model takes to account the short term and long term aging of the binder by changing the corresponding viscosity(NCHRP, 2004).

Studies on these models depict that all the models can be utilized to estimate mixture stiffness under specific circumstances. The Hirsch model incorporates the mixture properties; therefore, it can be adjusted for different mixtures. Although the De Benedito model gives accurate results, it is not reliable in very low and very high temperatures, and it is difficult to adjust the model for specific mixture conditions (Pellinen, et al., 2007).

Although major progress has been made in testing aged binders, the mechanical testing of the field aged sample is still missing. In fact, the mechanical tests are more reliable indicators of mixture properties because they account for all mixture components in the mix and not only the binder. The disk-shaped compact tension test (Wagoner, et al., 2005) and direct tension test of rectangular specimens at Texas A&M University are some of the state-of-the-art tests in this area.

Most of these studies are focused on the binder characterization and there have been few attempts to characterize the aging properties of asphalt mixtures using mechanical mixture tests (Burr, et al., 1993, Lee, et al., 2009, Mallick and Brown, 2004, Morian, et al., 2011, Woo, et al., 2008).

The deeper portion an of asphalt layer ages less than the parts near the surface. The stiffness profile in field asphalt layers, unlike that in laboratory compacted specimens, is not uniform because of the nonuniform air void distribution with depth and

the aging phenomenon (Brandes and Hirata, 2009, Kassem, et al., 2008, You, et al., 2009).

X-ray CT scan analysis of field layers shows that the initial stiffness profile is a C shaped curve. The asphalt layers immediately after placement have higher stiffness in the center of the layer compared to the upper and lower edges because the center part is hotter and it receives more compaction energy compared to the layers near the surface. Furthermore, the lower layers cannot be compacted well enough because these layers lose their temperature rapidly after placement on the cold base layer. This initial C-shaped stiffness profile changes due to binder aging with time. Binder aging also is more severe near the surface due to higher oxygen availability and sun radiation at the surface(Hintz, et al., 2011, Tan, et al., 2008).

However, recent studies confirm that oxygen can penetrate to depths well below the surface through interconnected air voids(Farrar, et al., 2006, Koohi, et al., 2011, Woo, et al., 2008). Figure 2, schematically shows the change of the stiffness gradient profile with the age of the AC layer. These curves match our findings concerning the changes in stiffness gradient with time. In other words, the stiffness profile is a C-shaped curve a short time after placement and as binder ages the stiffness gradient gets sharper near the surface and the aging extends to deeper levels (Koohi, et al., 2011).

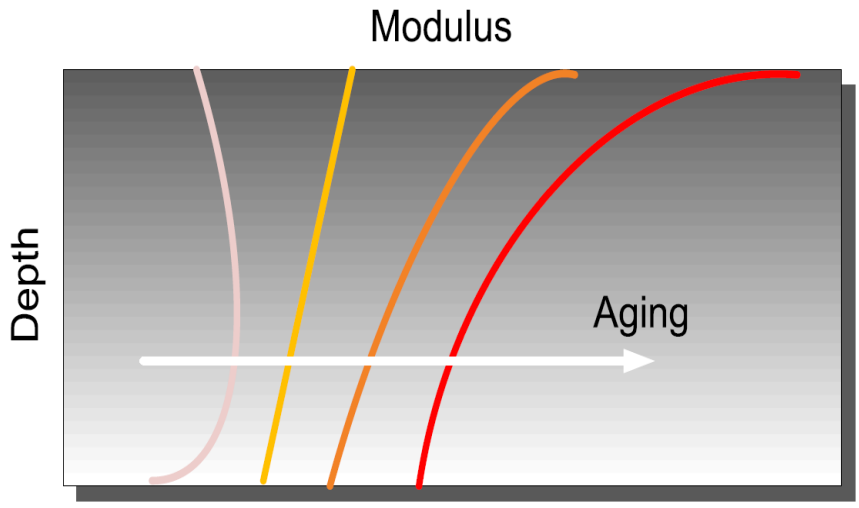

Figure 2.Change in stiffness profile with pavement age

The Direct Tension (DT) test is an efficient and quick test to obtain the undamaged viscoelastic properties of laboratory made AC mixtures (Chulseung and Roque, 2010, Epps and Monismith, 1970, Koh and Roque, 2010). Properties such as Poisson's ratio, complex modulus and corresponding master curves can be obtained via DT test by using linear viscoelasticity theory and the well-known correspondence principle(Luo and Lytton, 2010, Schapery, 1984).

Fracture and Healing Properties of Asphalt Mixtures

Asphalt layers experience the repeated loading, unloading as well as the rest periods because of the traffic and environmental conditions. The crack propagation from the bottom to the top and vice versa is a prominent distress in the asphalt layers.

Fortunately, each one of these phenomenon can be well explained by mechanistic-based models and various research projects have been conducted to develop and use such models(Harmelink, et al., 2008, Kim, et al., 2009, Luo, et al., 2010, Matsumoto, et al., 2010, Mun, et al., 2004, Svasdisant, et al., 2002, Wang, et al., 2003, Zhao, et al., 2010, Zou and Roque, 2011).

Different approaches have been used to characterize the crack initiation and propagation in asphalt layers, namely, conventional fatigue crack analysis (Harvey and Monismith, 1993, Ramsamooj, 1991, Tayebali, et al., 1996), continuum damage mechanics and fracture mechanics.

The traditional tests to measure the fatigue cracking susceptibility of mixes such as the four point bending beam test, are very expensive and time consuming (Kallas and Puzinauskas, 1971, Ramsamooj, 1991, Zhu, et al., 2009)

The continuum damage mechanics approach basically states that the micro structure of materials changes with deformations caused by external loadings without focusing on the crack initiation and propagation. Subsequently, the micro damage process results in the loss in material properties such as stiffness. Various models have been developed to explain these phenomena in different materials including some recent studies in asphalt (Abu Al-Rub, et al., 2010, Christensen Jr, et al., 2005, Darabi, et al., 2011, Wen and Bahia, 2009, Zhang and Huang, 2010, Zhao and Kim, 2003).

The fracture mechanics approach focuses directly on the crack geometry, initiation and propagation mechanisms. This approach is based on Paris's law for crack

propagation theory. However, the stress intensity factor in Paris's law applies only to elastic materials (Paris and Erdogan, 1963).

In viscoelastic media, the generalized J-integral based on the correspondence principle and pseudo strain energy concepts proposed by Schapery, is a powerful principle to address the crack propagation process (Cleveland, et al., 2003, Kuai, et al., 2009, Schapery, 1984, Schapery, 1975).

Asphalt like other viscoelastic materials restores part of its strength by healing. The study of the fracture or damage properties without considering the healing is incomplete and results in an underestimation of the number of load cycles to reach failure. Various research studies focused on the self-healing in different materials namely polymers and asphalt in recent years (Abu Al-Rub, et al., 2010, Brown, et al., 2002, Chowdary and Krishnan, 2006, Kessler, 2007, Kim and Little, 1989, Schapery, 1989, Shen, et al., 2010, Yufeng and Wanlin, 2006).

Different test methods have been used to characterize fracture properties of asphalt layers such as compacted disc-shape test, single-edge notched beam test and semi circular bending test(Hyunwook and Partl, 2012, Kim, et al., 2009, Li and Marasteanu, 2010, Wagoner, et al., 2005).

The Overlay Tester machine was initially designed to simulate the reflective cracking in asphalt overlays over rigid pavements. Subsequently the apparatus was used as a torture test to compare different mixtures by counting the number of load cycles to failure (Zhou, et al., 2007, Zhou and Scullion, 2003).

The Texas Overlay Tester (OT) is a capable multipurpose test apparatus. The OT was originally developed to determine the reflection cracking resistance of hot mix asphalt mixtures used in overlays over concrete joints (Germann and Lytton, 1979). This machine also has been used to study the behavior of the geosynthetic fabrics and grids inside the asphalt layers based on fracture mechanics concepts (Cleveland, et al., 2003, Cleveland, et al., 2002, Roque, et al., 2002).

As shown in Figure 3, the OT machine consists of two steel plates. One plate is fixed and the other can move back and forth to apply the desired repeating displacement. This machine has been modified several times since its first prototype (Germann and Lytton, 1979) and the latest version is more precise and portable. In this later model, specimens with the standard size of 150 mm long ,75 mm wide and 38 mm high can be tested .These specimens with this size can be easily cut from the cylindrical mixes compacted by the Gyratory compactor in the laboratory or cores taken from the field. As shown in Figure 3, the specimen is glued on the aluminum plates and subsequently the plates are mounted and fixed on the machine's steel platforms using pins (Zhou and Scullion, 2005). The time, load, opening displacement and temperature are recorded by the data acquisition system during the OT test. Figure 4 shows the OT machine during the test.

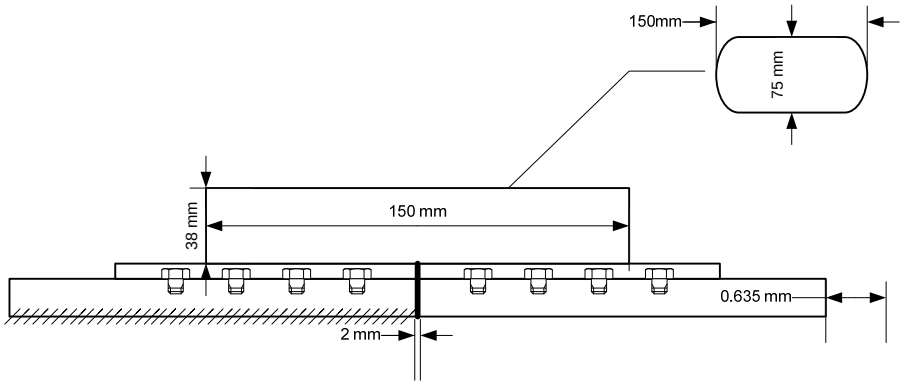

Figure 3.The OT setup

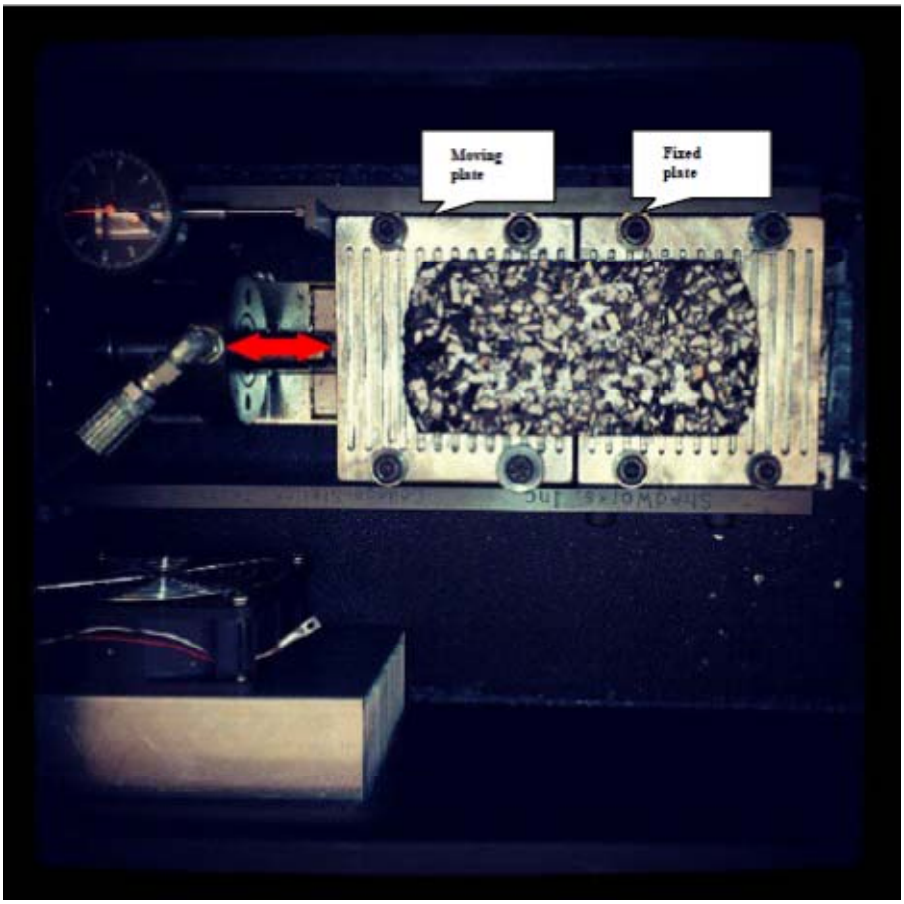

Figure 4.The OT machine during the test

The simplicity of the test led to its use as an index test for fatigue because in both reflection cracking and fatigue, the active mechanism is crack growth. The OT was selected to be used together with the Hamburg Wheel Tracking Test (HWTT) to establish a balanced asphalt mix design procedure to account for both fatigue and rutting distresses (Aschenbrener, 1995, Buchanan and Smith, 2005, Grebenschikov and Prozzi, 2011, Li, et al., 2011, Zhou, et al., 2007). This test was expected to be a good surrogate for the expensive and time consuming beam fatigue tests (Kallas and Puzinauskas, 1971, Ramsamooj, 1991, Zhu, et al., 2009).

The current OT analysis method relies on counting the load cycles to the failure and the failure criterion is satisfied when the initial maximum load is reduced by 93%. The resulting count on companion samples has proven to give a large variability. Especially, this method does not work well with coarse graded mixes and the Coefficient of Variation (COV) is over 30% (Walubita, et al., 2009).

Research has been conducted recently in TTI in order to find Paris's law constants. In this research, the crack length in each load cycle is measured with a Digital Correlation System (DIC). The results of this work indicated that the crack grows rapidly during few first load cycles after that the rate of growth decreases substantially with time (Jacobs, 1995, T.O.Medani and Molenaar, 2000, Zhou, et al., 2007, Zhou and Scullion, 2006).

The numerical modeling of the crack propagation in asphaltic materials has been studied using different methods in recent years(Cao, et al., 2011, Luo, et al., 2008, Luo, et al., 2011, Luo and Zheng, 2010, Wang and Li, 2012, Yu and Du, 2011). The cohesive

zone model has been successfully used to model the crack propagation in the viscoelastic materials. Different cracking scenarios such as brittle, quasi-brittle and ductile cracks can be modeled in this approach (Aragao and Kim, 2010, Braham, et al., 2012, Dong, et al., 2011, Kim, 2011, Li and Marasteanu, 2005, Liu and Wang, 2008, Paulino, et al., 2006, Seong Hyeok, et al., 2008, Song, et al., 2006, Zhang, et al., 2011, Zhao and Zhang, 2010).

Although major achievements have been accomplished in the numerical modeling of crack growth in asphalt mixtures but simulation of the field aged asphalt layers with stiffness gradient is still very difficult. Aged AC layers can be modeled using similar approaches used in analyzing the Functionally Graded Materials (FGM).In other words ,the aging mechanisms induces a gradient in the stiffness of the material with depth. This stiffness gradient can be modeled through assuming a continuous function for the stiffness through the structure's depth. The response of these materials to different loading and temperature scenarios have been already studied in various research projects (Fang, et al., 2007, Huang, et al., 2005, Mukherjee and Paulino, 2003, Wu and Luo, 2011).

CHAPTER III

COMPLEX STIFFNESS GRADIENT ESTIMATION OF FIELD-AGED ASPHALT CONCRETE LAYERS USING THE DIRECT TENSION TEST*

Part of the content used in this chapter has been already published in the Journal of Materials in Civil Engineering ASCE(Koohi, et al., 2011). The characterization of viscoelastic properties of the aged field asphalt mixtures has been a challenge for pavement engineers. Instead of characterizing full mixtures from the field cores, only the binder was extracted from the mixture and was evaluated for its aging properties. Since the binder is only one component of the mixture, the properties of the aged binder may not clearly indicate the properties of the aged field mixtures. This study presents a novel method to calculate the complex stiffness gradient of field aged specimen using a direct tension test. Since the field asphalt mixtures are not aged uniformly with the pavement depth, there is a modulus gradient through the thickness of the asphalt layer. The asphalt mixture is stiffer at the surface. As a result, rectangular specimens cut from field cores when tested in a direct tension test in Electro-Hydraulic servo machines with feedback frequency tend to oscillate. This phenomenon was used to establish a novel method to measure the stiffness gradient within the depth of the asphalt layer. The test results were

* Reprinted with permission from "Complex Stiffness Gradient Estimation of Field-Aged Asphalt Concrete Layers using Direct Tension Test" by Koohi, Y., Lawrence, J., Luo, R., and Lytton, R. ,2012. Journal of Materials in Civil Engineering, 24(7), 832-841, Copyright 2012, by ASCE, All rights reserved.

independently verified with a finite element model. A combination of signal processing, filtering and analytical methodology was used to find the complex stiffness gradient with depth of an asphalt layer. The results of this study can be used to improve different performance models and specification codes. This method was successfully used to characterize aged visco elastic properties of field cores obtained from different roads in Texas.

Methodology

Test Protocol Development

Recently, the direct tension test has been successfully used to find the asphalt mixtures' properties such as complex modulus of the laboratory fabricated samples (Luo and Lytton, 2010). The testing protocol for laboratory samples was modified to be used for field specimens. The different specimen geometries, gluing systems and machine adjustments were considered to find the most reliable test setup with accurate outputs. Table 1 shows part of the efforts has been made to design the final test setup.

Table 1.Summary of the test setup design procedure

Parameter Increased	Oscillation Amplitude	Sensitivity of Parameter	Comments
Cross section shape	decrease	low	Using the square cross section reduces the oscillation
Cross section area	decrease	high	Less oscillation amplitude in thicker samples
Gauge length	increase	medium	The gauge length should be three times larger than the largest aggregate size
Specimen height	decrease	medium	Sample heights less than 4 inches is not preferred due to stress concentration near endcaps
Controlling LVDT position	---	high	Controlling LVDT should be determined during the VEC test run at 50˚F (10°C)
Using less sensitive LVDTs	decrease	high	Using less sensitive LVDTs which filters machine vibration
Using universal support	decrease	low	

Material Preparation

The field samples tested in this research were gathered from different Texas roads. The complete information (such as the construction date, mixture properties, coring date, coring location, etc.) was collected for each core. The cores were taken in different time sequences to study the effect of aging time on the stiffness gradient. To determine the effect of traffic, cores were also taken from both the wheel path and shoulder.

The test specimen is a rectangular sample cut from a cylindrical field core as shown in Figure 5. The length and width of the specimen are 102 and 76 millimeters, respectively. The thickness of the specimen varies between 38 to 76 millimeters based on the asphalt layer thickness.

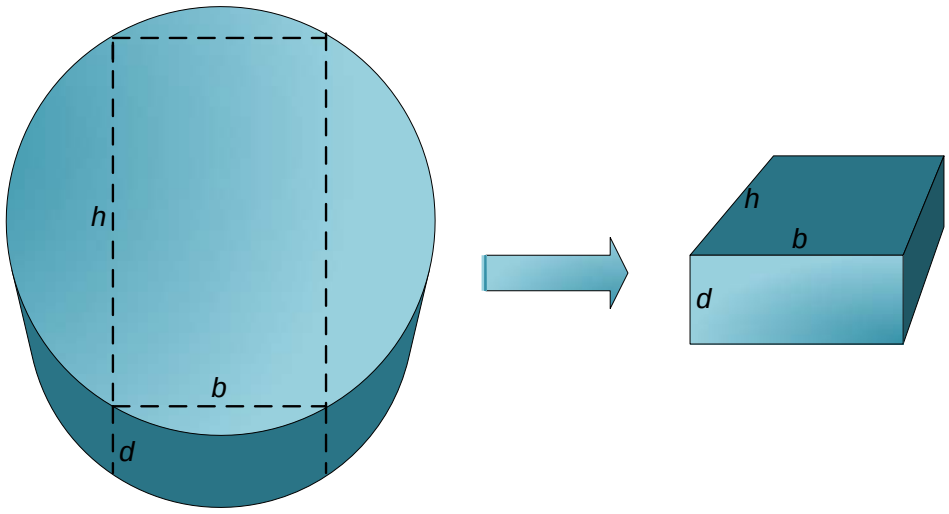

Figure 5.The rectangular cut specimen from the field core

After cutting the specimen, a steel end cap was glued to each end of the specimen. A special gluing jig was used to make sure that the specimen was perfectly centered between the steel end caps. The cutting and gluing processes should be done very carefully to avoid any misalignment which causes undesired oscillations in the direct tension test.

Test Setup

A specimen and the arrangement of the Linear Variable Displacement Transducers (LVDTs)are shown in Figure 6. As shown in the Figure 6, six LVDTs were mounted on the specimen, including a vertical LVDT that was used to measure the vertical displacement at the pavement surface, another vertical LVDT used to measure the vertical displacement at the bottom of the asphalt layer, and two vertical LVDTs used to measure the displacements at the center of the layer. Two horizontal LVDTs were also installed to measure horizontal displacements at the surface of the pavement and the bottom of the layer. Figure 7 shows a specimen during the test in the test chamber. The test was a non-destructive direct tension test with monotonically increasing load. The specimen was stretched to a maximum strain of 100 micro-strains to prevent any crack propagation. The test was performed at different temperatures in order to evaluate the effect of temperature on the stiffness gradient function. It took 10

minutes to run this test at each temperature with two hours between changes of temperatures to allow the specimen to reach the temperature equilibrium.

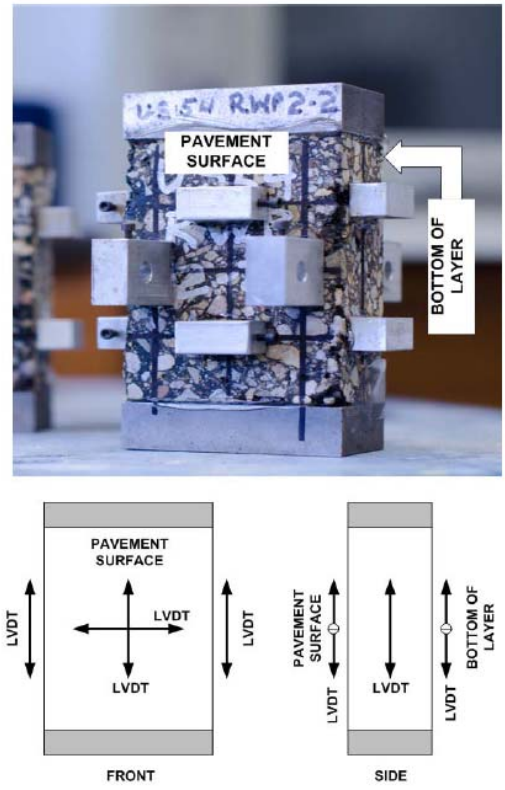

Figure 6.The setup with six LVDTs

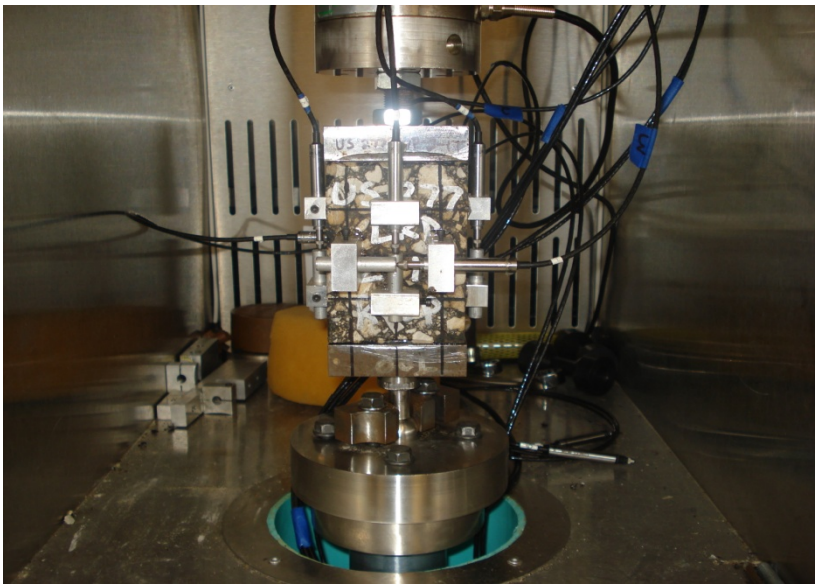

Figure 7.Test setup and LVDT arrangements

Theory

Electro-Hydraulic Servo Machines

The servo electro-hydraulic machines are widely used in industry and also material testing. Different loading patterns can be applied to the material using these machines. These machines usually use oil pressure transducers and photoelectric encoders to measure the load and displacement, respectively.

The machine uses linear electronic actuators to apply a specified load pattern at a desired rate. This actuator uses a signal processing algorithm to adjust the oil pressure in the loading apparatus with the programmed load pattern. The actuator compares the oil

pressure and planned load frequently to apply the desired load pattern. Different machines use different algorithms and frequencies to adjust the load .The frequency with which data is collected by the actuator and compared with the desired load pattern is called feedback frequency. The new servo electro-hydraulic machines have feedback frequencies of 20 Hz which is much higher than previous models. In this study two different machines were used to find the complex stiffness gradient, an older machine with a feedback frequency of 2Hz and a new machine with feedback frequency of 20Hz.

In the direct tension test, the stress pattern that the feedback rate induces in the specimen with non-uniform stiffness is not uniform with the larger stress developing on the stiffer side of the specimen. The centroid of the force generated within the specimen is not aligned with the centroid of the applied load. This eccentricity creates a moment that causes the specimen to oscillate around the pinned support. The strain versus time outputs show different levels of strain and oscillating strain amplitudes in the front and back of the specimen. Figure 8 shows the outputs of the strains at the surface and bottom of the asphalt layer. As shown in Figure 8 the strain has a lower magnitude at the surface compared to those of the bottom.

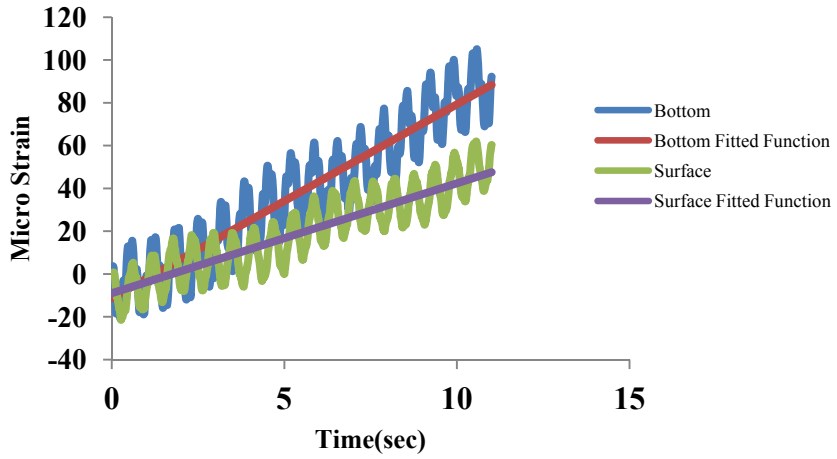

Figure 8.The strain output for the surface and bottom of the asphalt layer

As shown in Figure 6 the front and back of the specimen are the surface of the pavement and bottom of the layer, respectively. These oscillations have not been observed in the unaged lab specimens where the stiffness can be assumed to be uniform. Therefore, the observed oscillations for the specimens cored from aged pavements are related to the stiffness gradient.

Visco-elastic Force Determination

Test outputs and a finite element model simulation of the test indicate that the strain outputs of the direct tension test of a field-aged specimen tend to oscillate. The finite element model will be described in a later section of this dissertation. Figure 9

shows the free body diagram of a rectangular specimen in the direct tension test. As shown in Figure 9 it is assumed that strain changes linearly from the surface to the bottom of the layer. The illustrated stress pattern is expected to be induced inside the specimen. A power function was used to illustrate the stress pattern and stiffness gradient with depth. The equilibrium equations were used to determine the induced stress distribution in the specimen. Subsequently, the Laplace transform of the viscoelastic solution was easily obtained from the elastic solution using the correspondence principle (Bhattacharjee, et al., 2009, Mukherjee and Paulino, 2003, Park, et al., 1996).

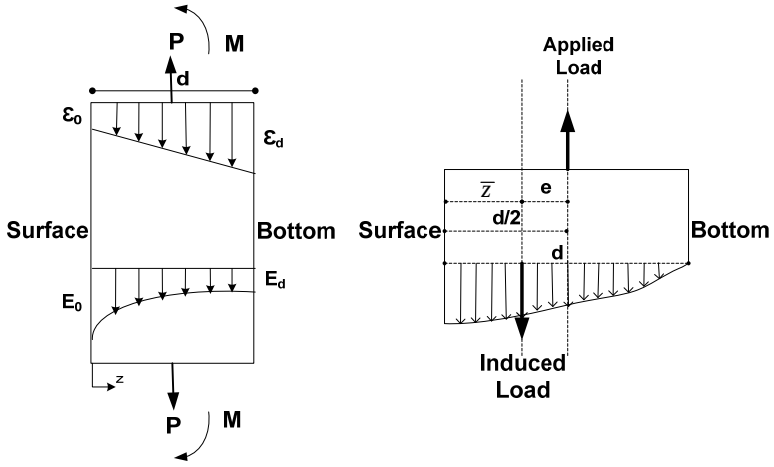

Figure 9.The rectangular specimen's free body diagram

Equation 1 shows the power function assumed to determine the elastic modulus with depth.

$$E(z) = E_d + (E_0 - E_d)(\frac{d-z}{d})^n \quad (1)$$

Where $E(z)$ is the elastic modulus at depth z; E_d and E_0 are the elastic modulus at the bottom and top of the asphalt layer, respectively; n is the model parameter; and d is the thickness of the rectangular specimen.

Equations 2 and 3 show the induced strain and stress in the specimen at depth z.

$$\varepsilon(z) = \varepsilon_0 + \frac{\varepsilon_d - \varepsilon_0}{d} z \quad (2)$$

$$\sigma(z) = E(z)\varepsilon(z) \quad (3)$$

where $\varepsilon(z)$ and $\sigma(z)$ are the strain and stress at the depth, z. ε_d and ε_0 are strains at the bottom and surface of the layer, respectively.

Substituting equations 1 and 2 into equation 3 gives the induced stress in depth z:

$$\sigma(z) = \varepsilon_0 E_d + \frac{\varepsilon_d - \varepsilon_0}{d} E_d z + \varepsilon_0 (E_0 - E_d)(\frac{d-z}{d})^n + \frac{\varepsilon_d - \varepsilon_0}{d}(E_0 - E_d)(\frac{d-z}{d})^n z \quad (4)$$

Equation 5 shows the induced internal force in the specimen, where b is the specimen thickness.

$$P = b \int_{z=0}^{z=d} \sigma(z) dz \quad (5)$$

The magnitude of the induced force is calculated by substituting the stress expression from equation 4 into Equation 5.

$$P = b\varepsilon_0 E_d d + b(\varepsilon_d - \varepsilon_0)E_d \frac{d}{2} + \frac{b\varepsilon_0(E_0 - E_d)d}{n+1} + \frac{b(\varepsilon_d - \varepsilon_0)(E_0 - E_d)d}{(n+1)(n+2)} \tag{6}$$

All of the material properties in Equation 6 are functions of time. Therefore, using the correspondence principle, frequency dependent properties can be obtained. The Laplace transform of both sides of the equation 6 is calculated. Equation 7 is the expression for the Laplace transform of the viscoelastic force. In the following equations the Laplace transform for function f is $\overline{f}(s) = \int_0^\infty f(t)e^{-st}d_t$.

$$\begin{aligned}\overline{P}(s) = s\overline{E}_d(s)\left[\overline{\varepsilon}_0(s)\left(1 - \frac{1}{2} - \frac{1}{n+1} + \frac{1}{(n+1)(n+2)}\right) + \overline{\varepsilon}_d(s)\left(\frac{1}{2} - \frac{1}{(n+1)(n+2)}\right)\right]bd + \\ s\overline{E}_0(s)\left[\overline{\varepsilon}_0(s)\left(\frac{1}{n+1} - \frac{1}{(n+1)(n+2)}\right) + \overline{\varepsilon}_d(s)\left(\frac{1}{(n+1)(n+2)}\right)\right]bd\end{aligned} \tag{7}$$

As shown in Figure 9, expression 8 shows the position of the stiffness centroid, expressions 4 and 6 are inserted into Equation 8 to find the stiffness centroid location, $\overline{z}$ .Equation 9 is the expression for $\overline{z}$.

$$\overline{z} = \frac{1}{P}\int_{z=0}^{z=d} bz\sigma(z)d_z \tag{8}$$

$$\overline{z} = \frac{d\left[\varepsilon_0\left(\frac{1}{6} - \frac{(n+1)+k(n+5)}{(n+1)(n+2)(n+3)}\right) + \varepsilon_d\left(\frac{1}{3} - \frac{2(k-1)}{(n+1)(n+2)(n+3)}\right)\right]}{\left[\varepsilon_0\left(\frac{1}{2} + \frac{k-1}{n+2}\right)\right] + \left[\varepsilon_d\left(\frac{1}{2} + \frac{k-1}{(n+1)(n+2)}\right)\right]} \tag{9}$$

The moment induced in the section can be found by substituting the values of force and eccentricity from Equations 7, 9 and 11 into Equation 10.The result is shown in Equation 10.

$$\overline{M}(s) = \overline{P}(s)\overline{e}(s) \tag{10}$$

$$e = \frac{d}{2} - \bar{z} \tag{11}$$

$$\bar{M}(s) = s\bar{E}_d(s).bd^2\left(\varepsilon_0(s)\left(\frac{t_0}{2} - r_0\right) + \varepsilon_d(s)\left(\frac{t_d}{2} - r_d\right)\right) \tag{12}$$

$$r_0 = \frac{1}{6} - \frac{n(k+1)+5k+1}{(n+1)(n+2)(n+3)} \tag{13}$$

$$r_d = \frac{1}{3} - \frac{2(k-1)}{(n+1)(n+2)(n+3)} \tag{14}$$

$$t_0 = \frac{1}{2} + \frac{(k-1)}{(n+2)} \tag{15}$$

$$t_d = \frac{1}{2} + \frac{(k-1)}{(n+1)(n+2)} \tag{16}$$

Equations 17, 18 and 19 are strain amplitude values at the surface, bottom and center of the specimen, respectively, where I is the moment of inertia.

$$\Delta\bar{\varepsilon}_0(s) = \frac{\bar{M}(s)\bar{z}(s)}{I.s\bar{E}_0(s)} \tag{17}$$

$$\Delta\bar{\varepsilon}_d(s) = \frac{\bar{M}(s)\left[d - \bar{z}(s)\right]}{I.s\bar{E}_d(s)} \tag{18}$$

$$\Delta\bar{\varepsilon}_c(s) = \frac{\bar{M}(s)\left[\frac{d}{2} - \bar{z}(s)\right]}{I.s\bar{E}_c(s)} \tag{19}$$

Using Equation 1 the value for the dynamic modulus in the center ($s\bar{E}_c(s)$) can be calculated at (z=d/2) then by substituting the $s\bar{E}_c(s)$ value in Equation 19, Equation 20 will be obtained.

$$s\bar{E}_c(s) = s\bar{E}_d(s)\left[\frac{2^n - 1 + k}{2^n}\right] \tag{20}$$

Equation 21 shows the final format of the magnitude of the complex modulus at the bottom of the specimen as a function of specimen geometry, viscoelastic force, n and k values, where k in this Equation is the ratio of the surface modulus to the bottom modulus. The Equations 21 and 22 were used to calculate the complex modulus at the surface and bottom of the asphalt layer.

$$s\bar{E}_d(s) = \frac{\bar{P}(s)}{bd\left\{\bar{\varepsilon}_0(s)\left[\frac{1}{2} + \frac{k-1}{n+2}\right] + \bar{\varepsilon}_d(s)\left[\frac{1}{2} + \frac{k-1}{(n+1)(n+2)}\right]\right\}} \tag{21}$$

$$s\bar{E}_0(s) = k.s\bar{E}_d(s) \tag{22}$$

n and k Estimation

The n and k values are dictated by the shape of the stiffness gradient curve throughout the depth. As shown in Figure 3, the stiffness centroid is not the geometric centroid and this eccentricity generates a moment. By substituting the expressions for $\bar{M}(S)$, $\bar{z}(s)$ and $s\bar{E}_c(s)$ into Equations 17 to 19, the expressions 23 and 24 can be obtained. The n and k values can be obtained by solving the corresponding system of equations.

$$\frac{\Delta\bar{\varepsilon}_0(s)}{\Delta\bar{\varepsilon}_d(s)} = \frac{1}{k}.\frac{\bar{\varepsilon}_0(s).r_0 + \bar{\varepsilon}_d(s).r_d}{\bar{\varepsilon}_0(s).(t_0 - r_0) + \bar{\varepsilon}_d(s).(t_d - r_d)} \tag{23}$$

$$\frac{\Delta\bar{\varepsilon}_c(s)}{\Delta\bar{\varepsilon}_d(s)} = \frac{2^n}{2^n - 1 + k} \cdot \frac{\bar{\varepsilon}_0(s).(\frac{t_0}{2} - r_0) + \bar{\varepsilon}_d(s).(\frac{t_d}{2} - r_d)}{\bar{\varepsilon}_0(s).(t_0 - r_0) + \bar{\varepsilon}_d(s).(t_d - r_d)} \quad (24)$$

$\Delta\bar{\varepsilon}_d(s)$, $\Delta\bar{\varepsilon}_c(s)$ and $\Delta\bar{\varepsilon}_0(s)$ are the bottom ,center and top oscillating strain amplitudes ,respectively.

Data Analysis

The output results of different test machines in the direct tension test of the field samples vary because of the different feedback rate used in the test machines. With lower feedback rates, a simpler analysis method can be used which is called the band width determination. Though the higher feedback rates provide more accurate results, these outputs are harder to analyze as well. This occurs because the machine corrects the applied load more frequently and the amplitude made by the stiffness gradient is more difficult to filter. To solve this problem, a combination of filtering and signal processing was employed.

Band Width Method

To find the values of the n and k using Equations 23 and 24, the Laplace transform of the strain amplitudes should be calculated. For this purpose, the factors of Equations 25 and 26 were fitted to the actual force and strain outputs, respectively.

$$f(t) = a(1 + e^{-bt}) \tag{25}$$

$$\varepsilon(t) = a(1 + e^{-bt}) \tag{26}$$

Then, in each data sampling sequence, the difference between the strain value and the fitted function was calculated. The result is a band the width of which is the oscillation amplitude. The upper and lower boundaries of the band are also sinusoidal functions. To find upper and lower boundaries of this band, a local maximum and minimum finder algorithm was used. This algorithm basically filters the points inside the band and gives the upper and lower points. Then a sinusoidal function shown in Equation 27 was used to fit to these boundary points. The a_1 and a_2 parameters are shown in Figure 10 and Figure 11.The band width is the difference between the upper and lower boundary functions.

$$y(t) = a_1 + a_2(1 - \cos(\omega t)) \tag{27}$$

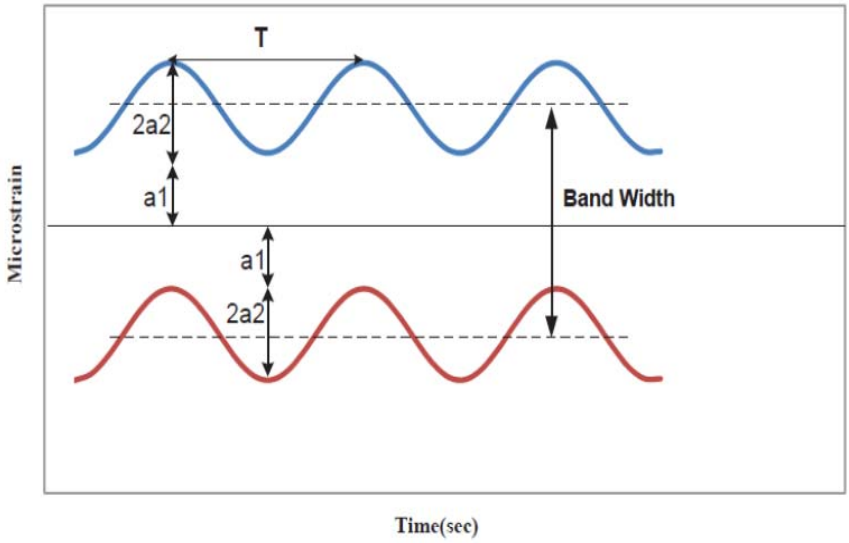

Figure 10.The lower and upper band, phase angle=0

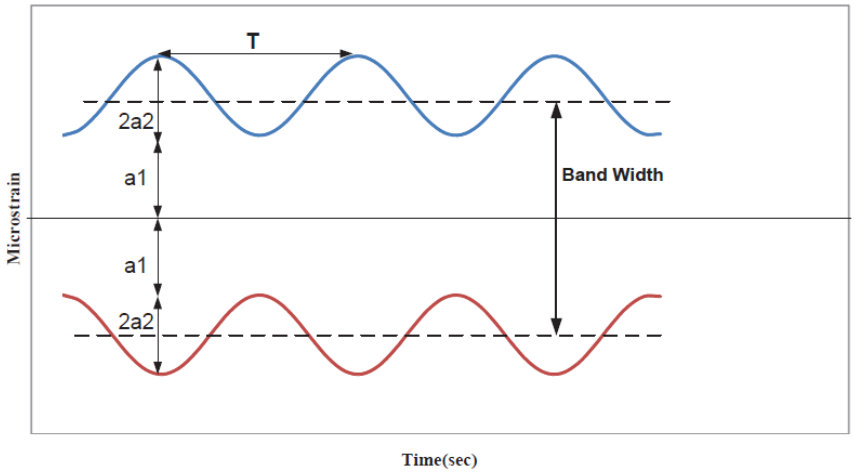

Figure 11.The lower and upper bands, phase angle=90

The upper and lower boundaries of the bands can be in the same phase as in Figure 10 or with a 90 degree phase difference as in Figure 11, in each case the band

width can be calculated using Equations 28 and 30, respectively. The viscoelastic solution of the Equations 28 and 30 were calculated in Equations 29 and 31 by applying the correspondence principle to the elastic equations.

$$\Delta\varepsilon = 2a_1 + a_2 \tag{28}$$

$$\Delta\bar{\varepsilon} = \frac{2a_1 + a_2}{s} \tag{29}$$

$$\Delta\varepsilon = 2a_1 + 2a_2\left(1 - \cos\left(\omega t\right)\right) \tag{30}$$

$$\Delta\bar{\varepsilon}(s) = \frac{2}{s}\left(a_1 + a_2\right) - \frac{2a_2 s}{s^2 + \omega^2} \tag{31}$$

The parameter ω is the induced radian frequency in the specimen in response to the machine's feedback frequency. According to the correspondence principle, the Laplace transform variable s can be substituted by $i\omega_2$, where ω_2 is the radian frequency of the machine's feedback rate.

Moving Average Filtering of the Response

In the high feedback rates, filtering the noise from the stiffness gradient induced oscillation is more difficult. In this case, after finding the difference between the strain measurement and the fitted function value in each sampling time, it was found that the resultant difference function is symmetric. This resultant function is shown in Figure 12, and it is clear that the upper band lags behind the lower band by 90 degrees. Therefore the square of the symmetric difference function results in a saw tooth function with the

same frequency, as shown in Figure 13.Subsequently a moving average filter was used to smooth the saw tooth function from the previous step. Finally, the square root of the smoothed function was calculated to find the response function components, such as frequency, a_1 and a_2 using Equation 14. In Figure 12 through Figure 15, this process can be followed step by step.

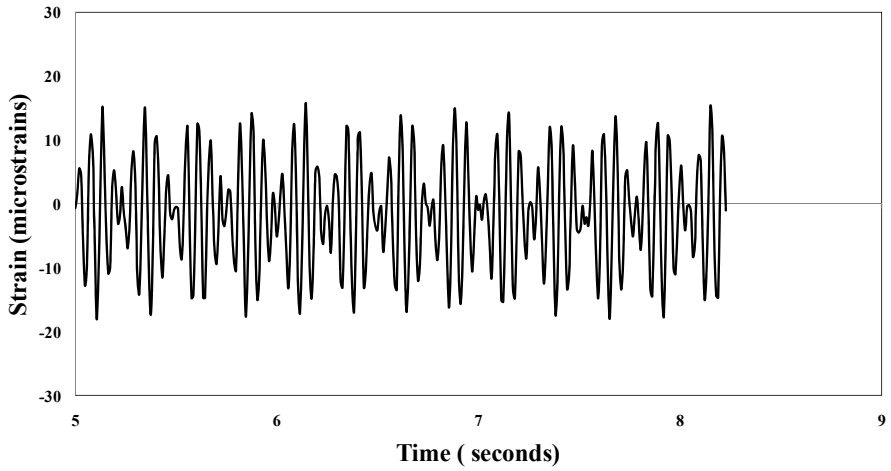

Figure 12. The difference function versus time

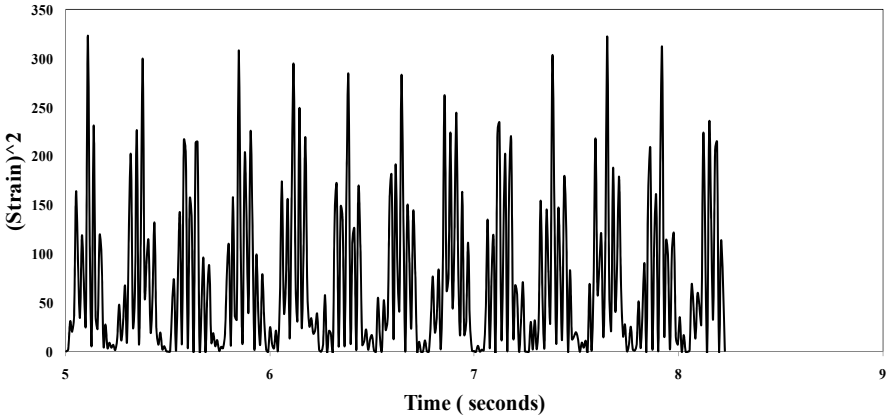

Figure 13. The square of the difference function versus time

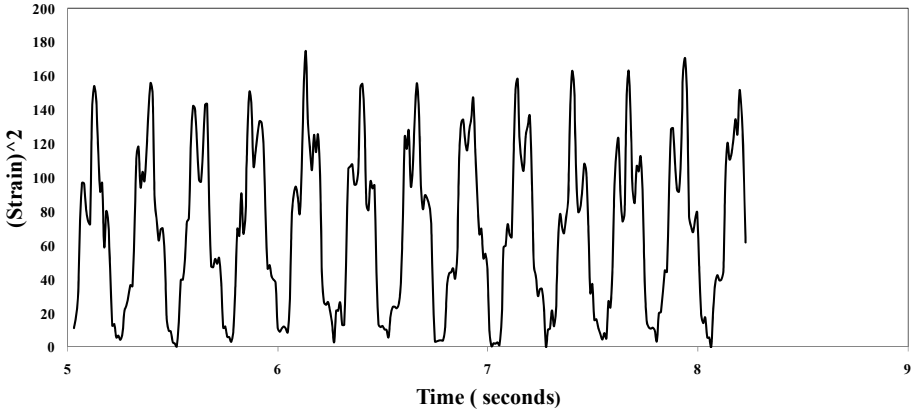

Figure 14. The smoothed function using the moving average filter

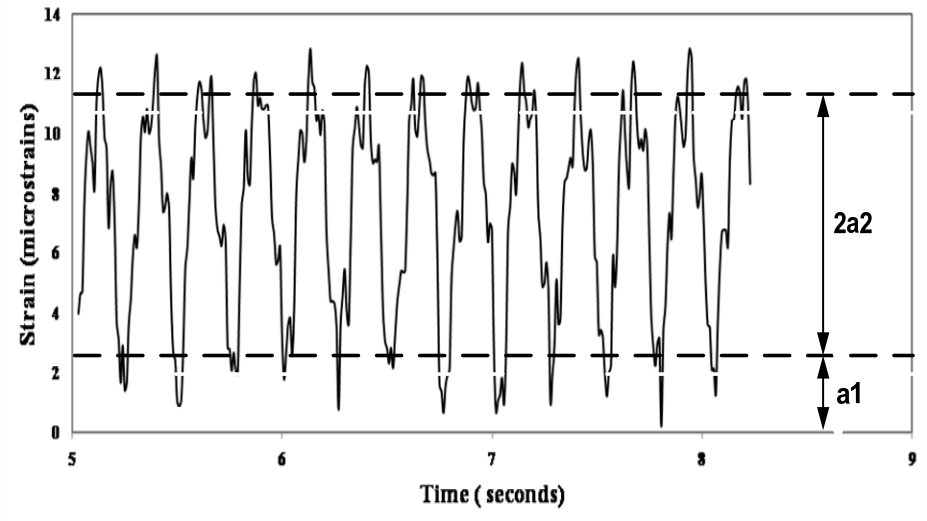

Figure 15. The square root of the smoothed function

After finding the oscillation amplitudes in the top and bottom of the specimen using the described methods .The strain amplitudes together with the Laplace transform of the strain fitted functions were inserted into equations 23 and 24 to be solved for n and k. The viscoelastic solution for these equations results in complex number solutions for n and k, indicating that both n and k have magnitude and phase angle and are frequency dependent. Afterward, values of n and k at the feedback frequency of 20 Hz were used in Equations 21 and 22 to determine the complex modulus at the surface and bottom of the asphalt layer.

The complex stiffness gradient function was determined by putting the n value, the complex modulus at the surface and bottom of the asphalt layer in Equation 1.

Finite Element Verification

For further confirmation, the direct tension test is simulated using the commercial finite element software Abaqus to verify the specimen responses. Figure 16 shows the boundary conditions which were used in the model. The loading arm which is attached to the upper endcap moves in a rigid sleeve that prevents it from any lateral movement or rotation. At the same time, the lower end is fixed with a pin support that allows rotation only but not lateral movement. To simulate rigid endcaps on the top and bottom of the specimen, the nodes on both ends were tied to a reference point that forced these nodes to remain in the same plane during the simulated displacement application.

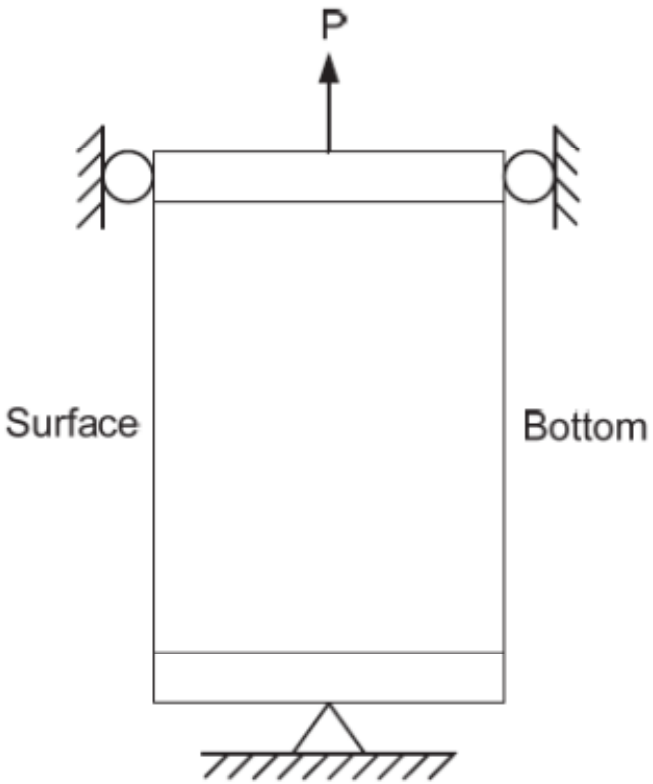

Figure 16.Boundary conditions of the finite element model

The specimen tends to show lateral displacement in the center height of the sample which is caused by the induced moments in the specimen because of the modulus gradient. However, the lateral fixtures of the test machine do not allow lateral displacements at the top and bottom of the sample. Because of the feedback rate, this test applies a sinusoidal force at the top of the specimen. Consequently, the reaction forces are also expected to be sinusoidal. It is not trivial to measure the exact reaction forces applied to the specimen by the top fixtures. However, both the actual machine load and subsequently the feedback response are sinusoidal. Therefore, a sinusoidal increasing

displacement in the form of Equation 32 was used in the Abaqus model to simulate both actual machine displacement and the feedback rate effect for the displacement control tests. The frequency of the applied displacement represents the feedback controlled displacement. This displacement magnitude represented in Equation 32 is the same as the upper endcap displacement in the actual test but the actual feedback rate may not be a smooth curve like this.

$$d(t) = a.t + b.\sin(c.t) \tag{32}$$

To simulate the stiffness gradient with depth, the original model was partitioned into eight sub-sections. Different viscoelastic moduli were assigned to each section to create the stiffness gradient with depth. The Poisson's ratio was assumed to be constant in all sub-sections. The viscoelastic properties of the specimen were defined using Prony series' parameters as shown in Equation 33.These parameters were measured on lab compacted asphalt mixtures and were assumed to be the same for all subsections. The magnitudes of the complex moduli of the subsections were obtained from the stiffness gradient analysis of a field-aged specimen using the aforementioned procedure at the frequency of 2 Hz, 20°C. The material properties used in the model are listed in Table 2

$$G(\tau) = G_{\infty} + \sum_{i=1}^{n} G_i e^{-\frac{\tau}{\tau_i}} \tag{33}$$

where, G_{∞} is the long term complex modulus and τ_i is the relaxation time. The long term complex modulus was assumed to be zero in this model.

Table 2.The material properties in the finite element model

Section	Modulus(MPa)	Poisson's Ratio	Prony series' G_i	Prony series' τ_i
1	7046	0.3	0.37	6.75
2	6316	0.3	0.37	6.75
3	5578	0.3	0.37	6.75
4	4847	0.3	0.37	6.75
5	4116	0.3	0.37	6.75
6	3378	0.3	0.37	6.75
7	2648	0.3	0.37	6.75
8	1910	0.3	0.37	6.75

The visco/elastic analysis module in Abaqus was used to analyze the model with viscoelastic properties. The model response was matched closely to the response of the field aged specimen and it conformed to the LVDT outputs very accurately. Figure 17 shows the strain versus time in the surface, and bottom of the specimen in both an actual test and the corresponding finite element model. As shown in Figure 17, in both the actual outputs and the model, the stiffer side has both the lower amplitude and strain compared with the bottom of the sample. There are some differences between the actual test response and the numerical model outputs in both magnitude and phase angle. This may be because of the model material property assumptions, the specimen misalignment and the assumed smooth feedback rate function. Figure 18 shows the maximum principal stress contours and the deformed shape of the specimen at the end of the test. As shown in Figure 18 the specimen rotates on the pin support and there is a stress concentration

near the upper corner of the stiffer side. The test used in this numerical verification was conducted using a machine with the 2Hz feedback rate.

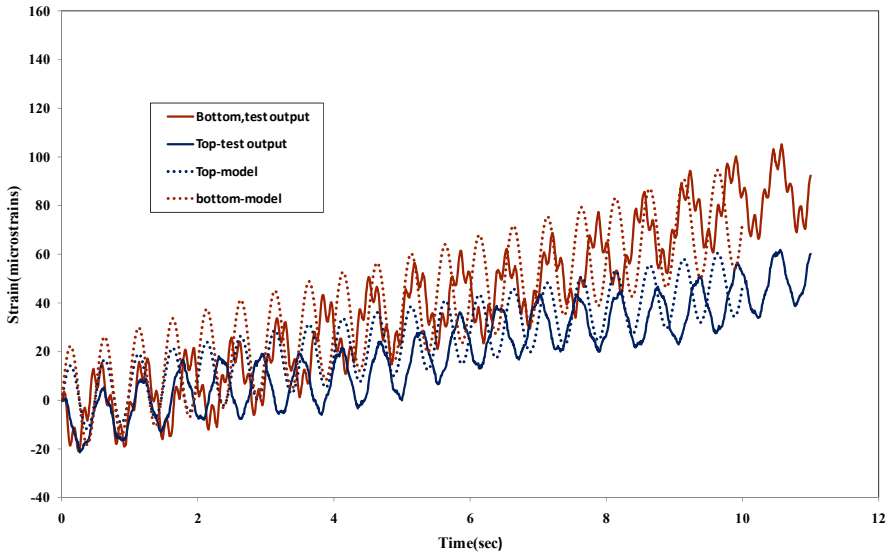

Figure 17.The FE model outputs versus actual test results

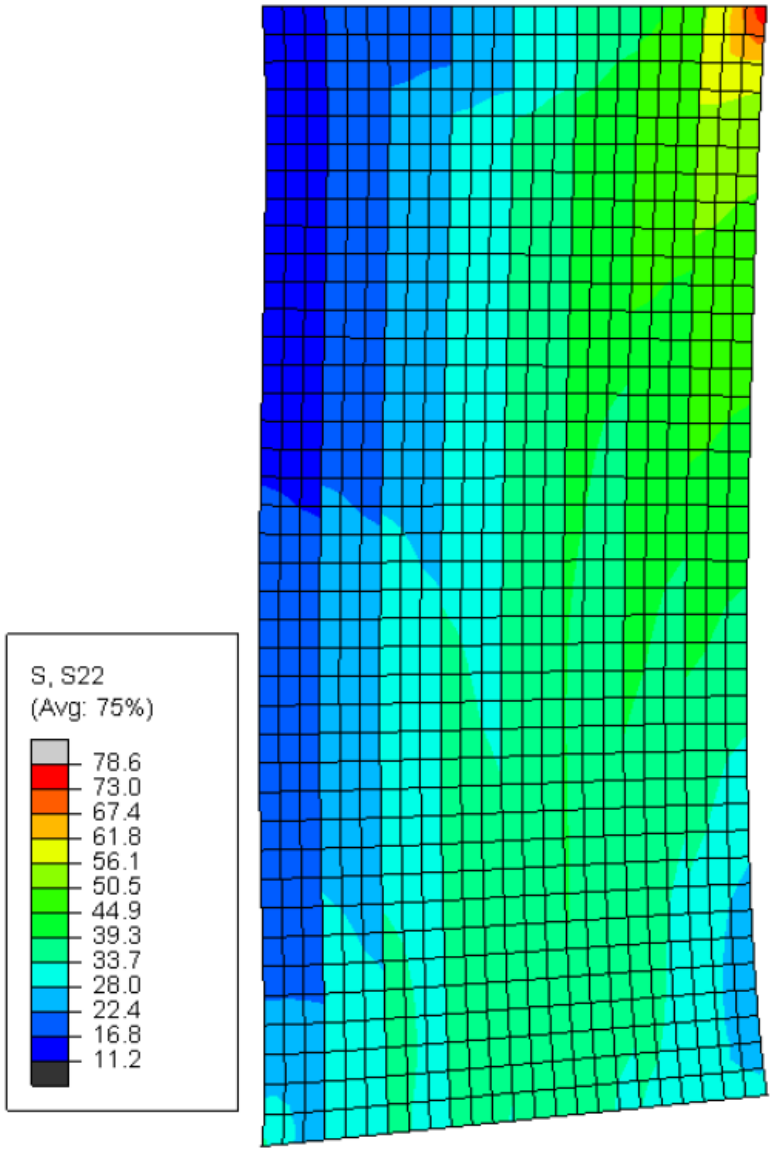

Figure 18.The deformed mesh with principal stress contours

Results

The field aged cores obtained from two different pavement sections, US82 and US277 in Texas, were tested and analyzed with the described methodology. All of the specimens were tested with 20 Hz feedback frequency.

Stiffness Gradient Analysis of Field Cores from US82

The US-82 asphalt concrete layer was constructed in July 2008. A PG 70-28 binder was used in this mixture. The mix design binder content was 6.2%. The cores were taken from both shoulder and wheel path in December 2009, and they were tested using a servo electro-hydraulic machine with a feedback rate of 20 Hz. The asphalt layer thickness in this road was 76 millimeters and the final test specimen was 50 millimeters thick. The specimens were tested at 10 and 20 °C.

The high feedback rate of the test machine resulted in a very noisy response; therefore, the moving average filtering method was used to determine the n and k values. Table 3 shows the analysis results for the n, k and the magnitudes of complex modulus ($|E^*|$),at the surface and bottom of the test specimens at 10 and 20°C.

The analysis results listed in Table 3 show that the k value increases with test temperature however the absolute value of the k phase angle decreases. Figure 19shows the stiffness gradient for the EBS-2-5 sample at 10 and 20°C. As observed from Figure 19, the stiffness gradient shifts to the left as the test temperature increases.

Table 3.Stiffness gradient analysis for the cores from US277

Sample ID	Coring Location	Age (Months)	T (C)	n	n Phase Angle (degrees)	k	k Phase Angle (degrees)	$\|E^*\|$ Surface (MPa)	$\|E^*\|$ Bottom (MPa)
EBS-2-5	Shoulder	17	10	2.24	-55	3.91	-65	5296	1354
EBS-2-5	Shoulder	17	20	3.28	-51	4.21	-60	4024	956
EBS-2-4	Shoulder	17	10	3.11	-47	4.44	-62	6214	1400
EBS-2-4	Shoulder	17	20	3.06	-31	4.85	-48	2744	566
RWP-2-6	Wheel Path	17	10	2.73	-65	3.98	-69	8714	2179
RWP-2-6	Wheel Path	17	20	1.78	-61	3.92	-66	4314	1100

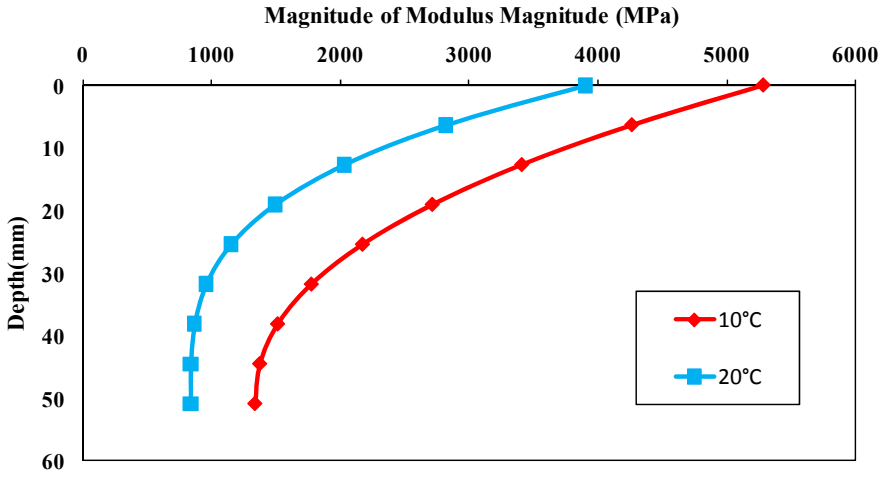

Figure 19.The stiffness gradient curve for the ESB-2-5 at 10and 20 C

Stiffness Gradient Analysis of Field Cores from US277

The US-277 asphalt concrete layer was constructed in April 2008. A PG 70-28 binder was used in this mixture and the design binder content was 4.2%. The cores were collected in 2008 ,2009,2010 and 2011. The asphalt concrete layer thickness in this road was 76 millimeters and the final test specimen was a 50 millimeters thick specimen. The specimens were tested in 10, 20 and 30°C. The results for n and k values for each year are listed in Table 4 through Table 7.

Table 4.Stiffness gradient analysis for the cores of the road US 277 for year 1

Sample ID	Coring Location	Age (years)	T (C°)	n	n Phase Angle (degrees)	k	k Phase Angle (degrees)	$\|E^*\|$ Surface (MPa)	$\|E^*\|$ Bottom (MPa)
NBS-1-5	Shoulder	1	10	4.32	-48.57	2.91	-38.22	5515.12	1893.43
NBS-1-5	Shoulder	1	20	3.79	-72.31	2.06	-65.21	1722.83	837.02
NBS-1-4	Shoulder	1	10	3.84	-57.91	3.07	-61.22	4354.38	1419.56
NBS-1-4	Shoulder	1	20	N/A	N/A	N/A	N/A	N/A	N/A
RWP-1-2	Wheel Path	1	10	5.31	-86.51	2.14	-24.12	3822.18	1790.02
RWP-1-2	Wheel Path	1	20	4.59	-34.52	3.79	-29.12	3708.88	977.33
RWP-1-5	Wheel Path	1	10	5.32	-75.75	1.46	-11	3774.59	2586.91
RWP-1-5	Wheel Path	1	20	3.79	-72.31	2.06	-65.11	1722.83	837.02

Table 5.Stiffness gradient analysis for the cores of the road US277 for year 2

Sample ID	Coring Location	Age (years)	T (C°)	n	n Phase Angle (degrees)	k	k Phase Angle (degrees)	$\|E^*\|$ Surface (MPa)	$\|E^*\|$ Bottom (MPa)
NBS-2-3	Shoulder	2	10	3.95	-48.41	2.41	-41.02	4971.25	2073.87
NBS-2-3	Shoulder	2	20	3.84	-46.42	2.34	-40.02	2529.66	1080.20
NBS-2-1	Shoulder	2	10	3.51	-41.12	2.43	-66.03	5736.31	2355.94
NBS-2-1	Shoulder	2	20	5.32	79.79	1.55	-11.01	2952.13	1905.44
RWP-2-1	Wheel Path	2	10	3.81	-74.21	2.38	-73.02	6299.15	2644.35
RWP-2-1	Wheel Path	2	20	3.44	-68.71	2.25	-77.01	3316.67	1474.99
RWP-2-3	Wheel Path	2	10	3.91	-73.81	2.53	-71.02	6948.05	2743.01
RWP-2-3	Wheel Path	2	20	3.87	-71.52	2.04	-61.05	2283.59	1119.02

Table 6.Stiffness gradient analysis for the cores of the road US277 for year 3

Sample ID	Coring Location	Age (years)	T (C°)	n	n Phase Angle (degrees)	k	k Phase Angle (degrees)	$\|E^*\|$ Surface (MPa)	$\|E^*\|$ Bottom (MPa)
NBS-3-1	Shoulder	3	10	3.94	-58.41	2.09	-47.02	6309.94	3013.01
NBS-3-1	Shoulder	3	20	3.91	-58.61	2.07	-47.03	3625.26	1754.30
NBS-3-1	Shoulder	3	30	3.92	-59.01	2.19	49.03	2351.75	1073.85
NBS-3-3	Shoulder	3	10	3.63	51.14	1.65	42.01	3925.13	2378.69
NBS-3-3	Shoulder	3	20	3.93	-61.61	2.48	-54.02	4317.95	1738.11
NBS-3-3	Shoulder	3	30	3.81	-61.06	2.41	-56.01	1886.36	786.27
RWP-3-1	Wheel Path	3	10	3.9	-67.41	1.98	-55.02	6176.18	3129.91
RWP-3-1	Wheel Path	3	20	3.75	-50.61	1.81	41.02	1996.14	1103.98
RWP-3-1	Wheel Path	3	30	3.74	65.01	2.19	60.01	2062.98	941.20
RWP-3-3	Wheel Path	3	10	3.86	-55.01	2.03	-45.02	6071.39	2991.71
RWP-3-3	Wheel Path	3	20	3.78	-67.61	2.02	-59.01	3212.73	1594.27
RWP-3-3	Wheel Path	3	30	3.82	-55.98	2.08	-47.01	1076.98	517.52
RWP-3-1T	Treated	3	10	3.65	-70.81	1.87	-64.01	4046.8	2169.71
RWP-3-1T	Treated	3	20	4.11	63.68	1.36	12.01	2141.39	1573.11
RWP-3-1T	Treated	3	30	N/A	N/A	N/A	N/A	N/A	N/A
RWP-3-2T	Treated	3	10	5.35	-74.71	1.41	-9.42	4093.98	2905.79
RWP-3-2T	Treated	3	20	3.74	65.35	1.71	54.01	2729.16	1603.44
RWP-3-2T	Treated	3	30	5.32	71.72	1.37	-8.21	1224.3	891.56

Table 7.Stiffness gradient analysis for the cores of the road US277 for year 4

Sample ID	Coring Location	Age (years)	T (C°)	n	n Phase Angle (degrees)	k	k Phase Angle (degrees)	$\|E^*\|$ Surface (MPa)	$\|E^*\|$ Bottom (MPa)
NBS-4-2	Shoulder	4	10	3.7	-61.61	2.38	-60.01	8033.56	3376.84
NBS-4-2	Shoulder	4	20	5.26	81.68	1.62	-16.02	3077.33	1895.36
NBS-4-2	Shoulder	4	30	3.78	-53.11	1.95	-44.04	1965.97	1007.17
NBS-4-4	Shoulder	4	10	N/A	N/A	N/A	N/A	N/A	N/A
NBS-4-4	Shoulder	4	20	3.73	-58.10	2.24	-53.02	3797.89	1695.42
NBS-4-4	Shoulder	4	30	N/A	N/A	N/A	N/A	N/A	N/A
RWP-4-1	Wheel Path	4	10	3.75	-63.21	2.06	-55.03	5444.9	2648.96
RWP-4-1	Wheel Path	4	20	3.85	-55.71	2.01	-45.01	2326.04	1158.25
RWP-4-1	Wheel Path	4	30	N/A	N/A	N/A	N/A	N/A	N/A
RWP-4-3	Wheel Path	4	10	3.73	-68.61	1.76	-58.02	6156.35	3488.19
RWP-4-3	Wheel Path	4	20	3.91	-69.91	2.09	-59.11	3171.39	1514.50
RWP-4-3	Wheel Path	4	30	3.79	-71.61	2.06	-63.12	1602.12	777.03
RWP-4-1T	Treated	4	10	3.78	-66.72	1.86	-56.12	5654.14	3047.01
RWP-4-1T	Treated	4	20	5.31	72.79	1.39	-8.21	2267.21	1625.92
RWP-4-1T	Treated	4	30	3.69	64.13	1.78	54.12	882.77	496.97
RWP-4-4T	Treated	4	10	3.82	64.24	1.73	51.05	4578.58	2648.34
RWP-4-4T	Treated	4	20	3.9	-64.12	1.94	-51.02	2578.22	1329.10
RWP-4-4T	Treated	4	30	N/A	N/A	N/A	N/A	N/A	N/A

The test results from US-277 during a four year period shows that the aging in the first few months after construction is very severe near the surface and it extends to

the deeper parts of the layer with time. The asphalt layers were softer in the first and second year; therefore, the test results only were obtained for 10º and 20° C and there were not enough data to complete the analysis for 30ºC.

Figure 20 shows the magnitude of the complex modulus over a four year period in the shoulder and wheel path. As shown in Figure 20 the modulus increases in the shoulder during the four year period but the modulus in the wheel path decreases after second year because of the surface treatment of the road in the second year.

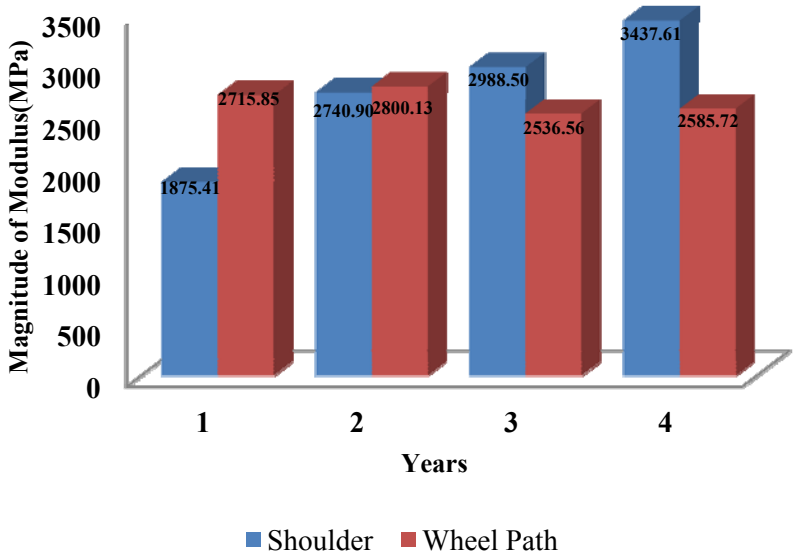

Figure 20.Magnitude of complex modulus in the shoulder and wheel path over a four year period

The results of the student's t-test analysis indicate that there is not enough evidence to prove that the aging in the shoulder is different from the aging in the wheel path which is under more severe traffic load.

Table 8 shows the statistical analysis of the 10C test at year 1.Table 9 through Table 11 show the statistical analyses for years 2 , 3 and 4 respectively. As shown in the statistical analysis summaries, the modulus at the surface and bottom of the asphalt layer increase with age. The Coefficient of variation for all parameters including the moduli is less than 30% and it is acceptable for field specimens. It should be noted that the data from path way and shoulder have been mixed in this analysis since according to t-statistic analysis there is no evidence that the traffic has a significant influence on aging. The statistical analysis for 20C and 30C tests are presented in Appendix A.

Table 8.Statistical summary of the stiffness gradient at 10C in year 1

Sample ID	Coring Location	Age	Test Temperature	n	k	Modulus at Surface	Modulus at Bottom
US-277-NBS-1-5	S	1	10C	4.32	2.91	5515.11	1893.44
US-277-NBS-1-4	S	1	10C	3.84	3.07	4354.38	1419.56
US-277-RWP-1-2	W	1	10C	5.31	2.14	3822.18	1790.02
US-277-RWP-1-5	W	1	10C	5.32	1.46	3774.59	2586.91
μ				4.70	2.39	4366.56	1922.48
б				0.74	0.74	809.55	487.44
COV				15.78	31.11	18.54	25.35

Table 9.Statistical summary of the stiffness gradient at 10C in year 2

Sample ID	Coring Location	Age	Test Temperature	n	k	Modulus at Surface	Modulus at Bottom
US-277-NBS-2-3	S	2.00	10C	3.95	2.40	4971.25	2073.87
US-277-NBS-2-1	S	2.00	10C	3.50	2.43	5736.31	2355.94
US-277-RWP-2-1	W	2.00	10C	3.81	2.38	6299.15	2644.35
US-277-RWP-2-3	W	2.00	10C	3.91	2.53	6948.05	2743.01
μ				3.79	2.44	5988.69	2454.29
б				0.20	0.07	839.77	302.14
COV				5.35	2.79	14.02	12.31

Table 10.Statistical summary of the stiffness gradient at 10C test in year 3

Sample ID	Coring Location	Age	Test Temperature	n	k	Modulus at Surface	Modulus at Bottom
US-277-NBS-3-1	S	3.00	10C	3.94	2.09	6309.94	3013.01
US-277-NBS-3-3	S	3.00	10C	3.63	1.65	3925.13	2378.69
US-277-RWP-3-1	W	3.00	10C	3.90	1.98	6176.18	3126.91
US-277-RWP-3-3	W	3.00	10C	3.86	2.03	6071.39	2991.70
μ				3.83	1.94	5620.66	2877.58
б				0.14	0.20	1134.56	337.85
COV				3.59	10.19	20.19	11.74

Table 11.Statistical summary of stiffness gradient at 10C in year 4

Sample ID	Coring Location	Age	Test Temperature	n	k	Modulus at Surface	Modulus at Bottom
US-277-NBS-4-2	S	4.00	10C	3.70	2.38	8033.56	3376.85
US-277-RWP-4-1	W	4.00	10C	3.75	2.06	5444.90	2648.97
US-277-RWP-4-3	W	4.00	10C	3.73	1.76	6156.35	3488.20
μ				3.73	2.07	6544.93	3171.34
б				0.03	0.31	1337.36	455.80
COV				0.76	14.87	20.43	14.37

Figure 21 shows the stiffness gradient curves in different time sequences for the shoulder specimens at 10°C. Figure 21 shows that the aging is very severe in the top 12 millimeters, and after time, the sample ages more at a greater depth.

Figure 22 shows the change of the stiffness gradient over a four year period in the wheel path. The results indicate that the bottom of layer continues to become harder in four year period whereas the stiffness of the surface stays relatively constant after the second year. This may happen due to the traffic load.

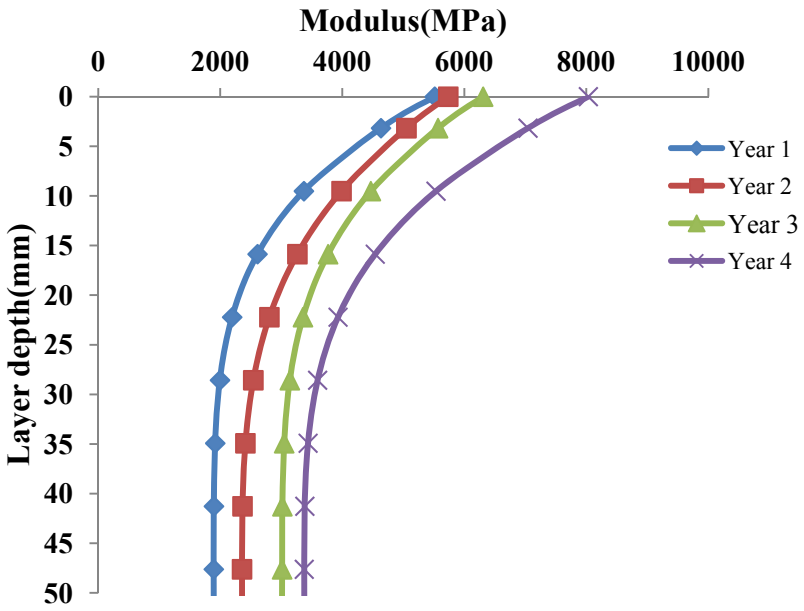

Figure 21.The change of the stiffness gradient curve over a four year period on Shoulder

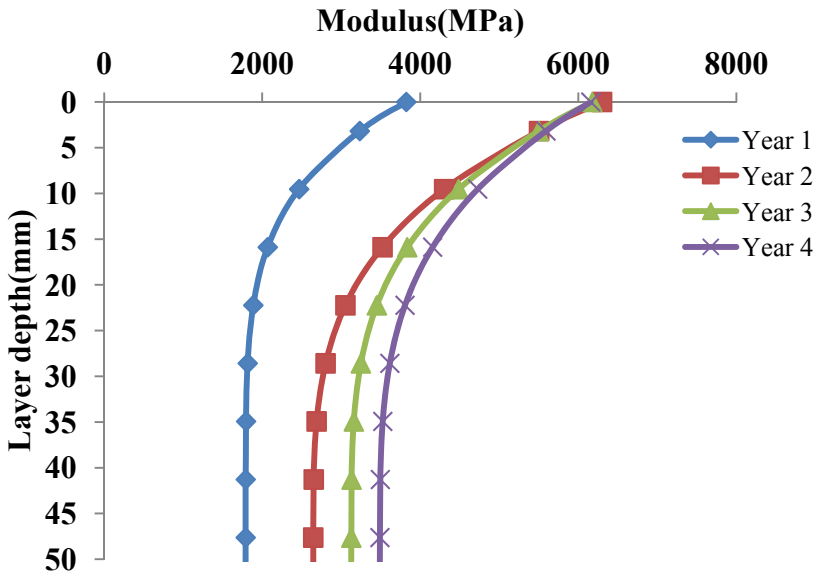

Figure 22.The stiffness gradient change over a period of 4 years at the wheel path

There is an exceptionally low value of modulus at some 20 degree tests which may occur due to the previous sample damage during the 10°C test.

In tests at all temperatures greater strains occur on the low modulus face which can exceed the strain above which damage occurs. The tests at all temperatures were made with the same level of machine displacement control, suggesting that greater displacement restrictions should have been used at the lower temperature. In future tests, more restrictions will be used on the applied strain levels at 10°C.

Concluding Remarks

This study shows that the direct tension test can be used as a rapid test without inducing damage to find the viscoelastic properties of the field samples namely, the stiffness gradient with the depth, which can be used in different performance prediction models. The methodology described in this paper can be used in different machines with different feedback frequencies by changing the applied frequency rates in the corresponding equations.

Based on the data analyzed in this study, it is clearly observed that the stiffness increase due to the aging process is quick and severe in the top 0.5 inches a few months following pavement construction, and as the pavement ages, aging extends deeper into the layer. The stiffness gradient function behavior with time is a complicated phenomenon which requires the analysis of data obtained from several samples taken at different times from the same section. Major progress has been accomplished in the calculation of the stiffness gradient function with depth. Furthermore, the relation of the n and k factors to mixture and binder properties and the pavement age can now be determined in future studies, leading to improvements in aging models used in predicting pavement performance.

CHAPTER IV

METHODOLOGY TO FIND THE HEALING AND FRACTURE PROPERTIES OF LABORATORY COMPACTED ASPHALT MIXES USING OVERLAY TESTER

In this chapter, the pseudo strain energy concept and Paris's law were tailored according to the OT test conditions to obtain fracture and healing properties of the asphalt mixes in the same test. By applying this methodology, the OT can be used not only to obtain the number of load cycles to reach a standard crack length but also the fracture and healing properties of the asphalt mixes for different quality assurance and performance prediction purposes.

The test method modifications and sample preparation techniques which have been conducted by TTI researchers have reduced the variability of the results. This variability has several causes all of which will be explained at the conclusion of this study. The study reported in this research was undertaken to determine the cause of the high degree of variability and to develop methods of using OT data that are much more consistent and precise. This has been accomplished through the application of fracture mechanics.

The FE program output is used in a constitutive model to predict the crack growth in a field asphalt layer under the repeated loading. The FE model together with

constitutive fracture mechanics based model is able to estimate the crack growth rate, fracture properties, and healing properties of the laboratory asphalt mixtures.

This new methodology uses a combination of fracture mechanics principles and Finite Element (FE) simulation to calculate the crack growth rate, fracture and healing properties of laboratory compacted asphalt mixtures. The correspondence principle and also Paris's law were used in this methodology (Paris and Erdogan, 1963, Schapery, 1989, Schapery, 1975).

Methodology

The methodology will be described in this research will include three main modules:

- Finite Element Model to find the strain profiles above the crack tip
- The crack growth analysis module
- The fracture and healing characterization module

Figure 23 illustrates the three main modules of the methodology. There are also some modifications in the test procedure.

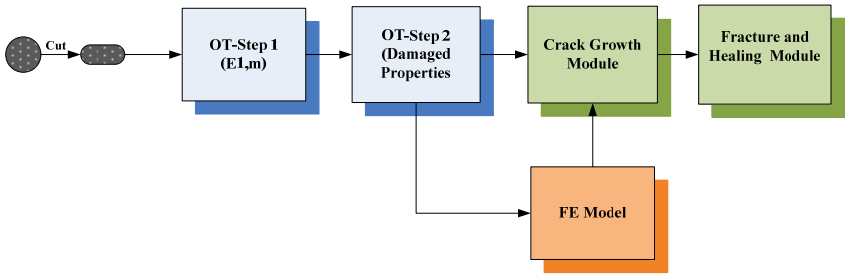

Figure 23.The analysis of the laboratory compacted specimen via OT Test

Finite Element Duplication of the Test

Boundary Conditions

As part of this research, the test procedure was simulated in ABAQUS. The test is modeled in a 2D format for an elastic material. It was assumed that Poisson's ratio is 0.3 for modeling purposes.

Figure 24 shows the boundary conditions used in the FE model. As shown in Figure 24, the left portion of the specimen is fixed and the right portion moves back and forth in the horizontal direction. The crack initiates from the bottom of the specimen above the opening and closing joint and grows vertically to the top.

The model was defined in both plane stress and plane strain conditions .The results were identical. However the plane stress condition is more appropriate for this model because the specimen is very thin.

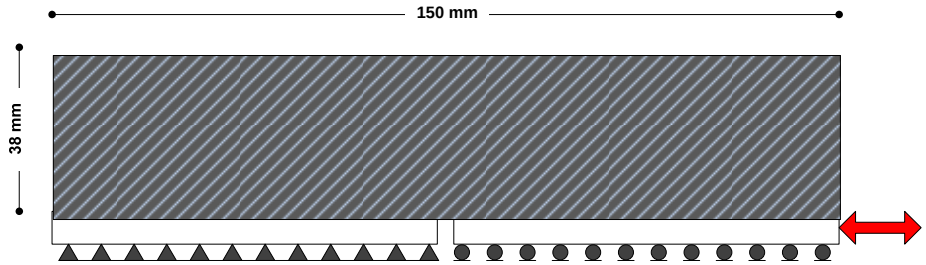

Figure 24.The boundary conditions of the FE model

The crack with different lengths was modeled and the contour integral method was used to define the crack tip function. Figure 25 shows the deformed specimen and the corresponding principal stress distribution in the specimen when the crack length is 15.875 mm and the opening is 0.635 mm.

Since the test is displacement controlled, the strain profiles above the tip of the crack remain the same, regardless of the magnitude of the elastic modulus. This information was used to predict the crack length in each cycle, as the strain profiles above the tip of the crack depend only on the maximum displacement magnitude.

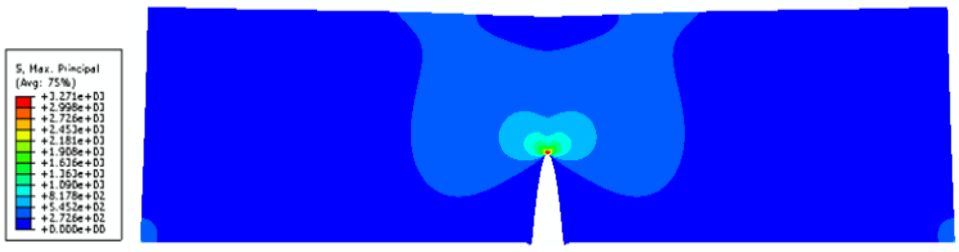

Figure 25.The deformed specimen and principal stress contours

The computed strain profiles for four different crack lengths are plotted against specimen depth in Figure 26. As seen in Figure 26, as the crack advances, the area under the strain profiles in the intact material decreases. In this study, the change of the area under the strain curve for different crack lengths was used to estimate the actual crack length in each load cycle. In specimens thicker than 40 mm, the strain in the upper 10 mm becomes compressive.

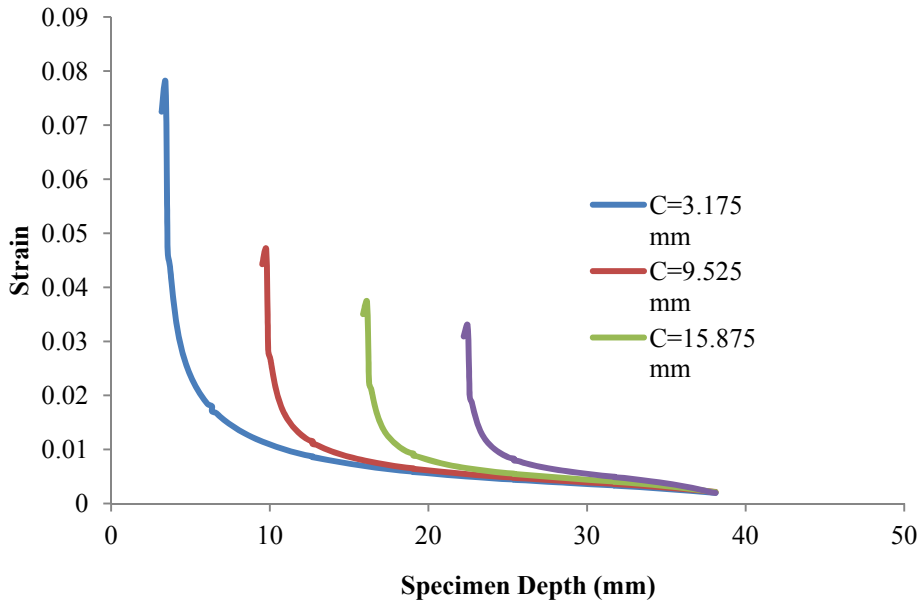

Figure 26.Strain profiles above the tip of the crack at different crack Depths

Effect of Sample Geometry on Test Results

Counting the number of the load cycles to the failure has been used to compare the asphalt mixtures; However, users reported a lot of variability in this method. This may happen for different reasons. A sensitivity analysis was conducted to compare the strain profile contours above the crack. The results showed that in the specimens thicker than 38 millimeters (1.5 inches) the upper parts of the specimen will be in the compression or very small tensile strains; therefore, as crack enters these low tensile strain or compressive zones the crack growth rate decreases significantly.

Figure 27 shows the strain profiles above two specimens with the same crack length and different thicknesses. As shown in Figure 27 the thicker specimen has a compressive zone which delays the crack growth. Unlike the method of counting the load cycles ,the methodology that will be described in this research will estimate the crack growth function versus the load cycles which is already related to the strain profiles above the crack tip; therefore, the problem of the high variability only occurs in the case in which the load cycles to the failure are counted.

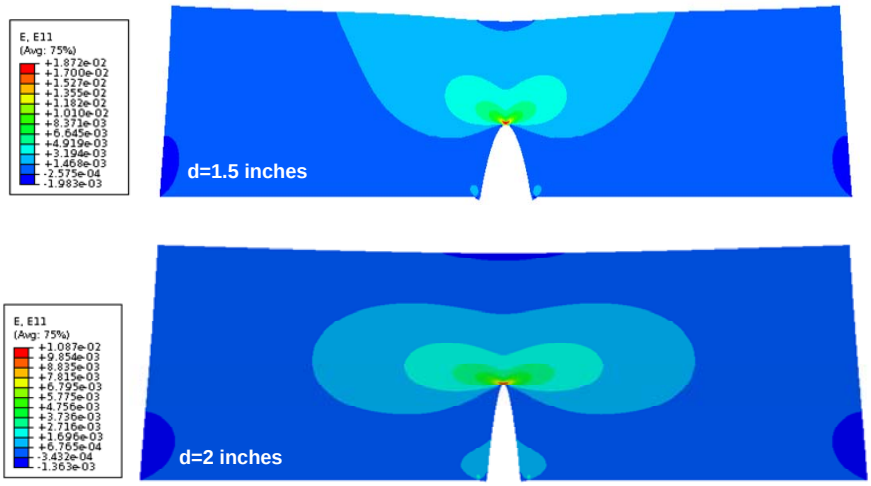

Figure 27.Effect of specimen thickness on the strain contours above the crack

Additionally, the effect of the destructive displacement opening is not very significant in the size of the compressive zone above the crack. However, as expected the larger displacement results in the larger compressive and tensile strains, but unlike the thickness the shape of the strain contours above the crack remains the same. Figure 28 shows the strain profiles above the crack for different maximum openings.

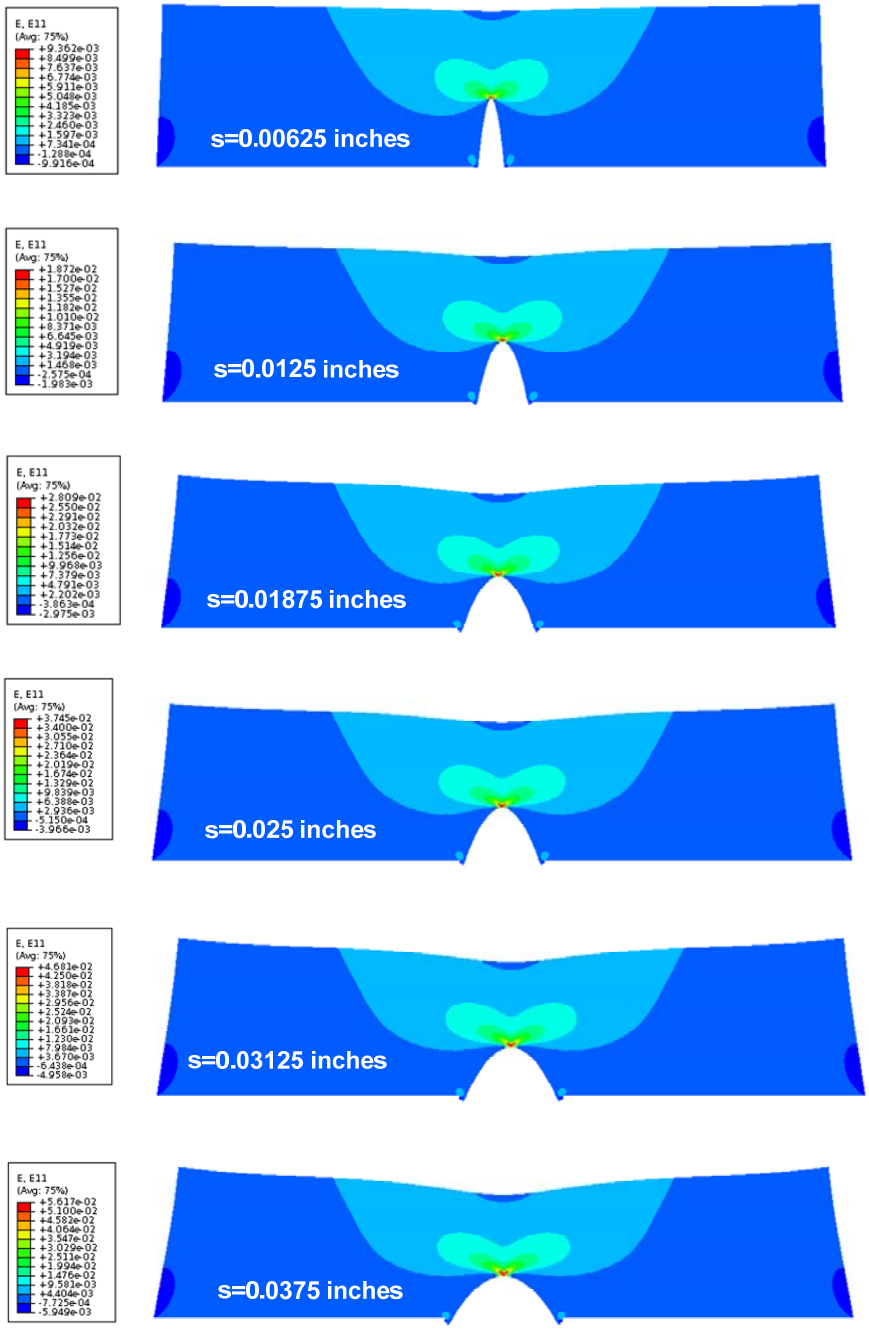

Figure 28.Effect of the gap opening on the strain contours above the crack

Stress Intensity Factor and J-integral

The FE simulation results show that the energy release rate decreases as the crack grows. In order to understand the crack propagation process in the OT test, the stress intensity factor and J-integral were calculated with time as the crack grows. The FE simulation was used to obtain the changes in the stress intensity factor and J-integral against crack length. The crack in the OT test is a Mode I tensile crack. The crack growth rate is controlled by the size of the stress intensity factor, K_I which is defined in Equation 34.

$$K_I = \sigma\sqrt{\pi C} \tag{34}$$

where σ is stress and C is the half crack length.

Figure 29 shows that the stress intensity factor for Mode I reduces significantly as the crack grows. This graph is for a test specimen with uniform modulus.

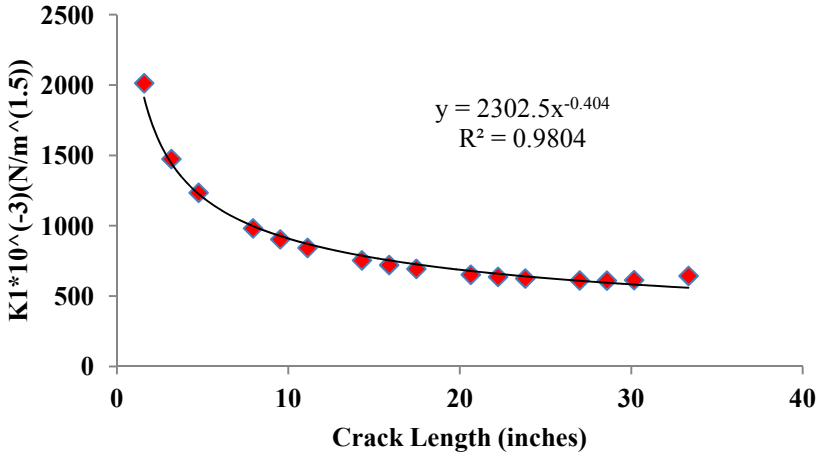

Figure 29.The stress intensity factor versus crack length

The same trend can be seen in Figure 30 for the J-integral (strain energy release rate) which is related to fracture toughness under Mode I loading at the tip of the crack (Yoda, 1980).

$$J_I = K_I^2\left(\frac{1-\nu^2}{E}\right) \tag{35}$$

where K_I, ν and E are the Stress Intensity Factor, Poisson's ratio and Young's modulus, respectively.

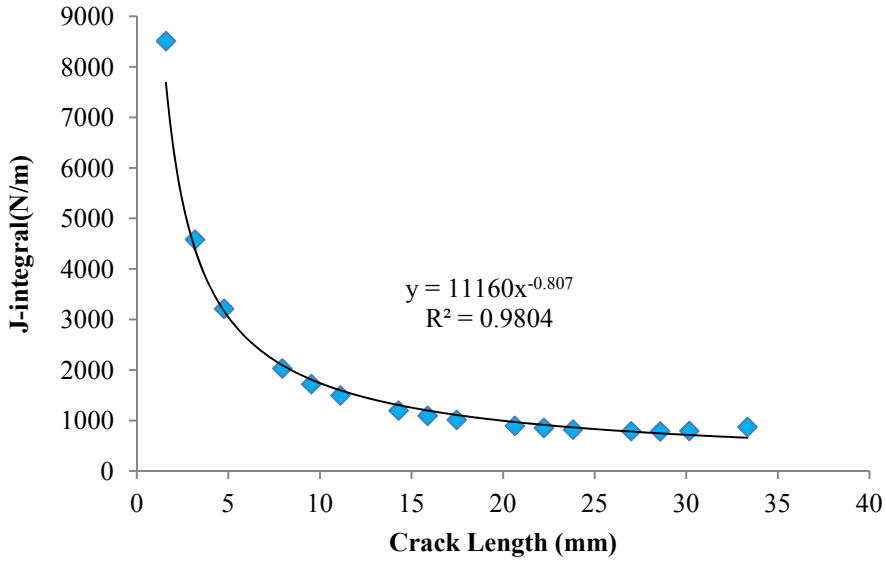

Figure 30.J-integral versus the crack length

Development of the Crack Growth Estimation Model

As mentioned previously, one of the objectives of this research was to develop a method of predicting the crack growth rate with load cycles. The convolution integral was used to represent the time dependent properties of the asphalt.

The time dependent stress in a linear visco elastic material can be calculated using Equation 36.

$$\sigma(t) = \int_0^t E(t-\tau)\frac{d\varepsilon(\tau)}{d\tau}dt \qquad (36)$$

where σ and ε are the Linear Visco Elastic (LVE) stress and strain, respectively; t designates a specific time; and τ is a time-integration variable.

As the outputs collected by the OT machine are load, displacement and time, Equation 36 should be converted to a load-displacement equation. This transformation is done by Equation 37.

$$\sigma(t) = \frac{P_{LVE}(t)}{A} \tag{37}$$

where $P_{LVE}(t)$ is the measured viscoelastic force and A is the intact area (the area above the crack tip).

The first part of the test is designed to obtain the undamaged properties of the asphalt mixes. The displacements in the nondestructive test are limited to ensure that there is no crack growth.

The relaxation modulus is given by the form shown in Equation 38.

$$E(t-\tau) = E_1.(t-\tau)^m \tag{38}$$

where E_1 and m are the undamaged tensile mixture properties which are determined by regression analysis. The loading pattern for this test is shown in Figure 31.

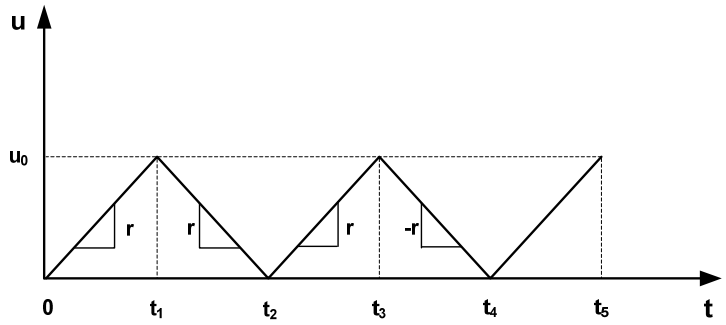

Figure 31.The loading pattern in OT test

The data from the first load cycle in the nondestructive test was used to obtain the undamaged properties. First the percentage of the maximum opening at the time $t < t_1$ is calculated using Equation 39.

$$\frac{u(t)}{u_0} = \frac{t}{t_1} \tag{39}$$

where $u(t)$ is the displacement at time *t* and u_0 is the maximum displacement.

The elastic strain at time $t < t_1$ and opening *u* for no crack condition are shown in Equation 40.

$$\varepsilon(c=0, u(t), z) = \varepsilon(c=0, u_0, z)\frac{t^2}{t_1^2} \tag{40}$$

where $\varepsilon(c=0, u(t), z)$ is elastic strain at time *t* and depth *z*; and $\varepsilon(c=0, u_0, z)$ is the elastic strain at depth *z* at the maximum displacement. The viscoelastic force is calculated using Equation 39 and 40. The time dependent strain and the relaxation modulus values in the convolution integral are replaced by the corresponding values

from Equations 38 and 40, respectively. The final magnitude of the viscoelastic force is shown by Equation 41. It should be noted the $s(c=0)$ in Equation 41 is the integration of the strain profile curve over the depth of the specimen. This term is calculated with the FE model for the no crack condition using the nondestructive phase's displacement.

$$P_{LVE}(t)=\frac{2bE_1}{t_1^2}s(c=0)\frac{t^{2-m}}{(2-m)(1-m)} \tag{41}$$

in which $P_{LVE}(t)$ is measured by the load cell as a function of time and $s(c=0)$ is calculated using the integrated strain profiles that were calculated with the FE model. The unknown parameters in Equation 41, E_1 and m, are calculated using a linear regression method.

Subsequently, the viscoelastic force for the destructive cycles is calculated to find the actual crack length in each loading cycle.

Equation 42 applies to the destructive load cycles.

$$\varepsilon(z,t)=\frac{rt}{u_0}\varepsilon(z) \tag{42}$$

where t is a specific time and r is the slope of applied displacement with time.

The convolution integral is solved for both loading and unloading intervals. The maximum tension (loading) and compression (unloading) viscoelastic forces are shown in Equations 43 and 44, respectively.

$$\max.P_{LVE}(z=c)=\frac{E_1bt^{1-m}}{(1-m)t_1}s(c) \qquad 0<t<t_1 \tag{43}$$

$$\max.P_{LVE}(z=c) = bs(c)\frac{E_1 t^{1-m}}{(1-m)t_1} - 2bs(c)\frac{E_1(t-t_1)^{1-m}}{(1-m)t_1} \quad t_1 < t < 2t_1 \tag{44}$$

where $\max.P_{LVE}(z=c)$ is the measured maximum viscoelastic force within the specified time interval, b is the width of specimen, and $s(c)$ is the area under the strain profile above the tip of the crack length (c).

Figure 32 shows the area under strain profiles above the tip of the crack for different crack lengths for the test displacement.

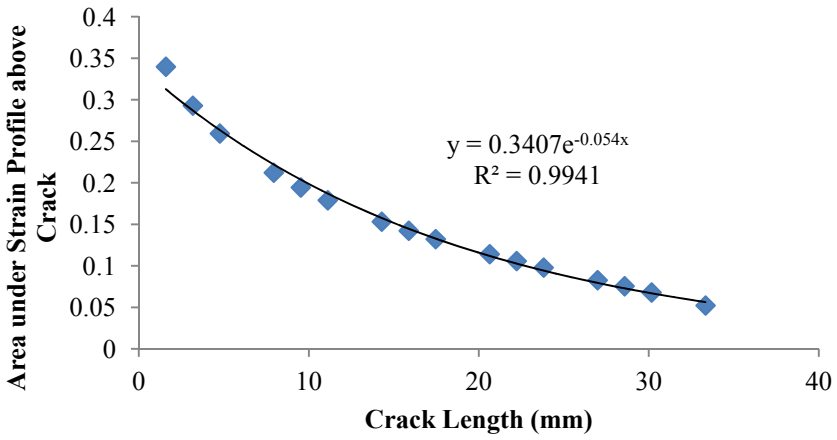

Figure 32.Area under strain profiles above the tip of the crack

In order to find the actual crack length in each cycle, the healing of the crack when the displacement is forced back to zero must be considered. The high magnitude of the compressive force in each cycle is responsible for the healing that occurs in a very

short time. As seen in Figure 32, the value of $s(c)$ decreases as the crack grows. Healing actually reduces the crack size, and as a result, the area under the strain profile above the tip of the crack increases. In order to include the healing effect, the areas under the strain profiles in tension and compression were calculated from Equations 43 and 44 and summed for each cycle. The resultant $s(c)$ was applied to the $s(c)$ versus crack length curve shown in Figure 32 to find the corresponding crack length.

Table 12 shows the systematic procedure to find the actual crack length in each load cycle.

Table 12.Systematic procedure to find the actual crack length in OT test

Step 1: Calculate the area under strain profiles for no crack condition using FE model
Step 2: Calculate the area under strain profile for various crack lengths and estimate the function
Step 3: Conduct the undamaging test, 10 cycles with maximum opening of 0.05mm
Step 4: Conduct the damaging test, 150 cycles with opening of 0.635 mm
Step 5: Use the load-time data, step 3 and Step 1 output to find the E_1 and m values in Equation 41.
Step 6: Find $(s_t(c))_i$ and $(s_c(c))_i$ for each cycle using outputs of step 4, 5, and Equations 43 and 44.
Step 7: Find $(s(c)_{total})_i = (s_t(c))_i + (s_c(c))_{i-1}$ to consider the effect of healing occurs in each cycle.
Step 8: Use the $s(c)_{total}$ and step 2 output function to find the crack length in this cycle.
Step 9: Repeat steps 6 to 8 for all cycles to find the crack length in each cycle
Step 10: Fit the power function of the crack length versus the load cycles.

Fracture and Healing Properties Estimation

As discussed before each loading cycle contains both fracture and healing phases and the test results show that a large amount of healing occurs during each displacement cycle.

The fracture and healing properties can be determined from OT test outputs using the dissipated pseudo work principle very efficiently.

The pseudo displacement is calculated by Equation 45.

$$U_r(t) = \frac{P_{LVE}(t)}{k_r} \tag{45}$$

where $P_{LVE}(t)$ is the linear viscoelastic force and k_r is the reference stiffness which is the value of the maximum load in the first load cycle divided by the maximum opening. Figure 33 shows the pseudo displacement plotted against the measured load in a specific load cycle. The dissipated pseudo work area under the tensile loading part is related to the crack growth and the dissipated work area under the compressive loading part is related to the healing which occurs in each load cycle.

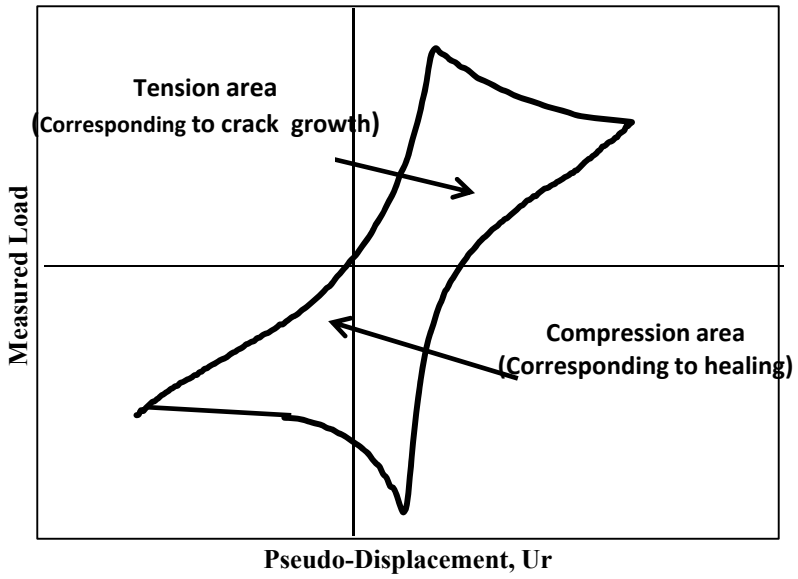

Figure 33.Pseudo-displacement versus the measured visco-elastic load

By obtaining the crack length and dissipated pseudo work as functions of the displacement cycles, the pseudo J-integral is calculated using Equation 46 for both healing and fracturing modes.

$$J_R = \frac{\frac{\partial W_{R1}(N)}{\partial N}}{\frac{\partial (c.s.a)}{\partial N}} \tag{46}$$

where the J_R is the pseudo J-integral, N is the number of load cycles, $\frac{\partial W_{R1}(N)}{\partial N}$ is the rate of change of dissipated pseudo work and $\frac{\partial (c.s.a)}{\partial N}$ is the rate of change of the crack surface area. The conventional form of Paris' law (Paris and Erdogan, 1963) shown in Equation 47, is usually used to predict the crack growth response of different materials (Atzori, et al., 2008, Bilir, 1990, Pugno, et al., 2006).

$$\frac{dC(N)}{dN} = A(J_R)^n \tag{47}$$

where $C(N)$ is the crack length on the Nth load repetition.

The conventional version of Paris' law does not give realistic results because the energy release rate decreases as the crack grows in the OT test. Therefore, the format shown in Equation 48 and 49 is used to determine the Paris' Law's fracture and healing coefficients, respectively.

$$\frac{dC(N)}{d(N)}_{-} = A\left[\frac{W_{R1}(N)}{c.s.a}\right]^n \tag{48}$$

$$\frac{dC(N)}{d(N)}_{-} = B\left[\frac{W_{R1}(N)}{c.s.a}\right]^m \tag{49}$$

where

$$c.s.a = 2bC(N) \tag{50}$$

$$I = \frac{K_r}{K_n} \tag{51}$$

For each cycle the areas under the tension and compression of pseudo work-load curves are calculated. Then the area is multiplied by the *I* factor which is the ratio of the initial pseudo-stiffness, K_r, divided by the damaged pseudo stiffness in the nth load cycle. The corrected area is divided by the intact cross section to find the values of WR_t and WR_c in each cycle.

The power function is used to fit to the curves of WR_t and WR_c against load cycles. The resultant power functions together with the actual crack growth function are inserted into Equations 48 and 49 to find the healing and fracture properties using regression analysis. Equations 52 and 53 show the crack growth and the Pseudo-dissipated work functions, respectively. Equations 54 and 55 are the results of the regression analysis for A and n. The same equations can be used to find the B and m values.

$$C = d \cdot N^e \tag{52}$$

$$\frac{W_{R1}(N)}{2bC(N)} = a \cdot N^b \tag{53}$$

$$n = \frac{e-1}{b} \tag{54}$$

$$A = \frac{d \cdot e}{a^n} \tag{55}$$

Figure 34 and Figure 35 show the change of the WR_t and WR_c versus the load cycles. The area Pseudo dissipated work decreases as the load cycles increase.

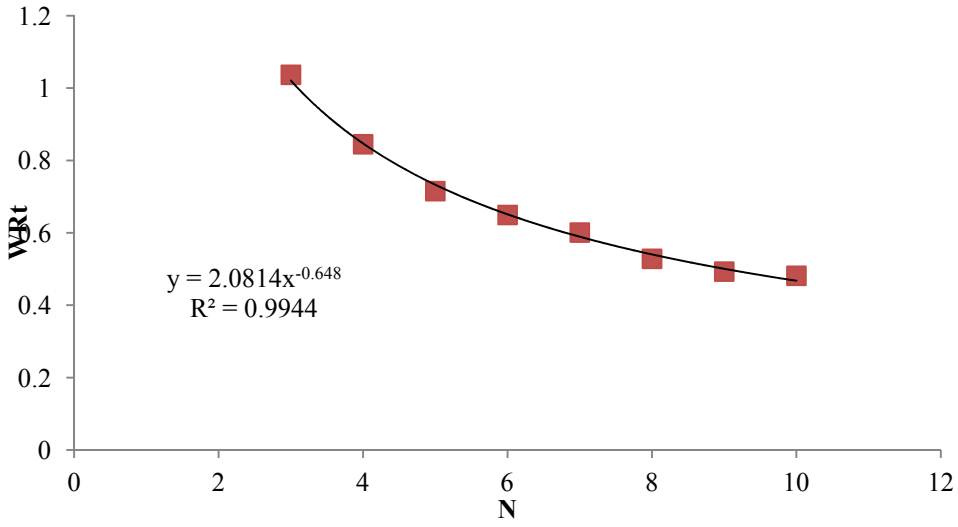

Figure 34.Fracture pseudo work versus load cycles

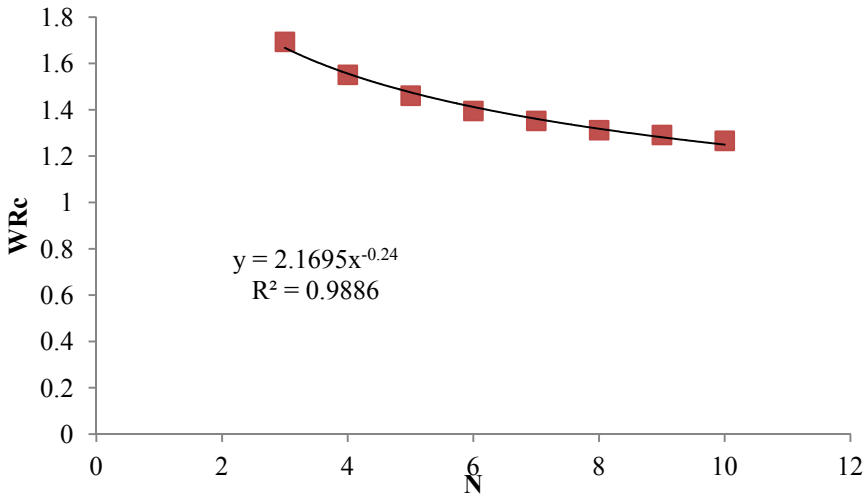

Figure 35.Healing pseudo work versus load cycles

Table 13 illustrates the systematic procedure to determine the fracture and healing properties of the asphalt mix.

Table 13. Systematic procedure to find fracture and healing properties of asphalt mix in OT test

Step 1: Calculate the viscoelastic force with time using the outputs of Table 1 procedure and Equations 43 and 44
Step 2: Find the Pseudo displacement with time using step1 and Equation 45
Step 3: Sketch the Pseudo displacement against the measured load for each cycle
Step 4: Calculate the areas under the compression and tension parts of the each loop (Figure 33)
Step 5: Correct the areas by multiplying the factor I from Equation 51.
Step 6: Divide the area by the area of the intact cross section to find WR_t and WR_c for each cycle.
Step 7: Repeat steps 1 to 6 for all cycles
Step 8: Sketch WR_t and WR_c against load cycles
Step 9: Fit the power function to the WR_t and WR_c against load cycles' curves
Step 10: Use Equations 48 and 49, the outputs of step 9 and the actual crack growth curve to find fracture and healing coefficients using linear regression.

Experiment

Materials

In order to illustrate the methodology with actual test results, a Texas type D mix with a PG 67-22 grade binder was analyzed with the testing analysis method. The binder content of the mix was 5.2%. The specimens were molded at two different air void contents, 4 and 7 percent to compare the effect of air void content on the crack growth, fracture, and healing properties of the mixes. Three replicates of each air void category

were used to evaluate the consistency of the model. The laboratory compacted cores were cut to the standard specimen geometry and the specimens were glued on the aluminum plates.

Test Procedure

The test is conducted in two steps: the nondestructive test and the crack growth test. Figure 36 shows the nondestructive and destructive loading patterns. The nondestructive phase includes 10 load cycles with an opening of 0.05 mm and the destructive phase includes 150 load cycles with a maximum opening of 0.635mm. All tests are conducted at 25 Cº.

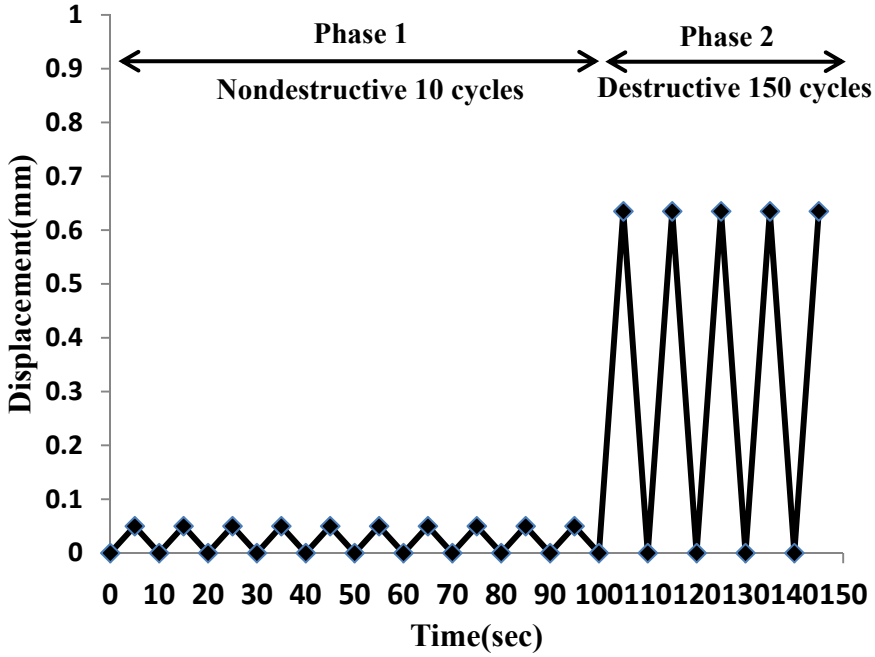

Figure 36.Loading pattern for nondestructive and destructive tests

Results

The test outputs were analyzed to obtain both damaged and undamaged properties. Table 14 and Table 15 show the results for the undamaged, fracture and healing properties.

The numbers of cycles for the crack to grow a length of 25 mm is counted for two reasons: (a) to reduce length of time required for the test, and (b) because counting cycles after crack enters the top 6 mm low strain zone in thin samples produces inconsistent results. As was noted before in thicker sample the top zone is in compression according to FE analysis results and the crack growth rate decreases

substantially in this zone. The coefficient of variation (COV) for the number of cycles corresponding to the crack length of 25 mm is calculated to demonstrate the consistency of the methodology compared to previous methods. The COV values for the number of load cycles of mixes A and B are 19 and 16 percent, respectively.

Table 14.Dameged and undamaged properties of the mixture type A using OT test

Mix Properties			Undamaged Properties		Damaged Properties			Healing Properties	
ID	Percent Air (%)	Binder Content (%)	E_1 (MPa)	m	N	A	n	B	m
A-1	4.2	5.2	253.805	0.42	56	0.046	1.720	0.019	3.430
A-2	4.4	5.2	257.432	0.41	44	0.035	1.190	0.021	2.320
A-3	4.2	5.2	246.451	0.4	65	0.038	1.374	0.023	2.461
μ	4.267	5.2	252.529	0.41	55	0.040	1.428	0.021	2.737
б	0.115	0	5.649	0.01	10.536	0.006	0.269	0.002	0.604
COV	2.706	0	2.237	2.439	19.156	14.335	18.844	9.524	22.078

Table 15.Damaged and undamaged properties of the mixture type B using OT test

Mix Properties			Undamaged Properties		Damaged Properties			Healing Properties	
ID	Percent Air (%)	Binder Content (%)	E_1 (MPa)	m	N	A	n	B	m
B-1	6.90	5.20	172.444	0.530	44	0.030	1.750	0.016	3.040
B-2	7.40	5.20	189.350	0.480	36	0.049	1.470	0.051	2.580
B-3	7.40	5.20	193.791	0.547	50	0.024	1.640	0.011	2.825
μ	7.233	0	185.195	0.519	43.333	0.034	1.620	0.026	2.815
б	0.289	0	11.264	0.035	7.024	0.013	0.141	0.022	0.230
COV	3.991	0	6.082	6.744	16.209	38.013	8.708	83.825	8.176

In addition, the undamaged properties are very consistent. The COV values for the undamaged relaxation moduli of mixes A and B are 2.23 and 6.08 percent, respectively. According to Table 14, the fracture and healing COV parameters are below the 30% level which was a characteristic of the previous method of using the overlay tester.

The average number of cycles corresponding to 25 mm crack growth is higher in mix A compared with mix B. This happens because of the lower air voids of mix A relative to mix B.

As mentioned previously a large amount of healing occurs during each load cycle. The higher magnitude of the m values in both mixes also confirms this observation.

Previous methods of analyzing OT test data by counting the number of load cycles for the crack to reach the top of the sample have shown coefficients of variation of much greater than 30 percent especially for coarse-graded mixes (Walubita, et al., 2009).

Figure 37 depicts the actual crack growth against loading cycles. As shown in Figure 37, the crack grows very quickly during first few load cycles and the rate of crack growth decreases substantially after that.

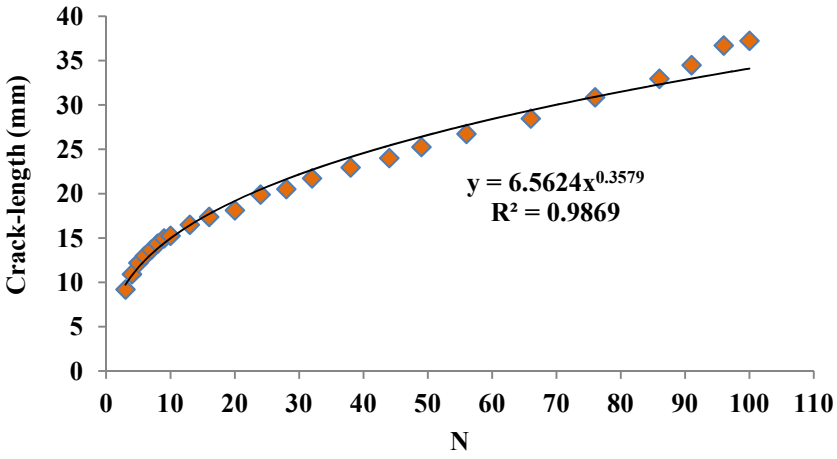

Figure 37.Actual crack growth for a laboratory compacted mixture with 4% air void

Concluding Remarks

The results of this research show that the OT machine can be used as a quick and robust test for determining fracture and healing properties of asphalt mixes and a calculated number of load cycles for the crack to reach a standard length. The latter permits a direct comparison of the fracture resistance of different mixes. The accuracy and repeatability of this method has been demonstrated to be superior to previous methods of using the same test apparatus. In addition, the analysis of the crack growth and pseudo work dissipation produces both fracture and healing properties.

CHAPTER V

THE ESTIMATION OF VISCOELASTIC PROPERTIES OF IN-SITU ASPHALT MIXTURES VIA DIRECT TENSION TEST AND OVERLAY TESTER TEST

The viscoelastic characterization of asphalt layers in the field is more challenging than that of laboratory compacted mixtures due to the aging of the binder and other enviromental factors in the field. The methodology developed in this study uses two efficient and popular tests, the Direct Tension (DT) and the Texas Overlay Tester (OT) tests, to find the viscoelastic properties of aged asphalt concrete mixtures in tension.

The DT test outputs under a monotonically increasing load were analyzed using a novel method to find the stiffness gradient of asphalt mixtures in the field. Subsequently the OT test outputs were analyzed using fracture mechanics principles together with a Finite Element (FE) model to calculate the fracture and healing properties of aged asphalt mixtures in the field.

A user-defined material subroutine (UMAT) in Abaqus has been developed to simulate the response of the aged AC layers as functionally graded materials under the repeated loadings. The FE program output is used in a constitutive model to predict the crack growth in a field asphalt layer under the repeated loading. The FE model together with constitutive fracture mechanics based model is able to estimate the crack growth rate, fracture properties, and healing properties of the field-aged asphalt mixtures. This

subroutine can be independently used with different FE models to simulate aged asphalt concrete in various test methods.

This chapter describes a testing protocol which includes the procedure to extract the field cores, DT test and OT test to calculate the viscoelastic properties of the field-aged AC mixtures.

The methodology described in this chapter was verified using actual field cores from a 10 year old road in Arizona. The results indicate that the viscoelastic properties of the asphalt concrete layers in the field can be successfully determined using DT and OT tests based on fracture mechanics principles and numerical simulation of the test procedure.

Methodology

The OT laboratory protocol has been tailored to be applied to the field samples. Figure 38 shows the main modules of the methodology which are described in this dissertation. The procedure includes:

- Extraction of the three identical cores from the field
- One core is used for the X-ray CT-scan and binder extraction procedure, and the other two will go through DT and OT tests
- The DT test outputs are analyzed using the stiffness gradient calculation module

- The OT test and the stiffness gradient outcomes are plugged into the FGM numerical module to calculate the crack growth pattern
- The FGM output is used in another analytical module to calculate the healing and fracture properties of the AC
- It should be noted that the DT test is a nondestructive test; therefore, the test protocol can be completed with two replicates instead of three because the same sample can be used after the DT test for the binder extraction . The analytical and numerical models will be discussed in greater detail in the following sections.

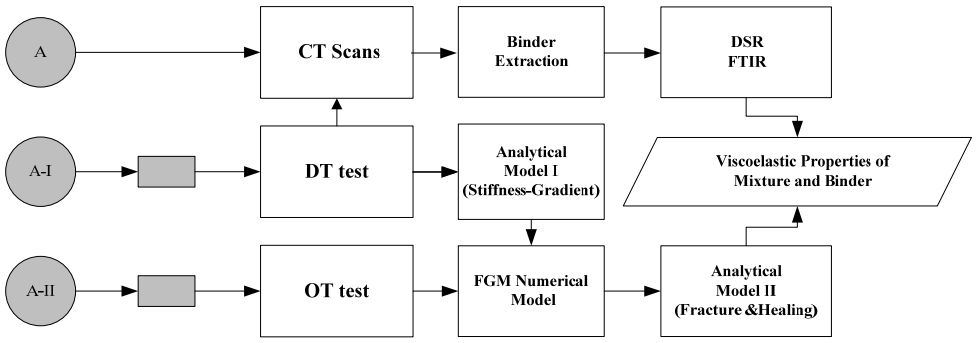

Figure 38.General procedure of the test protocol of field samples

Stiffness Gradient Calculation via Direct Tension Test

A rectangular specimen is cut from the field core used for the DT test and steel endcaps are glued to both ends of the rectangular specimen. Six Linear Variable

Differential Transformers (LVDTs) are installed on each specimen of which four LVDTs measure the strain at the surface, bottom and the center of the asphalt layer and the other two record the horizontal strains at the surface and the bottom of the asphalt concrete layer. The rectangular field specimens oscillate under the monotonically increasing loads and these oscillations can be tracked in the strain outputs. The oscillations occur due to the effect of the feedback frequency and the stiffness gradient. The test is conducted at three different temperatures and each test takes about 3 hours to complete including the time required for the test sample to reach to the equilibrium temperature.

The analytical model assumes that the strain changes linearly with depth and the complex modulus of the asphalt layer changes from a higher modulus at the surface to a lower modulus at the bottom following a power function. Equations 56 and 57 show the stiffness gradient function and the relation between the modulus at the surface and the modulus at the bottom of the asphalt concrete layer in the field.

$$E(z) = E_d + (E_0 - E_d)(\frac{d-z}{d})^n \tag{56}$$

$$E_0 = k.E_d \tag{57}$$

where $E(z)$ is the magnitude of the complex modulus at depth z ; E_0 and E_d are the magnitudes of the complex modulus at the surface and the bottom of the AC layer, respectively; n and k are model parameters; and d is the thickness of the specimen. The exponent n is an indication of the sharpness of the stiffness profile. In the other words as n value increases the stiffness changes become sharper near the surface.

The analytical model uses a procedure which includes the signal processing to find the amplitude and frequency of the oscillations at the surface, center and the bottom of the AC layer. Then, using an analytical method based on linear viscoelasticity and the correspondence principle, the complex modulus gradient function is calculated. The detailed process has been described in a previously published paper(Koohi, et al., 2011).This test and the corresponding analytical model estimates the stiffness gradient function with depth for the field specimen in the feedback frequency at three different temperatures.

Numerical Simulation of Functionally Graded Material

The FGM Model Applications

Less oxygen is available for the aging mechanism for the deeper portions of asphalt layer within the pavement structure. Therefore, asphalt mixtures in the field are usually stiffer at the surface because of more oxygen availability and more solar radiation at the surface. The stiffness gradient in the pavement layers usually is defined by dividing the pavement layer into smaller sublayers each of which has different stiffness modulus. Obviously , this method increases the errors in the strain and stress calculations in the FE models(Dave, et al., 2008).In this approach , every single layer will have different stiffness modulus and these properties should be redefined once the number of sublayers is increased to obtain more accurate results.

The error caused by assuming multiple layer, each with a discrete stiffness can be remedied by assigning a continuous function for the stiffness as a function of depth, such that the stiffness modulus changes as a function of the coordinates of each material point inside the pavement. Therefore, in this dissertation a FGM-UMAT is used, such that the user has the flexibility to assign a function of the structural coordinate without the need to redefine the values of the stiffness modulus for each sub-layer. More accurate results can be obtained simply by redefining the FE mesh without the need to redefine the stiffness modulus of every single layer. Therefore, the accuracy of the gradient function can be defined by the user with the coarseness of the FE mesh because the UMAT is defined at the integration points in the mesh and the number of the integration points can be increased by using a finer mesh. A user defined material subroutine (UMAT) in Abaqus was developed to define the stiffness gradient with depth in the asphalt layer. The model has been developed for a general case which includes three dimensional stress, plane stress and plane strain cases. It can be used as a subroutine along with the various simulated field asphalt concrete models to define the aging, stiffness and Poisson's ratio changes with the thickness of the asphalt concrete layer.

Strain Profiles Calculation above the Crack Tip using FE-FGM Model

As previously discussed, a power function was used that fits well to the actual stiffness gradient profiles in the field-aged asphalt concrete layers. The previously developed FE simulation of the OT test was modified for the field specimens. The

thickness of the field specimens was 50 millimeters (Woo, et al.) rather than the 38 millimeters (1.5 inches) used in the laboratory specimens. The opening of the gap was decreased from 0.635 millimeters (0.025 inches) to 0.3175 millimeters (0.0125 inches) because aged field samples are more brittle than laboratory made specimens and therefore break more easily under larger displacements. Figure 39 schematically shows the OT test configuration for a field specimen.

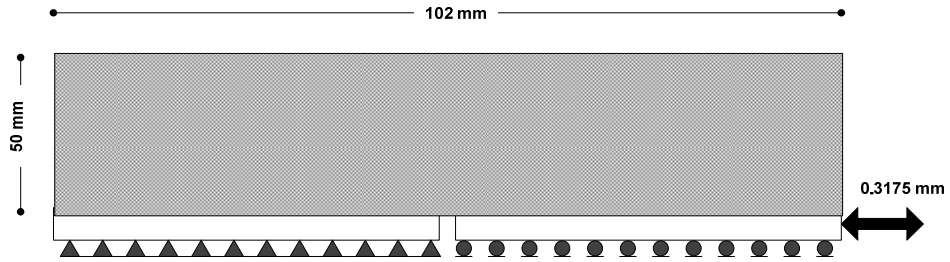

Figure 39.The OT test configurations of field specimens

The stiffness gradient function was plugged into the UMAT, and subsequently the OT simulation together with the subroutine was run via Texas A&M supercomputer facility to find the strain profiles above the tip of the crack for different crack lengths. Figure 40 shows the strain profiles above the crack for a specimen with n value of 4.9 and k value of 1.42 where n is the power of the stiffness gradient function and k is the ratio between the surface and the bottom moduli. The magnitude of the stiffness modulus for this specimen is 6728 MPa and 4736 MPa at the surface and bottom of the

layer, respectively. As shown in Figure 40, some parts of the layer thickness are in the compression, and when the crack enters this compressive zone, it will take more load cycles for the crack to grow through the thickness of the layer .This observation clearly explains the reason for the fact that counting the number of the load cycles to the failure is not a reliable method to compare AC mixtures.

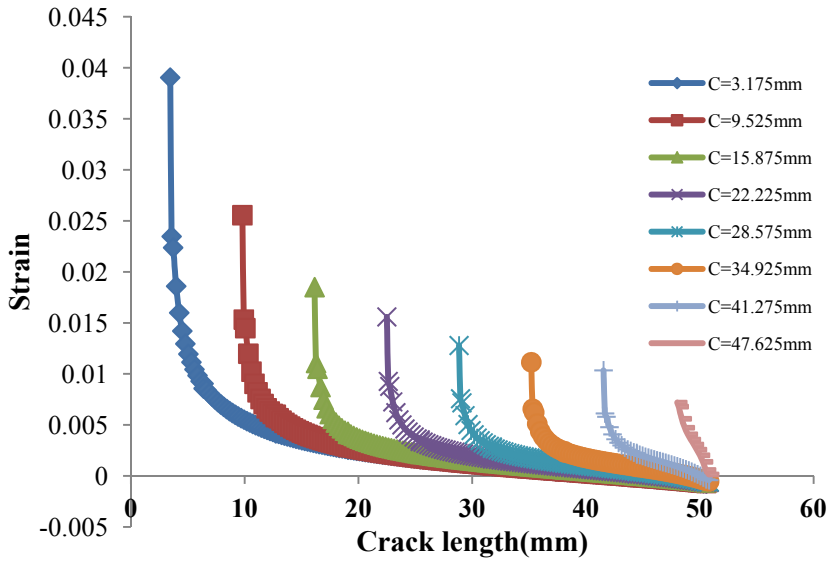

Figure 40.Strain profiles above the crack tip for different crack lengths in field specimens

Sensitivity Analysis via FE Model

Additionally, a sensitivity analysis was conducted for a specific crack length in a field specimen to study the effect of the stiffness gradient function shape on different

variables in the test. For this purpose, the model was run for a specimen with a crack length of 22.225 millimeters (0.875 inches) for different gradient curves by changing the n value but using a constant k value. The J-integral, stiffness profile, horizontal strain profile and the maximum principle stress contour are some of the outputs that were compared in this study.

As shown Figure 41 as the n value increases, more of the specimen is in compression. An n value equal to zero represents the uniform stiffness profile or laboratory condition and the higher n values show a greater stiffness gradient near the surface. The author's experience with field specimens shows that the n value usually increases with age. This simulation confirms that a larger portion of the specimen will be under compression in highly aged specimens; therefore, even with very small openings during the OT test the number of load cycles is not a reliable criterion to compare two specimens. Figure 42 shows the change in the maximum principal stress contour for different stiffness profiles.

Figure 43 shows that the J-integral at the tip of the crack decreases for the various stiffness profiles as the n value increases. The J-integral decreases as the stiffness gradient near the surface of the AC layer increases. This means that the available energy for the crack to grow during the OT test in the specimens with a sharper stiffness gradient near the surface is less than that for the less aged specimens. This graph also explains the variability of the OT test in highly aged specimen. As crack enters to the portions that are less aged, the crack growth rate decreases significantly.

As previously discussed the results of the stiffness gradient model are plugged into the FGM numerical model to find the strain profiles above the crack for various crack lengths in the aged field specimen. After that a replicate specimen is tested via OT and the data are analyzed using the fracture and healing module along with the outputs from the FE program. The FORTRAN code for the UMAT model is presented in appendix B.

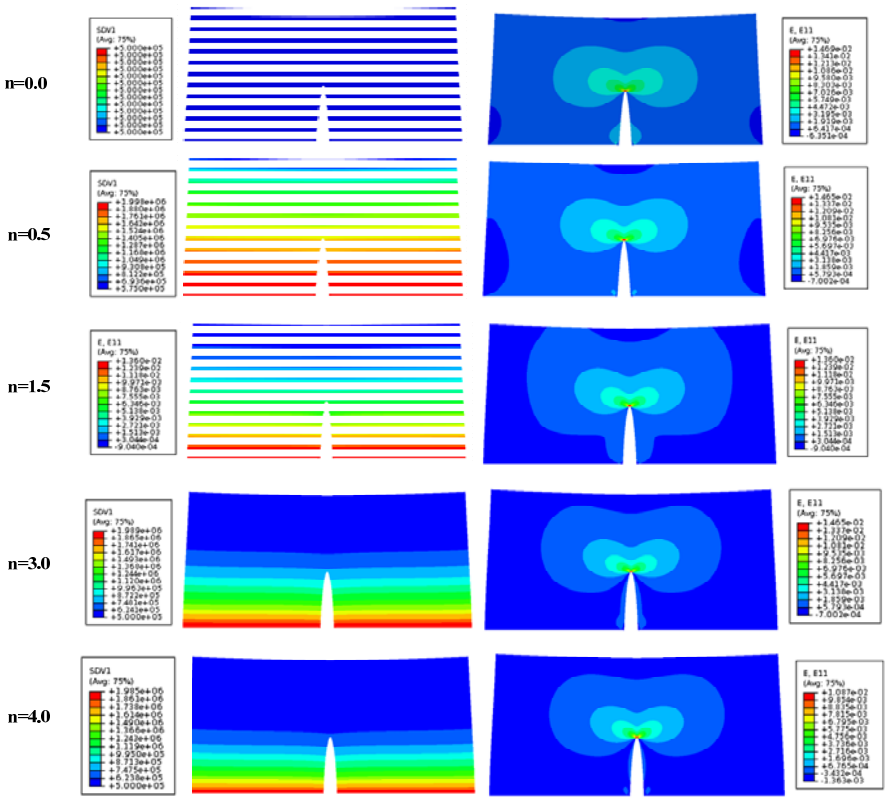

Figure 41.Modulus and horizontal strain contours for different stiffness profiles

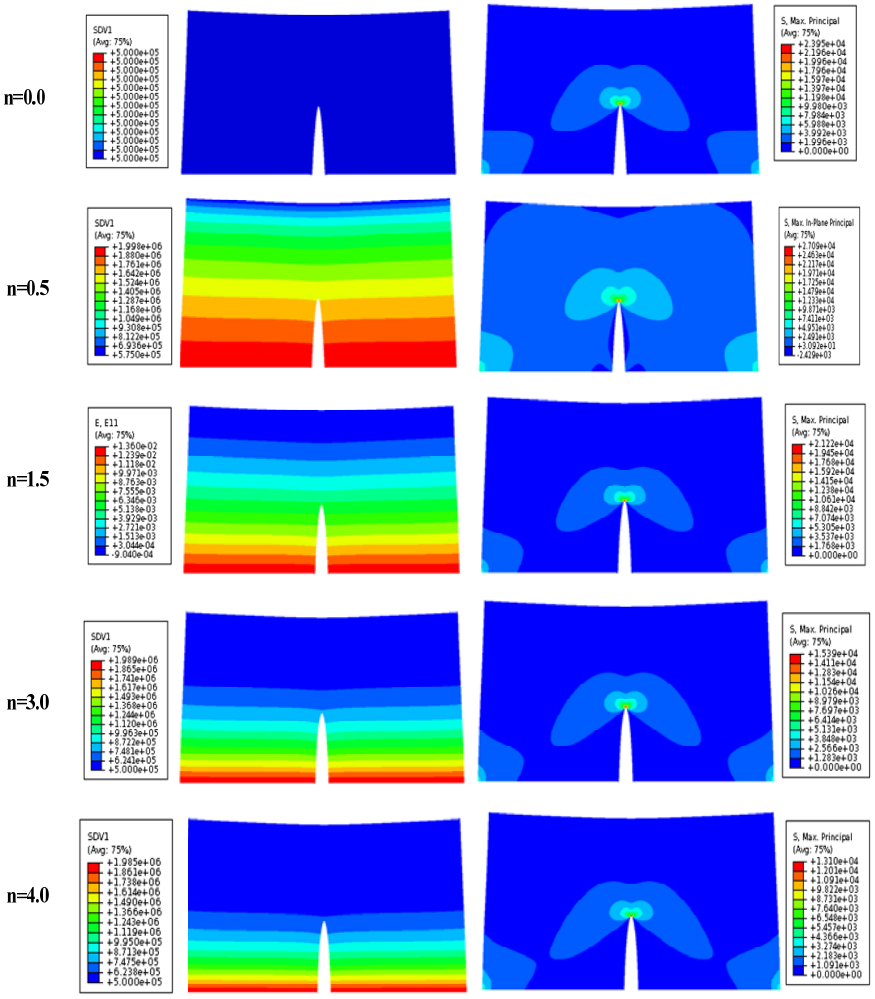

Figure 42.Modulus and maximum principal stress contours for different stiffness gradient profiles

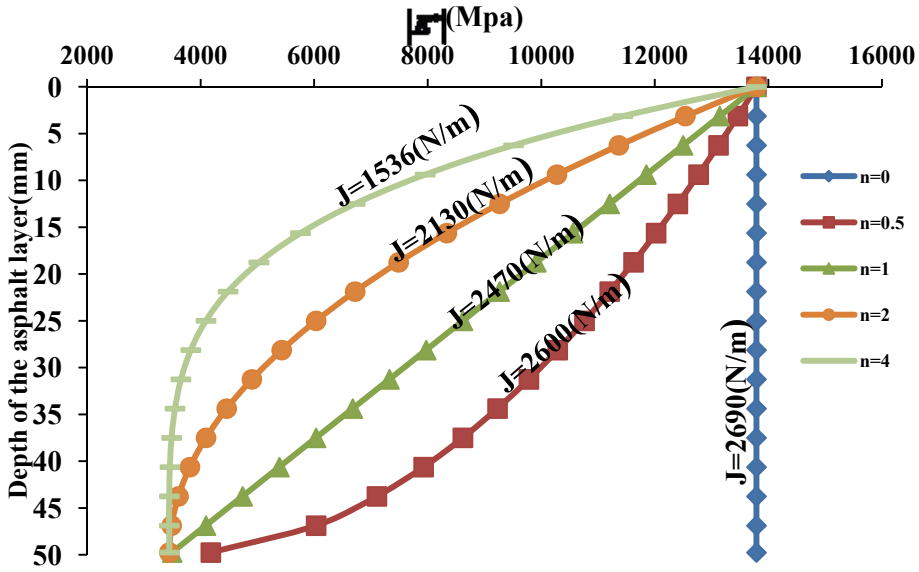

Figure 43.Magnitude of J-integral for an specimen with different stiffness profiles for crack length of 22.225 mm

Estimation of the Fracture and Healing Properties via OT test

The OT test was initially designed to test asphalt overlays on rigid pavements for the prediction of reflective cracking. The test apparatus consists of a stationary and a moving plate. A rectangular AC specimen is needed for this test similar to that used for the DT test. The specimen is glued onto the aluminum plates which are then fixed on the machine. The repeated displacement is applied to the specimen by moving one of the plates back and forth. The load and the displacement with time are recorded via an acquisition system. The machine has been used as a torture test to compare the performance of different asphalt mixtures; however, a high degree of variability has been reported by the users. The test consists of two steps; the first step is a nondestructive test

which is used to measure the undamaged properties such as m value and the relaxation modulus and the second step is the destructive test which is used to measure the fracture and healing properties of the AC. This method includes the calculation of the viscoelastic force in each cycle as a function of the area under strain profile above the crack tip .

By measuring the force in each cycle the area under the strain profile in the intact thickness above the crack is calculated; furthermore, the FE output gives the strain profiles for different crack lengths. Therefore, as the area under strain profile above the crack in each cycle is calculated, the corresponding crack length in each load cycle can be found. Equations 58 and 59 give the calculated viscoelastic force for each loading and unloading cycle.

$$\max.P_{LVE}(z=c)=\frac{E_1 b t^{1-m}}{(1-m)t_1}s(c) \qquad 0<t<t_1 \quad (58)$$

$$\max.P_{LVE}(z=c)=bs(c)\frac{E_1 t^{1-m}}{(1-m)t_1}-2bs(c)\frac{E_1(t-t_1)^{1-m}}{(1-m)t_1} \qquad t_1<t<2t_1 \quad (59)$$

where $\max.P_{LVE}(z=c)$ is the measured maximum viscoelastic force within the specified time interval, b is the width of specimen, and $s(c)$ is the area under the strain profile above the tip of the crack length .

Additionally, the pseudo displacement is calculated by Equation 60.

$$U_r(t)=\frac{P_{LVE}(t)}{k_r} \quad (60)$$

where $P_{LVE}(t)$ is the linear viscoelastic force and k_r is the reference stiffness which is the value of the maximum load in the first load cycle divided by the maximum opening. After the crack length in each load cycle is calculated, the viscoelastic force and pseudo displacement for each cycle are calculated. By graphing the pseudo displacement versus the measured force, a closed loop is obtained in which the area under the loop is the pseudo work for each cycle. The dissipated pseudo work has positive and negative portions in which the area under the tensile loading portion is related to the crack growth and the area under the compressive loading portion is related to the healing which occurs in each load cycle. The observations of test results show that a significant amount of healing occurs in each closing displacement cycles.

The change of the pseudo work is used to find the Paris's laws fracture and healing parameters.

A similar methodology to that for the laboratory compacted specimen is used for the field-aged asphalt concrete layers with few modifications. The strain profiles for the field aged asphalt concrete layers are estimated using the previously described FGM-FE model and a smaller displacement is applied to the field specimen because they are more brittle.

The output of the stiffness gradient model from the DT test gives the magnitude of the complex modulus at the feedback frequency which is 20 Hz in the machine that was used in the test. However, the modulus obtained from the OT test is measured at a different frequency; therefore, the Equation 61 is used to transfer the modulus to the desired frequency if it is needed in the calculations.

$$\left|E^*_{(\frac{1}{2t})}\right|(OT) = \left|E^*_{(\omega)}\right|(DT).\left(\frac{1}{2t\omega}\right)^m \tag{61}$$

where $\left|E^*_{(\frac{1}{2t})}\right|$ and $\left|E^*_{(\omega)}\right|$ are the magnitudes of the moduli in the OT test and DT tests, respectively. The m is the undamaged parameter which is obtained from the nondestructive part of the OT test, t is the loading time in the OT test and ω is the angular velocity of the DT machine.

Experiment

Materials

The cores used in this experiment were taken from roads in Arizona as a part of the Asphalt Research Consortium (ARC) project. Three identical cores were extracted from each section. Two replicates were tested in this study and the third replicate was tested for binder extraction purposes by another team. The road sections were built in 2001 and the binder PG 76-16 from West Texas blend was used in the AC mixture. The binder design percentage was 4.8%. Table 16 shows the geometry, the Rice and bulk specific gravity of the mixtures used in the test procedure. The AC layer was constructed in two construction lift.

Table 16.The general information about the field cores

Field Core	Year	Construction Lift	Specific Gravity	Rice	Thickness(mm)
AZ1-1A-3S	2001	Upper Lift	2.328	2.484	70.91
		Lower Lift	2.252	2.480	67.05
AZ1-1B-3S	2001	Upper Lift	2.347	2.486	64.16
		Lower Lift	2.237	2.489	65.00
AZ1-2A-3S	2001	Upper Lift	2.300	2.477	61.84
		Lower Lift	2.294	2.474	61.79
AZ1-2B-3S	2001	Upper Lift	2.283	2.487	57.49
		Lower Lift	2.305	2.491	63.11
AZ1-3A-3S	2001	Upper Lift	2.302	2.472	59.91
		Lower Lift	2.282	2.493	69.08
AZ1-3B-3S	2001	Upper Lift	2.279	2.479	54.96
		Lower Lift	2.279	2.499	74.61
AZ1-4A-3S	2001	Upper Lift	2.323	2.471	68.76
		Lower Lift	2.287	2.488	59.45
AZ1-4B-3S	2001	Upper Lift	2.326	2.496	67.69
		Lower Lift	2.278	2.495	68.96

First the cores are cut to the construction lifts then one replicate was X-rayed to find the air void distribution.

Sample Preparation for DT Test

One of the extracted replicates was cut to a rectangular specimen to be tested by applying the monotonically increasing load. The thickness of each lift was between 60 and 70 millimeters; therefore, a thickness of 50 millimeters was selected for the rectangular specimens. The specimen for this test must be cut and glued precisely because small misalignment in the endcaps results in errors. The test is a non-destructive test and the maximum allowable strain level in the LVDTs are limited to 100 microstrain. Figure 44 illustrates the process of the specimen preparation which includes

the cutting, gluing the endcaps and installing the LVDTs. The detailed specimen preparation has been described in a previously published paper(Koohi, et al., 2011).

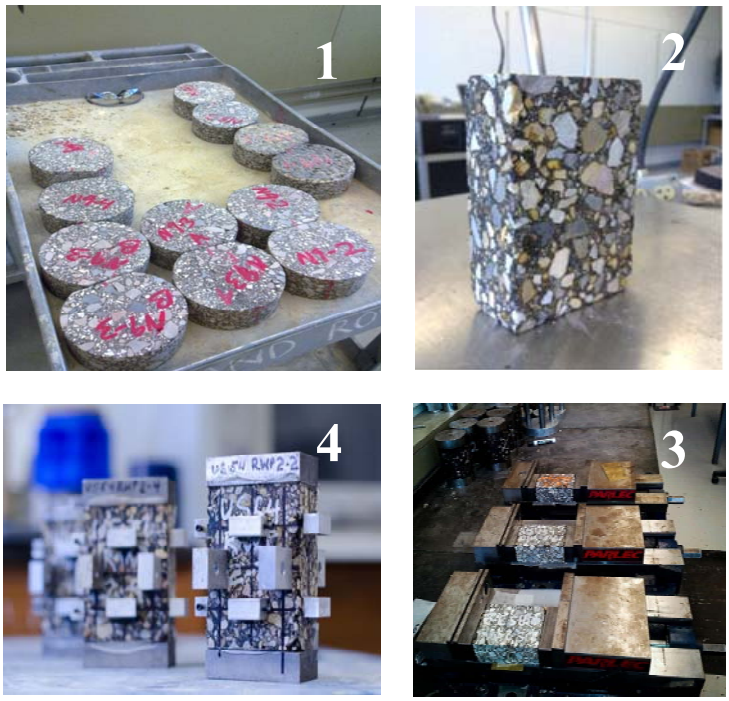

Figure 44.Sample preparation in DT test

Sample Preparation for OT Test

The sample preparation for the OT test is shown in Figure 45. Unlike the laboratory compacted specimens, the field specimens were very brittle and also thicker in size; therefore, the maximum displacement gap for the destructive part of the test was reduced to provide enough time for the crack to grow through the depth of the specimen.

The loading pattern consisted of 10 cycles of nondestructive displacements to get the undamaged properties and 200 cycles of the destructive displacements to measure the fracture properties. Figure 46 shows the loading pattern for the OT test in the field specimens. The nondestructive displacement was 0.05 millimeters (0.002 inches)and the displacement of the destructive test was 0.32 millimeters (0.0125 inches) .The surface of the asphalt layer was glued to the aluminum plates because the calculation of the fracture properties of the top down cracking was the purpose of this study.

Figure 45.Sample preparation for OT test

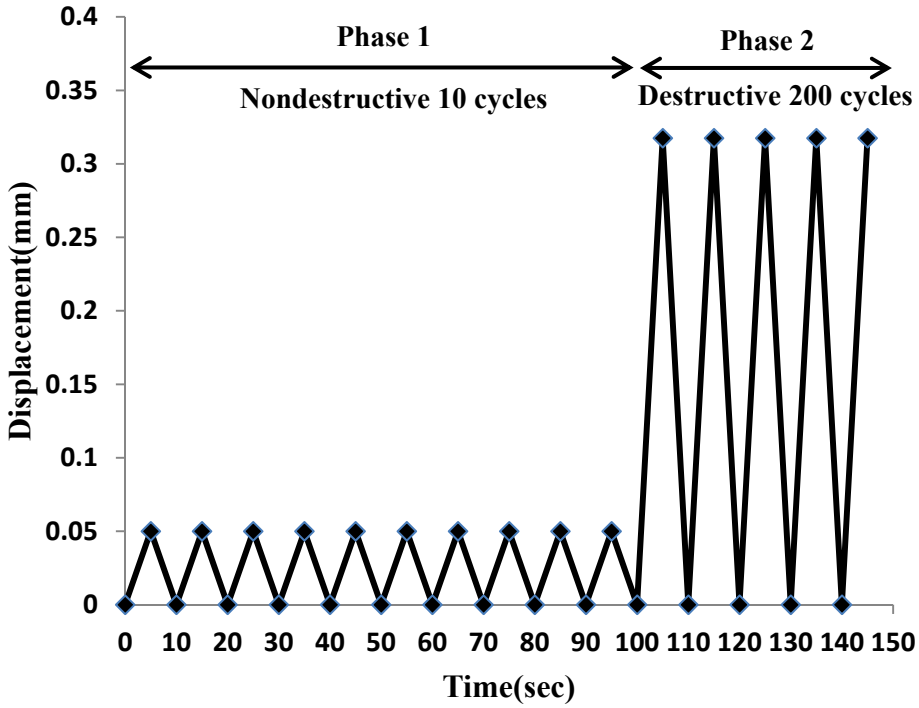

Figure 46.Loading pattern for field specimen in OT test

Results

Results for Stiffness Gradient Analysis

The outputs of the DT test were analyzed using the stiffness gradient calculation methodology. Table 17 shows the results for the stiffness gradient analysis. The magnitudes of the complex moduli for specimens were all in a reasonable range. The phase angles for all of the specimens were very small because the asphalt layer was very

aged and stiff. The n and k parameters were also complex numbers and their magnitudes and phase angles are shown in Table 17.

In the two of the specimens tested at 30ºC test the analysis was not completed, because the specimen was very soft and the test ended very fast; therefore, there was not enough measured data to complete the analysis.

Figure 47 shows the stiffness gradient of field aged specimen, AZ1-2A, at three different temperatures (10ºC, 20ºC and 30ºC) . The results show that, like other properties of the asphalt mixtures, the stiffness gradient curve is a function of loading frequency and temperature. The high n values indicate that the stiffness gradient is very high near the surface. The stiffness gradient profiles for the bottom lifts clearly show that the aging extends to the very deep levels of the asphalt layer. As the asphalt layer ages the k value decreases and the n value increases and the profile is relatively uniform in the deeper levels of a very aged specimen.

Table 17.Results of the stiffness gradient analysis for Arizona samples

Sample ID	Coring Location	Test Temperature	n	n Phase Angle	k	k Phase Angle	Surface Modulus(MPa)	Bottom Modulus(Psi)
AZ1-1A	Top Lift	20.00	4.57	-61.19	1.37	-6.71	4636	3386
AZ1-2A	Top Lift	20.00	4.14	-57.73	2.62	-46.70	5274	2009
AZ1-3A	Top Lift	20.00	4.57	-74.14	2.97	-51.28	7851	2640
AZ1-4A	Top Lift	20.00	4.29	-56.79	2.86	-44.58	5565	1943
AZ1-1A	Bottom Lift	20.00	1.71	-68.70	3.52	-73.32	4508	1281
AZ1-2A	Bottom Lift	20.00	3.69	56.46	1.45	17.19	3180	2185
AZ1-3A	Bottom Lift	20.00	4.95	83.51	1.67	-22.57	5097	3056
AZ1-4A	Bottom Lift	20.00	3.46	-61.73	1.91	-58.73	7736	4057
AZ1-1A	Top Lift	10.00	4.90	64.48	1.42	-1.61	6729	4737
AZ1-2A	Top Lift	10.00	3.18	-69.99	1.55	-70.74	6930	4481
AZ1-3A	Top Lift	10.00	4.39	-68.93	3.24	-55.18	13114	4047
AZ1-4A	Top Lift	10.00	3.62	-69.96	1.99	-66.27	8597	4324
AZ1-1A	Bottom Lift	10.00	3.51	-73.63	1.82	-71.76	7095	3895
AZ1-2A	Bottom Lift	10.00	4.11	-48.95	2.91	-40.82	11449	3938
AZ1-3A	Bottom Lift	10.00	2.31	-3.98	1.42	-6.87	4861	3423
AZ1-4A	Bottom Lift	10.00	5.19	68.53	1.36	-4.21	9620	7054
AZ1-1A	Top Lift	30.00	0.00	0.00	0.00	0.00	0	0
AZ1-2A	Top Lift	30.00	3.49	-65.42	1.83	-61.19	2232	1222
AZ1-3A	Top Lift	30.00	5.06	66.83	1.45	-1.97	2980	2054
AZ1-4A	Top Lift	30.00	4.13	-57.77	2.62	-47.17	3144	1201
AZ1-1A	Bottom Lift	30.00	3.36	-77.29	1.56	-77.39	2049	1315
AZ1-2A	Bottom Lift	30.00	3.24	-62.80	1.42	-57.09	1919	1354
AZ1-3A	Bottom Lift	30.00	0.00	0.00	0.00	0.00	0	0
AZ1-4A	Bottom Lift	30.00	4.07	-56.74	2.60	-46.87	3127	1201

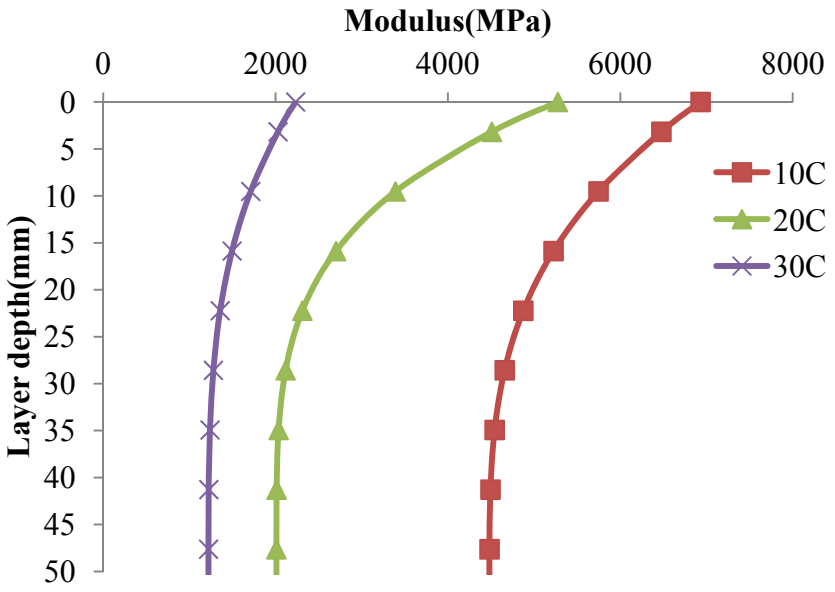

Figure 47.Stiffness gradient of field specimen AZ1-2A in three different temperatures

As expected, the average of the n values, which shows the sharpness of the stiffness gradient curve near the surface was higher in the top lifts compared to the bottom lifts. As shown in Figure 48, the top lift in the specimen, AZ1-3A, has a sharper gradient because of the oxygen availability and the solar radiation. Both n and k values are lower in the bottom lifts and bottom lift profiles are more uniform.

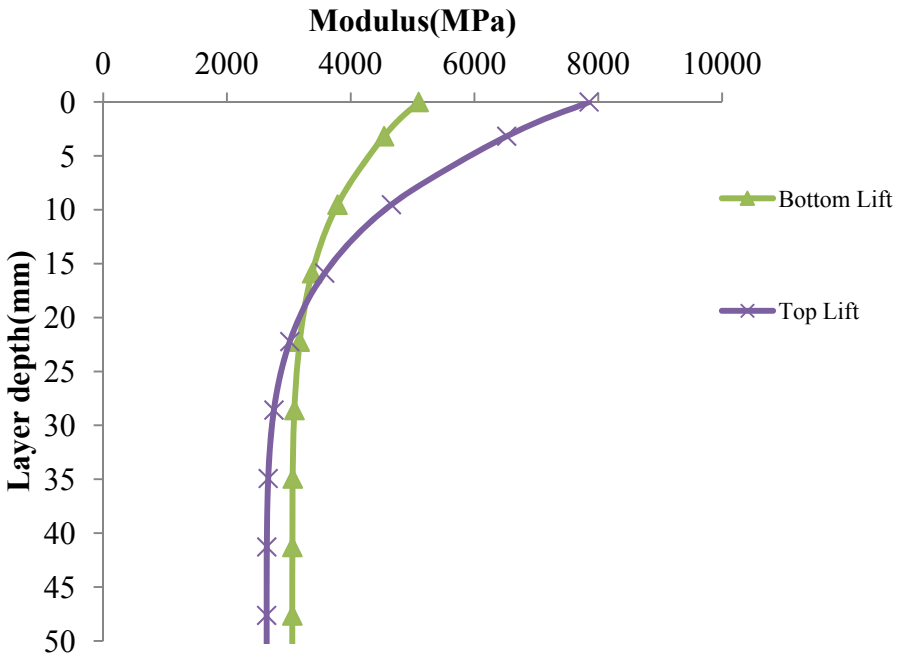

Figure 48.Stiffness gradient profiles of the top lift and bottom lift of the field asphalt specimen AZ1-3A

Strain Profiles above the Crack

The results of the stiffness gradient analysis were used in the FGM numerical model to calculate the area under the strain profiles above the tip of the crack. It should be noted that the modulus calculated in the DT test was at the frequency of 20Hz which was different from the test frequency of the OT test; therefore, Equation 61 was used to calculate the modulus value in the desired frequency .

Figure 49 shows the area under the strain profiles above the crack for different crack lengths of an aged field specimen. This area decreases as the crack grows and a

logarithmic function was found to be the best fit for this change. This graph is used to find the actual crack growth in the OT test. As shown in Figure 49 there is a very sharp decrease in the area under the strain profiles as the crack grows. This observation also is confirmed with the change of the J-integral versus crack length.

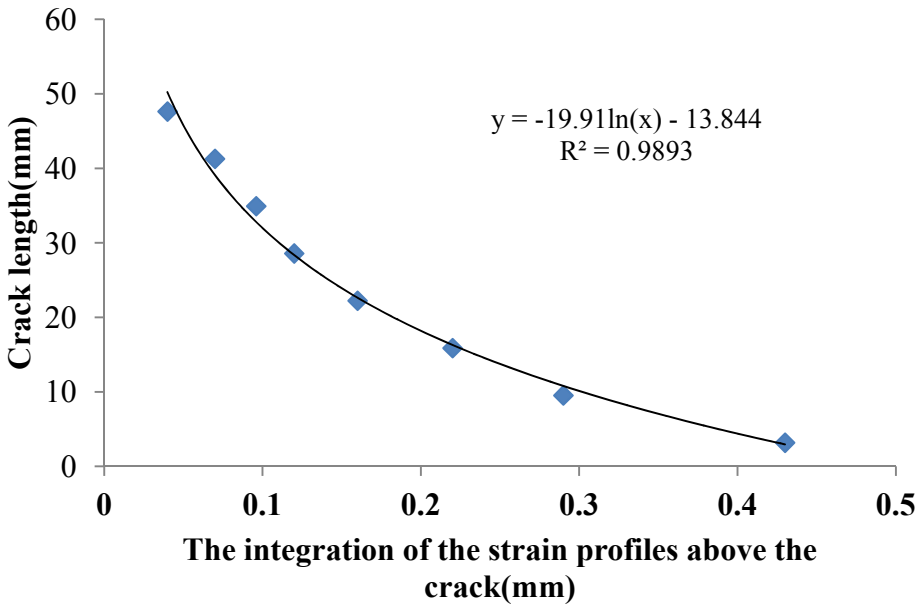

Figure 49. Integration of the strain profiles above the crack for various crack lengths

Results for the Fracture and Healing Properties

The OT test was conducted in two steps (nondestructive and destructive) to find the undamaged and damaged properties of the field specimens. Table 18 shows the

undamaged and damaged properties of the field specimen. The results for specimen AZ1-4 did not converged during the analysis. All of the results were calculated in 20ºC because the OT test is conducted at 20ºC. The coefficients A and n are the modified Paris's law's fracture parameters and B and m are the modified Paris's law's healing parameters. Equations 62 and 63 show the modified Paris's law for the fracture and the healing.

$$\frac{dC(N)}{d(N)} = A\left[\frac{W_{Rt}(N)}{c.s.a}\right]^{n} \tag{62}$$

$$\frac{dC(N)}{d(N)} = B\left[\frac{W_{Rc}(N)}{c.s.a}\right]^{m} \tag{63}$$

where $c.s.a = 2bC(N)$, $W_{Rt}(N)$ and $W_{Rc}(N)$ are the function of the tensile and compressive Pseudo strain work expressed as a function of load repetitions, respectively.

The larger values of B indicate the large amount of healing which occurs in each closing load cycle.

Table 18.The viscoelastic properties of aged asphalt mixtures from Arizona

Sample ID	Lift	E1 (MPa)	A	n	B	m	Crack Growth Function(mm)
AZ1-1	Top	825	0.025	2.32	0.92	6.64	$C = 11.92N^{0.1698}$
AZ1-1	Bottom	987	0.035	1.55	0.19	4.6	$C = 9.0297N^{0.2909}$
AZ1-2	Top	687	0.008	2.54	0.0057	9.29	$C = 19.2963N^{0.1736}$
AZ1-2	Bottom	778	0.016	2.46	0.0045	8.6	$C = 24.4297N^{0.183}$
AZ1-3	Top	911	0.026	1.87	0.08	3.44	$C = 9.3218N^{0.2536}$
AZ1-3	Bottom	671	0.027	1.89	0.048	4.19	$C = 15.5067N^{0.2037}$
AZ1-4	Top	776	N/A	N/A	N/A	N/A	$C = 39.2988N^{0.0609}$
AZ1-4	Bottom	418	N/A	N/A	N/A	N/A	$C = 39.7281N^{0.0706}$

Figure 50 shows the crack growth versus the displacement repetitions in the OT test of the field-aged specimen. The curves are similar to the crack growth curves for a laboratory compacted specimen but unlike the laboratory compacted specimen, there is a significant crack growth in the first few load cycles because the asphalt concrete near the surface is highly stiff and brittle. As shown in Figure 50 the crack growth rate slows down very rapidly as the crack enters the compressive zone, this especially can be seen in the mixtures with higher n values because a larger portion of the specimen will be in compression in these specimens.

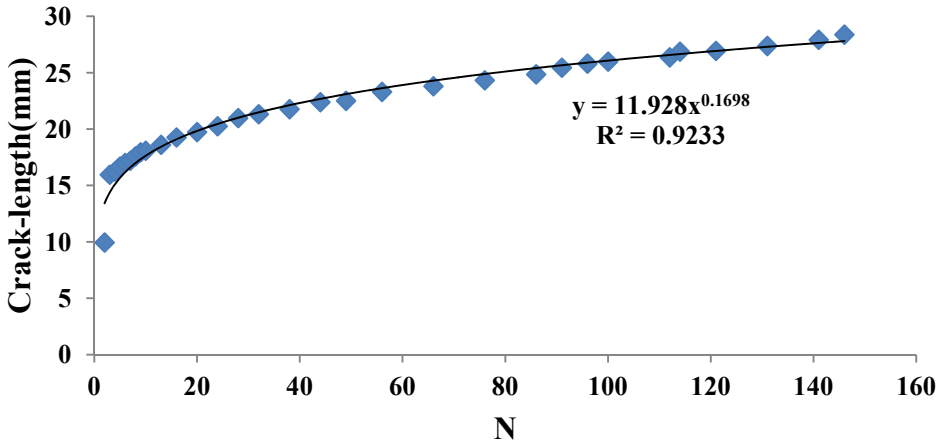

Figure 50.Actual crack growth versus load repetitions in an Arizona specimen

Concluding Remarks

The characterization of the viscoelastic properties of the field asphalt concrete layers is more challenging than that of the laboratory compacted specimen because of the aging of the binder and other enviromental factors affecting the asphalt layer in the field. The methodology described in this dissertation is a fundamental and mechanistic approach to find viscoelastic properties of field specimens such as modulus, fracture and healing properties using quick and efficient tests. The methodology consists of different modules. The methodology has been successfully tested and verified using actual aged AC layers.

The FGM numerical subroutine which was developed and used in this procedure can be used independently in different test simulations of aged asphalt layers. The results

for the stiffness gradient, fracture and healing properties of the field aged asphalt mixtures in tension were characterized using DT and OT test by using analytical models together with FE simulations.

The evaluation of the field mixture viscoelastic properties together with the aged binder properties will be the next step in this study. The combination of the mixture viscoelastic properties of the asphalt mixture with the aged binder properties can explain most of the complexities involved in the characterization of the field AC performance models.

CHAPTER VI

CONCLUSION

The viscoelastic properties of field-aged specimens are much different from those of the laboratory compacted specimens. This dissertation followed a fundamental approach based on linear viscoelasticity and fracture mechanics to find the damaged and undamaged viscoelastic properties of both laboratory and field asphalt concrete mixtures. The tasks performed in this dissertation can be summarized as:

- Calculation of the undamaged complex modulus and its profile with depth using the DT test
- Estimation of the crack growth versus load cycles during the OT test for both laboratory and field specimens
- Development of a novel methodology to find both fracture and healing properties of field and laboratory compacted asphalt concrete mixtures
- Finite Element duplication of DT and OT tests to improve the accuracy of these test procedures
- Development of a FGM-UMAT subroutine to be used in different FE models of aged asphalt concrete

Unlike the laboratory specimen the stiffness gradient of field aged specimens are neither uniform nor constant with time and depth because of the nonuniform air void distribution and binder oxidative aging. The method developed in this study is able to successfully calculate the stiffness profile of the field aged asphalt mixtures using a

quick DT test. This test method has several advantages: it is nondestructive, accurate, quick and easy. The same specimen can be used for other tests such as binder extraction after the DT test since the test is nondestructive and a complete test procedure can be done in two days. Test of the field specimen using the direct tension test is more challenging than laboratory specimens because of the stiffness gradient and different thicknesses; therefore, several modifications were applied to the laboratory DT test protocol. The rectangular field specimen under monotonically increasing loads, tend to oscillate because the load is applied to the geometric centroid which is different from stiffness centroid in the field specimens due to the stiffness gradient and this eccentricity applies a moment on the specimen. This fact is also confirmed by numerical duplication of both laboratory and field specimens.

The methodology developed in this dissertation, calculates the stiffness profile of the field aged specimen using the frequencies and amplitudes of oscillations. The methodology uses a combination of linear viscoelastic theory and signal processing methods to find the amplitudes of oscillations. Subsequently strain outputs and oscillation amplitudes are used to find the gradient of the complex modulus of the aged asphalt layers in field.

The methodology was successfully used to analyze several field specimen namely several specimen from the US-277 highway in Texas both from the shoulder and wheel path throughout a four year period. In addition 11 year old field cores from Arizona were tested and analyzed using this methodology. The results indicate that the aging is more severe near the surface and it extends to the deeper levels in the asphalt

layer during the performance years. In contrast to the observations which indicate that the aging is limited to the near surface ,this study indicates that aging extends to much deeper levels. The student's t-statistics results show that the traffic does not have a significant effect on the aging and stiffness gradient profile of field layers.

The results of the stiffness gradient analysis can be used in different research and industry problems such as:

- Tracking the effect of aging on the stiffness profile of the asphalt layers in the field
- Improving the performance models using fundamental properties of the field-aged mixtures
- Studying the effect of different factors such as traffic, environmental conditions and construction methods on the stiffness profile and aging
- Using the continuous stiffness profile in FE models
- Comparing the stiffness profile of the aged mixture with the rheological tests of the extracted binder
- Correct and modify existing models of aging asphalt mixtures such as the Global Aging System (GAS).

Fracture and crack propagation is another important issue in pavement engineering. Any comprehensive test protocol must include both undamaged and damaged properties of the asphalt mixture. The OT test was selected to characterize the damaged properties of the mixture in this study. The OT is a test apparatus which was initially designed to simulate the reflective cracking of the asphalt overlays on the rigid

concrete slabs. The apparatus has been used by some states and consultants as a torture test to evaluate the fatigue resistance of the asphalt layers by simply counting the load cycles through to failure but substantial variability has been reported by these users.

The methodology designed in this study can successfully predict the crack growth versus load repetitions using fracture mechanics principles and numerical simulation of the test. FE duplication of the test method clearly shows that a compressive zone develops during the loading and unloading cycles in the specimen, and as crack enters into these compressive zones, the crack growth rate drops significantly. These compressive zones are the main reason for the variability of the test results.

The suggested test methodology and analysis technique are faster, less costly and more repeatable than previous methods of using the Overlay Tester. Additionally, this test can be used together with DT test to characterize the damaged properties of field specimens.

Several laboratory and field specimen have been analyzed using this method and the variability of the results were much less than the currently used load cycle counting method. It should be noted that the test method of field specimen is different from that of the laboratory compacted specimen because the field specimens are aged and brittle ;therefore the test specimens break during first few displacement repetitions . A smaller opening displacement has been used for field specimen testing to obtain enough load data for the analysis.

This methodology can be successfully used to study the crack propagation mechanisms in the top down , bottom up and reflective cracking in asphalt layers. In this

study the surface of the asphalt layer was glued to the testing plates to study the top down cracking .The bottom of the layer can be glued to the plates to study the bottom up cracks. Fracture mechanics principles together with Pseudo dissipated energy principles were used to find the fracture and healing properties of both the laboratory and field compacted specimens. Both the test observations and FE results indicate that substantial amount of healing occurs during each closing load cycle. Several field-aged specimen and laboratory compacted specimens have been tested and analyzed using this methodology.

The results can be used to compare the fracture and healing properties of different laboratory and field mixtures. It is also an efficient method to track the change in the fracture and healing properties of the field specimens with oxidative aging.

The FE simulation of the tests which were used in this study, was a great supportive source in understanding the response of the field specimen. The FE simulation of the DT test confirms that the origin of the oscillations in the strain outputs, was the stiffness gradient. This fact also was shown by testing the laboratory compacted specimens. The FE model of the OT test outputs were used to get the strain profiles above the crack tip. Additionally, the model describes the response of both field and laboratory specimens under repeated load. These models were used to improve the test methods to decrease the variability of the results.

As a part of this research a FGM-UMAT user-defined material subroutine has been developed to be used to model the stiffness gradient of the field aged specimen

.The stiffness gradient of the field layers is a perfect example of a functionally graded material.

The sensitivity analysis of the FE model shows that, as the asphalt layer ages the area of the compressive zone during the OT test of a field specimen increases. Therefore the crack growth rate significantly decreases as the crack enters to this compressive zone. Therefore counting the load cycles to reach failure results in a very high variability.

By the use of this UMAT any stiffness profile or even the gradient of the Poisson's ratio can be implemented as a continuous function in any FE model. Different responses of the aged asphalt under various loading scenarios and in different test methods can be monitored using this UMAT.

In the next step, the extracted binder data for same field specimens will be compared with the stiffness gradient results of the same cores to find the possible correlations between the binder rheology and the mixture stiffness. This will show the effect of other mixture components such as aggregate and air void distribution on the aging process .As previously mentioned the same specimen after the direct tension test can be used for binder extraction since the direct tension test is a nondestructive test.

In addition a previously developed self consistent micro mechanical model(Luo and Lytton, 2010) can be used to back calculate the binder and aggregate properties using the measured mixtures properties such as stiffness gradient. This model can be used as a powerful tool in asphalt mixture design. The desired stiffness and its changes

during the performance period will be inserted into the model and the proper aggregate and binder combination will be selected from available categories.

REFERENCES

Abd El Halim, A. E. H. O., and Haas, R. (1994). "Effect of field compaction method on fatigue life of asphalt pavements." *Transportation Research Record*(1469), 43-49.

Abu Al-Rub, R. K., Darabi, M. K., Little, D. N., and Masad, E. A. (2010). "A micro-damage healing model that improves prediction of fatigue life in asphalt mixes." *International Journal of Engineering Science*, 48(Copyright 2011, The Institution of Engineering and Technology), 966-990.

Akisetty, C., Xiao, F., Gandhi, T., and Amirkhanian, S. (2011). "Estimating correlations between rheological and engineering properties of rubberized asphalt concrete mixtures containing warm mix asphalt additive." *Construction and Building Materials*, 25(2), 950-956.

Anderson, D. A., Bahia, H. U., and Dongre, R. "Rheological properties of mineral filler-asphalt mastics and its importance to pavement performance." *Proc., Symposium on Effects of Aggregates and Mineral Fillers on Asphalt Mixture Performance, December 10, 1991 - December 10, 1991*, Publ by ASTM, 131-153.

Anderson, R. M. "Using superpave gyratory compaction properties to estimate the rutting potential of asphalt mixtures." *Proc., Asphalt Paving Technology 2002, March 18, 2002 - March 20, 2002*, Association of Asphalt Paving Technologist, 725-738.

Antes, P. W., Van Dommelen, A. E., Houben, L. J. M., Molenaar, A. A. A., and Parajuli, U. "Stress dependent behaviour of asphalt mixtures at high temperatures." *Proc., Asphalt Paving Technology 2003, March 10, 2003 - March 12, 2003*, Association of Asphalt Paving Technologist, 173-195.

Aragao, F. T. S., and Kim, Y.-R. "Modeling fracture and failure of heterogeneous and inelastic asphaltic materials using the cohesive zone concept and the finite element method." *Proc., GeoFlorida 2010: Advances in Analysis, Modeling and Design Conference, February 20, 2010 - February 24, 2010*, American Society of Civil Engineers (ASCE), 2662-2671.

Aschenbrener, T. (1995). "Evaluation of hamburg wheel-tracking device to predict moisture damage in hot-mix asphalt." *Transportation Research Record*(1492), 193-201.

Atzori, B., Lazzarin, P., and Meneghetti, G. (2008). "Fatigue strength assessment of welded joints: From the integration of paris' law to a synthesis based on the notch stress

intensity factors of the uncracked geometries." *Engineering Fracture Mechanics*, 75(Compendex), 364-378.

Bari, J., and Witczak, M. (2007). "New predictive models for viscosity and complex shear modulus of asphalt binders: For use with mechanistic-empirical pavement design guide." *Transportation Research Record: Journal of the Transportation Research Board*, 2001(-1), 9-19.

Bari, J., Witczak, M. W., You, Z., Solamanian, M., Huang, B., Mohseni, A., Dukatz, E., Chehab, G., Williams, C., and Christiansen, D. "Development of a new revised version of the witczak e predictive model for hot mix asphalt mixtures." *Proc., Association of Asphalt Paving Technologists -Proceedings of the Technical Sessions 2006 Annual Meeting, March 27, 2006 - March 29, 2006*, Association of Asphalt Paving Technologist, 381-424.

Bayat, A., and Knight, M. (2010). "Investigation of hot-mix asphalt dynamic modulus by means of field-measured pavement response." *Transportation Research Record*(2154), 138-145.

Beainy, F., Commuri, S., and Zaman, M. "Asphalt compaction quality control using artificial neural network." *Proc., 2010 49th IEEE Conference on Decision and Control (CDC 2010), 15-17 Dec. 2010*, IEEE, 4643-4648.

Bhattacharjee, S., Swamy, A., and Daniel, J. (2009). "Application of elastic-viscoelastic correspondence principle to determine fatigue endurance limit of hot-mix asphalt." *Transportation Research Record: Journal of the Transportation Research Board*, 2126, 12-18.

Bilir, O. G. (1990). "Relationship between the parameters c and n of paris' law for fatigue crack growth in a sae 1010 steel." *Engineering Fracture Mechanics*, 36(Compendex), 361-364.

Braham, A., Zofka, A., Li, X., and Ni, F. (2012). "Exploring the reduction of laboratory testing for the cohesive zone model for asphalt concrete." *International Journal of Pavement Engineering*, 13(4), 350-359.

Brandes, H. G., and Hirata, J. G. (2009). "An automated image analysis procedure to evaluate compacted asphalt sections." *International Journal of Pavement Engineering*, 10(2), 87-100.

Brandes, H. G., and Robinson, C. E. (2006). "Correlation of aggregate test parameters to hot mix asphalt pavement performance in hawaii." *Journal of Transportation Engineering*, 132(1), 86-95.

Brown, E. N., Sottos, N. R., and White, S. R. (2002). "Fracture testing of a self-healing polymer composite." *Experimental Mechanics*, 42(Copyright 2003, IEE), 372-379.

Buchanan, M. S., and Smith, B. J. (2005). "Performance evaluation of hot-mix asphalt using rotary loaded-wheel testing." National Research Council, 157-164.

Burr, B. L., Glover, C. J., Davison, R. R., and Bullin, J. A. (1993). "New apparatus and procedure for the extraction and recovery of asphalt binder from pavement mixtures." 20-29.

Cao, P., Feng, D.-c., Ma, H.-y., and Zuo, W.-x. (2011). "Numerical test of crack propagation path in asphalt beam using coupled extended finite element with field variable method." *Advanced Materials Research*, 250-253, 2754-2759.

Chatti, K., and Kim, T. (1999). "Effect of frequency-dependent asphalt concrete layer moduli on pavement response." *ASTM Special Technical Publication*(1375), 365-382.

Chatti, K., Mahoney, J. P., Monismith, C. L., and Moran, T. "Field response and dynamic modeling of an asphalt concrete pavement section under moving heavy trucks." *Proc., Proceedings of the 1995 4th International Symposium on Heavy Vehicle Weights and Dimensions, June 25, 1995 - June 29, 1995*, Int Forum Road Transp Technol, 189-200.

Chowdary, V., and Krishnan, J. M. "Characterization of healing in sand asphalt mixtures using a thermomechanical framework." *Proc., 2006 Airfield and Highway Pavement Specialty Conference, April 30, 2006 - May 3, 2006*, American Society of Civil Engineers, 467-478.

Christensen Jr, D. W., Bonaquist, R., Masad, E., Rowe, G., Brown, S., Chehab, G., and Radovsky, B. "Practical application of continuum damage theory to fatigue phenomena in asphalt concrete mixtures." *Proc., 2005 Meeting of the Association of Asphalt Paving Technologists, March 7, 2005 - March 9, 2005*, Association of Asphalt Paving Technologist, 963-1001.

Christensen Jr, D. W., Pellinen, T., and Bonaquist, R. F. "Hirsch model for estimating the modulus of asphalt concrete." *Proc., Asphalt Paving Technology 2003, March 10, 2003 - March 12, 2003*, Association of Asphalt Paving Technologist, 97-121.

Chulseung, K., and Roque, R. (2010). "Characterization of the tensile properties of open graded friction course mixtures based on direct and indirect tension tests." *Journal of Testing and Evaluation*, 38(4), JTE102687 (102612 pp.).

Cleveland, G., Lytton, R., and Button, J. (2003). "Using pseudostrain damage theory to characterize reinforcing benefits of geosynthetic materials in asphalt concrete overlays." *Transportation Research Record: Journal of the Transportation Research Board*, 1849(-1), 202-211.

Cleveland, G. S., Button, J. W., and Lytton, R. L. (2002). "Geosynthetics in flexible and rigid pavements overlay systems to reduce reflection cracking." Texas Transportation Institute, 298 p.

Daniel, J. S., and Kim, Y. R. (1998). "Relationships among rate-dependent stiffnesses of asphalt concrete using laboratory and field test methods." *Transportation Research Record*(1630), 3-9.

Darabi, M. K., Abu Al-Rub, R. K., Masad, E. A., Chien-Wei, H., and Little, D. N. (2011). "A thermo-viscoelastic-viscoplastic-viscodamage constitutive model for asphaltic materials." *International Journal of Solids and Structures*, 48(Copyright 2010, The Institution of Engineering and Technology), 191-207.

Dave, E. V., Buttlar, W. G., Paulino, G. H., and Hilton, H. H. "Graded viscoelastic approach for modeling asphalt concrete pavements." *Proc., Multiscale and Functionally Graded Materials 2006: (M&FGM 2006), 15-18 Oct. 2006*, AIP, 736-741.

Delaporte, B., Di Benedetto, H., Chaverot, P., and Gauthier, G. "Linear viscoelastic properties of bituminous materials: From binders to mastics." *Proc., Asphalt Paving Technology 2007 AAPT, March 11, 2007 - March 14, 2007*, Association of Asphalt Paving Technologist, 455-494.

Doh, Y. S., Amirkhanian, S. N., Thodesen, C., Bridges, W., and Kim, K. W. (2010). "Evaluation of statistical validity of some asphalt binder grade systems." *Journal of Testing and Evaluation*, 38(6), JTE102389 (102387 pp.).

Dong, Z., Xiaoming, H., and Yongli, Z. (2011). "Evaluation of the fracture resistance of asphalt mixtures based on bilinear cohesive zone model." *Journal of Testing and Evaluation*, 39(6), JTE103626 (103625 pp.).

Dongre, R., Myers, L., D'Angelo, J., Paugh, C., Gudimettla, J., Christensen, D., Heitzman, M., Page, G., Dukatz, E., and King, G. "Field evaluation of witczak and

hirsch models for predicting dynamic modulus of hot-mix asphalt." *Proc., 2005 Meeting of the Association of Asphalt Paving Technologists, March 7, 2005 - March 9, 2005*, Association of Asphalt Paving Technologist, 381-442.

Epps, J. A., and Monismith, C. L. (1970). "Infuence of mixture variables on the direct tensile properties of asphalt concrete." V 39, 207-241.

Fang, X. Q., Hu, C., and Huang, W. H. (2007). "Determination of dynamic effective properties in functionally graded materials." *Acta Mechanica*, 192(1-4), 49-63.

Farrar, J. M., Harnsberger, P. M., and Kenneth, P. T. "Evaluation of oxidation in asphalt pavement test sections after four years of service." *International Conference on Perpetual Pavement*,2006, 1-17.

Feipeng, X., Amirkhanian, S. N., and Junan, S. (2009). "Effects of various long-term aging procedures on the rheological properties of laboratory prepared rubberized asphalt binders." *Journal of Testing and Evaluation*, 37(4), 329-336.

Feng, Z., Yu, J., Zhang, H., and Kuang, D. "Preparation and properties of ageing resistant asphalt binder with various anti-ageing additives." *Proc., 2011 International Conference on Green Building, Materials and Civil Engineering, GBMCE 2011, August 22, 2011 - August 23, 2011*, Trans Tech Publications, 1062-1067.

Fonseca, O. A., and Witczak, M. W. "Prediction methodology for the dynamic modulus of in-place aged asphalt mixtures." *Proc., Proceedings of the 1996 Conference of the Association of Asphalt Paving Technologies: Asphalt Paving Technology, March 18, 1996 - March 20, 1996*, Assoc of Asphalt Paving Technologists, 532-572.

Germann, F. P., and Lytton, R. L. (1979). "Methodology for predicting reflection cracking life of asphalt concrete overlays.".

Glover, C. J., Davison, R. R., Ghoreishi, S. M., Jemison, H. B., and Bullin, J. A. (1989). "Evaluation of oven simulation of hot-mix aging by an ft-ir pellet procedure and other methods." *Transportation Research Record*(1228), 177-182.

Grebenschikov, S., and Prozzi, J. (2011). "Enhancing mechanistic-empirical pavement design guide rutting-performance predictions with hamburg wheel-tracking results." *Transportation Research Record*(2226), 111-118.

Hadley, W. O., Hudson, W. R., and Kennedy, T. W. (1970). "Correlation of indirect tensile test results with stability and cohesiometer values for asphalt-treated materials." V 39.

Hanson, D., King, G., Buncher, M., Duval, J., Blankenship, P., and Anderson, M. (2009). "Techniques for prevention and remediation of non-load related distresses on hma airport pavements(phase 1) ", 1-123.

Hanzik, V., and Luxemburk, F. (1978). "Properties of mastic asphalt at the continuous loading die eigenschaften von gussasphalt bei dauerbelastung." *Bitumen*, 40(1), 9-13.
Harmelink, D., Shuler, S., and Aschenbrener, T. (2008). "Top-down cracking in asphalt pavements: Causes, effects, and cures." *Journal of Transportation Engineering*, 134(1), 1-6.

Harvey, J., and Monismith, C. L. (1993). "Effects of laboratory asphalt concrete specimen preparation variables on fatigue and permanent deformation test results using strategic highway research program a-003a proposed testing equipment." 38-48.

Hintz, C., Velasquez, R., Li, Z., and Bahia, H. "Effect of oxidative aging on binder fatigue performance." *Proc., Asphalt Paving Technology 2011, AAPT, March 27, 2011 - March 30, 2011*, Association of Asphalt Paving Technologist, 527-545.

Huang, G., Wang, Y., and Yu, S. (2005). "A new multilayered model for in-plane fracture analysis of functionally graded materials (fgms)." *Acta Mechanica Sinica*, 37(1), 1-8.

Huang, S.-C., and Grimes, W. (2010). "Influence of aging temperature on rheological and chemical properties of asphalt binders." *Transportation Research Record*(Compendex), 39-48.

Huang, S.-C., and Grimes, W. (2010). "Influence of aging temperature on rheological and chemical properties of asphalt binders." *Transportation Research Record*(2179), 39-48.

Huang, S.-C., Tia, M., and Ruth, B. E. (1996). "Laboratory aging methods for simulation of field aging of asphalts." *Journal of Materials in Civil Engineering*, 8(Compendex), 141-152.

Hyunwook, K., and Partl, M. N. (2012). "Development of a double-torsion fracture test to predict channelized crack behaviors of asphalt concrete." *Construction & Building Materials*, 26(1), 694-700.

Jacobs (1995). "Crack growth in asphaltic mixes." PhD Thesis, University of Technology ,the Netherlands.

Jeong Ho, O., Fernando, E. G., Lee, S. I., and Holzschuher, C. (2012). "Correlation of asphalt concrete layer moduli determined from laboratory and nondestructive field tests." *Journal of Transportation Engineering*, 138(3), 361-370.

Jia, J., Zhang, X.-N., and Yuan, Y. (2005). "Rolling thin film oven test investigation for polymer modified asphalt." *Journal of Harbin Institute of Technology (New Series)*, 12(6), 635-638.

Juan, J., and Xiaoning, Z. "Modification of the rolling thin film oven test for modified asphalt." *Proc., 24th Annual Southern African Transport Conference, SATC 2005: Transport Challenges for 2010, July 11, 2005 - July 13, 2005*, Document Transformation Technologies cc., 979-986.

Kallas, B. F., and Puzinauskas, V. P. (1971). "Flexure fatigue tests on asphalt paving mixtures." *ASTM Special Technical Publication*(Compendex), 47-66.

Kandhal, P. S., and Cooley Jr, L. A. (2006). "Simulative performance test for hot mix asphalt using asphalt pavement analyzer." *Journal of ASTM International*, 3(5).

Karakouzian, M., Dunning, M., Hudyma, N., Avar, B., Bukhari, M., and Singh, A. K. "Comparison of in-place versus laboratory aged hma binder properties." *Proc., Airfield Pavements: Challenges and New Technologies, Proceedings of the Specialty Conference, September 21, 2003 - September 24, 2003*, American Society of Civil Engineers, 327-333.

Kassem, E., Masad, E., Chowdhury, A., and Claros, G. "Influence of field compaction pattern on asphalt pavement uniformity." *Proc., 2008 Annual Meeting of the Association of Asphalt Paving Technologists, AAPT, April 25, 2008 - April 30, 2008*, Association of Asphalt Paving Technologist, 257-298.

Kessler, M. R. (2007). "Self-healing: A new paradigm in materials design." *Proceedings of the Institution of Mechanical Engineers, Part G: Journal of Aerospace Engineering*, 221(Compendex), 479-495.

Kevern, J. T., Schaefer, V. R., and Wang, K. (2009). "Evaluation of pervious concrete workability using gyratory compaction." *Journal of Materials in Civil Engineering*, 21(12), 764-770.

Khan, Z. A., Al-Abdul Wahab, H. I., Asi, I., and Ramadhan, R. (1998). "Comparative study of asphalt concrete laboratory compaction methods to simulate field compaction." *Construction and Building Materials*, 12(6-7), 373-384.

Kim, H., Wagoner, M. P., and Buttlar, W. G. (2009). "Micromechanical fracture modeling of asphalt concrete using a single-edge notched beam test." *Materials and Structures/Materiaux et Constructions*, 42(5), 677-689.

Kim, J., Roque, R., and Byron, T. (2009). "Viscoelastic analysis of flexible pavements and its effects on top-down cracking." *Journal of Materials in Civil Engineering*, 21(7), 324-332.

Kim, S.-S. (2005). "Direct measurement of asphalt binder thermal cracking." *Journal of Materials in Civil Engineering*, 17(6), 632-639.

Kim, S., Park, J., and Kim, K. W. (2011). "Correlation analyses for implementation of binder properties for rut potential estimation of asphalt mixtures." *Journal of Testing and Evaluation*, 39(5).

Kim, Y.-R. (2011). "Cohesive zone model to predict fracture in bituminous materials and asphaltic pavements: State-of-the-art review." *International Journal of Pavement Engineering*, 12(4), 343-356.

Kim, Y. R., and Little, D. N. (1989). "Evaluation of healing in asphalt concrete by means of the theory of nonlinear viscoelasticity." *Transportation Research Record*(Compendex), 198-210.

Koh, C., and Roque, R. (2010). "Characterization of the tensile properties of open graded friction course mixtures based on direct and indirect tension tests." *Journal of Testing and Evaluation*, 38(4).

Koohi, Y., Lawrence, J. J., Luo, R., and Lytton, R. L. (2011). "Complex stiffness gradient estimation of field-aged asphalt concrete layers using the direct tension test." *Journal of Materials in Civil Engineering*, 1(Compendex), 401.

Kuai, H., Lee, H. J., Zi, G., and Mun, S. (2009). "Application of generalized j-integral to crack propagation modeling of asphalt concrete under repeated loading." *Transportation Research Record*(2127), 72-81.

Lee, S.-J., Amirkhanian, S. N., and Kim, K. W. (2009). "Laboratory evaluation of the effects of short-term oven aging on asphalt binders in asphalt mixtures using hp-gpc." *Construction and Building Materials*, 23(9), 3087-3093.

Leiva, F., and West, R. C. "Relationships between laboratory measured characteristics of hma and field compactability." *Proc., 2008 Annual Meeting of the Association of Asphalt Paving Technologists, AAPT, April 25, 2008 - April 30, 2008*, Association of Asphalt Paving Technologist, 183-219.

Li, P.-L., Ding, Z., and Zhang, Z.-Q. "Influence of aging on viscoelastic response of asphalt mixture." *Proc., 2011 International Conference on Civil Engineering and Building Materials, CEBM 2011, July 29, 2011 - July 31, 2011*, Trans Tech Publications, 3350-3353.

Li, P.-l., Zhang, Z.-q., Wang, B.-g., and Ding, Z. (2008). "Experimental research on thermo-oxidative aging for simulation of pavement asphalt aging." *Journal of Zhengzhou University Engineering Science*, 29(1), 119-123.

Li, P.-l., Zhang, Z.-q., Wang, B.-g., and Ding, Z. (2008). "Experimental research on thermo-oxidative aging for simulation of pavement asphalt aging." *Journal of Zhengzhou University Engineering Science*, 29(Copyright 2008, The Institution of Engineering and Technology), 119-123.

Li, P.-l., Zhang, Z.-q., Wang, B.-g., and Ding, Z. (2008). "Experimental research on thermo-oxidative aging of asphalt for simulation in the field hot climate." *Journal of Hebei University of Technology*, 37(4), 90-95.

Li, P., Zhang, Z., Li, H., and Wang, B. (2011). "Research on conditions of hamburg wheel tracking test and evaluating indicator for asphalt mixture." *Journal of Wuhan University of Technology (Transportation Science & Engineering)*, 35(1), 113-117.

Li, X.-J., and Li, L.-H. (2007). "Effect of field aging on properties of asphalt binder." *Jianzhu Cailiao Xuebao/Journal of Building Materials*, 10(2), 167-176.

Li, X., and Marasteanu, M. O. (2005). "Cohesive modeling of fracture in asphalt mixtures at low temperatures." *International Journal of Fracture*, 136(1-4), 285-308.

Li, X. J., and Marasteanu, M. O. "Using semi circular bending test to evaluate low temperature fracture resistance for asphalt concrete." *Proc., Proceedings of the Society for Experimental Mechanics, Inc.*, Society for Experimental Mechanics, 867-876.

Liu, J.-h., and Wang, D.-y. "Numerical simulation of a crack in the cement stabilized stone using cohesive zone models." *Proc., ICEM 2008: International Conference on Experimental Mechanics 2008, 8 Nov. 2008*, SPIE - The International Society for Optical Engineering, 737511 (737517 pp.).

Luo, H., Zhu, H.-p., and Chen, C.-y. (2008). "Modelling of crack propagation in asphalt pavements by the coupled efg and fe method." *Journal of Highway and Transportation Research and Development*, 25(9), 1-6.

Luo, H., Zhu, H.-P., Miao, Y., and Chen, C.-Y. (2010). "Simulation of top-down crack propagation in asphalt pavements." *Journal of Zhejiang University: Science A*, 11(3), 223-230.

Luo, R., and Lytton, R. L. (2010). "Characterization of the tensile viscoelastic properties of an undamaged asphalt mixture." *Journal of Transportation Engineering*, 136(Compendex), 173-180.

Luo, R., and Lytton, R. L. (2010). "Self-consistent micromechanics models of an asphalt mixture." *Journal of Materials in Civil Engineering*, 23(Compendex), 49-55.

Luo, R., and Lytton, R. L. (2011). "Self-consistent micromechanics models of an asphalt mixture." *Journal of Materials in Civil Engineering*, 23(Compendex), 49-55.

Luo, S., Qian, Z., and Chen, C. (2011). "Crack propagation simulation for epoxy asphalt concrete pavement." *Key Engineering Materials*, 460-461, 698-703.

Luo, Z.-f., and Zheng, C.-c. (2010). "Analysis on i - ii mixed-mode crack in asphalt mixture specimen by means of finite element method." *Journal of Hebei University of Technology*, 39(5), 109-113.

Mallick, R. B., and Brown, E. R. (2004). "An evaluation of superpave binder aging methods." *International Journal of Pavement Engineering*, 5(1), 9-18.

Masad, E., and Kassem, E. "Improving the field compaction of asphalt pavements using x-ray ct and imaging techniques." *Proc., 4th International Gulf Conference on Roads, November 10, 2008 - November 13, 2008*, CRC Press, 611-620.

Matsumoto, K., Niwa, Y., Nakayama, T., and Sakano, M. "An analytical study on the fatigue cracking of the top flange in steel railway through truss stringers." *Proc., 5th International Conference on Bridge Maintenance, Safety and Management, IABMAS 2010, July 11, 2010 - July 15, 2010*, Association for Computing Machinery, 2755-2758.

Memon, G. M., and Chollar, B. H. "Laboratory simulation of oxidative aging of asphalt." *Proc., Proceedings of the 1996 Symposium on Oxidative Behavior of Materials by Thermal Analytical Techniques, November 21, 1996 - November 22, 1996*, ASTM, 138-148.

Mirza, M. W., and Witczak, M. W. "Development of a global aging system for short and long term aging of asphalt cements." *Proc., Proceedings of the 1995 Conference of the Association of Asphalt Paving Technologists: Asphalt Paving Technology, March 27, 1995 - March 29, 1995*, Assoc of Asphalt Paving Technologists, 393-430.

Mohammad, L., Saadeh, S., Chenggang, Z., Cooper, S., Abadie, C., and Khattak, J. "Comparative study of the mechanical properties of hma mixture: Field vs laboratory." *Proc., Asphalt Paving Technology 2007 AAPT, March 11, 2007 - March 14, 2007*, Association of Asphalt Paving Technologist, 887-918.

Molenaar, A. A. A., Hagos, E. T., and van de Ven, M. F. C. (2010). "Effects of aging on the mechanical characteristics of bituminous binders in pac." *Journal of Materials in Civil Engineering*, 22(8), 779-787.

Molenaar, A. A. A., Hagos, E. T., and van de Ven, M. F. C. (2010). "Effects of aging on the mechanical characteristics of bituminous binders in pac." *Journal of Materials in Civil Engineering*, 22(Compendex), 779-787.

Mollenhauer, K., Pierard, N., Tusar, M., Mouillet, V., and Gabet, T. (2010). "Development and validation of a laboratory aging method for the accelerated simulation of reclaimed asphalt." *Journal of Wuhan University of Technology-Materials Science Edition*, 25(4), 631-636.

Morian, N., Hajj, E. Y., Glover, C. J., and Sebaaly, P. E. (2011). "Oxidative aging of asphalt binders in hot-mix asphalt mixtures." *Transportation Research Record*(2207), 107-116.

Motola, Y., and Uzan, J. (2007). "Anisotropy of field-compacted asphalt concrete material." *Journal of Testing and Evaluation*, 35(1), 103-105.

Mukherjee, S., and Paulino, G. H. (2003). "The elastic-viscoelastic correspondence principle for functionally graded materials, revisited." *Transactions of the ASME. Journal of Applied Mechanics*, 70(3), 359-363.

Mukherjee, S., and Paulino, G. H. (2003). "The elastic-viscoelastic correspondence principle for functionally graded materials, revisited." *Transactions of the ASME. Journal of Applied Mechanics*, 70(Copyright 2003, IEE), 359-363.

Mun, S., Guddati, M. N., and Kim, Y. R. "Fatigue cracking mechanisms in asphalt pavements with viscoelastic continuum damage finite-element program." National Research Council, 96-106.

Nazarian, S., and Alvarado, G. (2006). "Impact of temperature gradient on modulus of asphaltic concrete layers." *Journal of Materials in Civil Engineering*, 18(Compendex), 492-499.

NCHRP (2004). "Guide for mechanistic -emperical design of new and rehabilitated pavement structures,final report." National Cooperative Highway Research Program, Part 3.6-30.

Olard, F., Di Benedetto, H., Daniel, J. O. S., Roque, R., Kim, Y. R., Chehab, G., Radovsky, B., and Brown, S. "The "dbn" model: A thermo-visco-elasto-plastic approach for pavement behavior modeling." *Proc., 2005 Meeting of the Association of Asphalt Paving Technologists, March 7, 2005 - March 9, 2005*, Association of Asphalt Paving Technologist, 791-827.

Paris, P. C., and Erdogan, F. (1963). "A critical analysis of crack propogation laws." *Transactions of the ASME. Journal of Basic Engineering*, No.3(Series D), 85.

Park, S. W., Kim, Y. R., and Schapery, R. A. (1996). "Viscoelastic continuum damage model and its application to uniaxial behavior of asphalt concrete." *Mechanics of Materials*, 24(Compendex), 241-255.

Paulino, G. H., Seong Hyeok, S., and Buttlar, W. G. (2006). "A bilinear cohesive zone model tailored for fracture of asphalt concrete considering viscoelastic bulk material." *Engineering Fracture Mechanics*, 73(18), 2829-2848.

Pellinen, T., Zofka, A., Marasteanu, M., and Funk, N. "Asphalt mixture stiffness predictive models." *Proc., Asphalt Paving Technology 2007 AAPT, March 11, 2007 - March 14, 2007*, Association of Asphalt Paving Technologist, 575-625.

Peterson, R. L., Mahboub, K. C., Anderson, R. M., Masad, E., and Tashman, L. (2004). "Comparing superpave gyratory compactor data to field cores." *Journal of Materials in Civil Engineering*, 16(1), 78-83.

Peterson, R. L., Mahboub, K. C., Anderson, R. M., Masad, E., and Tashman, L. "Superpave&reg laboratory compaction versus field compaction." National Research Council, 201-208.

Phromsorn, C. J., and Kennedy, T. W. (1995). "Evaluation of laboratory methods simulating aging effects of asphalt binder." *Transportation Research Record*(1488), 13-20.

Pugno, N., Ciavarella, M., Cornetti, P., and Carpinteri, A. (2006). "A generalized paris' law for fatigue crack growth." *Journal of the Mechanics and Physics of Solids*, 54(Copyright 2006, The Institution of Engineering and Technology), 1333-1349.

Raad, L., Saboundjian, S., and Minassian, G. (2001). "Field aging effects on fatigue of asphalt concrete and asphalt-rubber concrete." *Transportation Research Record*(Compendex), 126-134.

Radziszewski, P., Kalabinska, M., and Pilat, J. "Rheological behaviour of rubber asphalt binder." *Proc., Proceedings of the 1996 12th International Conference on Solid Waste Technology and Management, November 17, 1996 - November 20, 1996*, Univ of Pennsylvania, 8pp-8pp.

Ramsamooj, D. V. (1991). "Prediction of fatigue life of asphalt concrete beams from fracture tests." *Journal of Testing and Evaluation*, 19(3), 231-239.

Ramsamooj, D. V. (1991). "Prediction of fatigue life of asphalt concrete beams from fracture tests." *Journal of Testing and Evaluation*, 19(Compendex), 231-239.

Renjie, Q., and Li, Y. "Study the test methods and pavement performance indexes about hard asphalt binder material." *Proc., 2009 International Conference on Measuring Technology and Mechatronics Automation (ICMTMA), 11-12 April 2009*, IEEE, 607-610.

Romero, P., and Roque, R. "Evaluation of long-term oven aging of asphalt mixtures (aashto pp2-95) on superpave thermal cracking performance predictions." *Proc., Proceedings of the 1996 Symposium on Progress of Superpave (Superior Asphalt Pavement): Evaluation and Implementation, December 10, 1996 - December 10, 1996*, ASTM, 151-168.

Roque, R., Birgisson, B., Sangpetngam, B., and Zhang, Z. "Hot mix asphalt fracture mechanics: A fundamental crack growth law for asphalt mixtures." *Proc., Asphalt*

Paving Technology 2002, March 18, 2002 - March 20, 2002, Association of Asphalt Paving Technologist, 816-827.

Schapery, R. A. (1984). "Correspondence principles and a generalized j integral for large deformation and fracture analysis of viscoelastic media." *International Journal of Fracture*, 25(3), 195-223.

Schapery, R. A. (1989). "On the mechanics of crack closing and bonding in linear viscoelastic media." *International Journal of Fracture*, 39(1-3), 163-189.

Schapery, R. A. (1975). "A theory of crack initiation and growth in viscoelastic media, part 1:Theoretical developement, part 2:Approximate methods of analysis, part 3: Analysis of continuous growth." *International Journal of Fracture*, 11.

Selim, A. A., and Ezz-Aldin, M. A. (1990). "Correlation between field and laboratory performance of liquid asphalt-based seal coats." *Transportation Research Record*(1259), 53-62.

Seong Hyeok, S., Paulino, G. H., and Buttlar, W. G. "Influence of the cohesive zone model shape parameter on asphalt concrete fracture behavior." *Proc., Multiscale and Functionally Graded Materials 2006: (M&FGM 2006), 15-18 Oct. 2006*, AIP, 730-735.

Shen, S., Chiu, H.-M., and Huang, H. (2010). "Characterization of fatigue and healing in asphalt binders." *Journal of Materials in Civil Engineering*, 22(Compendex), 846-852.

Sigurjonsson, S., and Ruth, B. E. (1990). "Use of gyratory testing machine to evaluate shear resistance of asphalt paving mixture." *Transportation Research Record*(1259), 63-78.

Singh, D., Zaman, M., and Commuri, S. "Effect of long term oven aging on dynamic modulus of hot mix asphalt." *Proc., Geo-Frontiers 2011: Advances in Geotechnical Engineering, March 13, 2011 - March 16, 2011*, American Society of Civil Engineers (ASCE), 4773-4781.

Solaimanian, M. "Field focused long term performance evaluation of asphalt concrete pavements." *Proc., 4th International Gulf Conference on Roads, November 10, 2008 - November 13, 2008*, CRC Press, 683-694.

Song, S. H., Paulino, G. H., and Buttlar, W. G. (2006). "Simulation of crack propagation in asphalt concrete using an intrinsic cohesive zone model." *Journal of Engineering Mechanics*, 132(11), 1215-1223.

Songqing, Z., and Jinfei, S. "Research on temperature-dependent complex permittivity for large-size heterogeneous asphalt mixture." *Proc., 2010 International Conference on Information and Automation (ICIA 2010), 20-23 June 2010*, IEEE, 2082-2086.

Soon-Jae, L., Amirkhanian, S. N., and Kim, K. W. (2009). "Laboratory evaluation of the effects of short-term oven aging on asphalt binders in asphalt mixtures using hp-gpc." *Construction & Building Materials*, 23(Copyright 2009, The Institution of Engineering and Technology), 3087-3093.

Soon-Jae, L., Hakseo, K., Akisetty, C. K., and Amirkhanian, S. N. (2008). "Laboratory characterization of recycled crumb-rubber-modified asphalt mixture after extended aging." *Canadian Journal of Civil Engineering*, 35(Copyright 2009, The Institution of Engineering and Technology), 1308-1317.

Svasdisant, T., Schorsch, M., Baladi, G. Y., and Pinyosunun, S. (2002). "Mechanistic analysis of top-down cracks in asphalt pavements." *Transportation Research Record*(1809), 126-136.

T.O.Medani, and Molenaar, A. A. A. (2000). "A simplified practical procedures for estimation of fatigue and crack growth characteristics of asphaltic mixes." *International Journal of Road Materials and Pavement Design*, 10.

Tan, Y., Wang, J., Xue, Z., Feng, Z., and Xu, H. "Laboratory study on ultraviolet aging behavior of asphalt binder and mixture." *Proc., 7th International Conference of Chinese Transportation Professionals Congress 2007: Plan, Build, and Manage Transportation Infrastructures in China, May 21, 2007 - May 22, 2007*, American Society of Civil Engineers, 752-759.

Tayebali, A. A., Deacon, J. A., and Monismith, C. L. (1996). "Development and evaluation of dynamic flexural beam fatigue test system." *Transportation Research Record*(1545), 89-97.

Tian, X.-G., Zheng, J.-L., and Zhang, Q.-S. (2004). "Effect of aging on viscoelastic performance of asphalt binder." *Journal of Traffic and Transportation Engineering*, 4(Compendex), 3-6.

Wagoner, M. P., Buttlar, W. G., and Paulino, G. H. (2005). "Disk-shaped compact tension test for asphalt concrete fracture." *Experimental Mechanics*, 45(3), 270-277.

Wagoner, M. P., Buttlar, W. G., Paulino, G. H., and Blankenship, P. "Investigation of the fracture resistance of hot-mix asphalt concrete using a disk-shaped compact tension test." National Research Council, 183-192.

Walubita, L. F., Umashankar, V., Hu, X., Jamison, B., Zhou, F., Scullion, T., Martin, A. E., and Dessouky, S. (2009). "New generation mix-designs:Laboratory teting and construction of the apt test sections." TTI.

Wang, H., Hao, P., and You, Z. "Characterization of the viscoelastic property of asphalt mastic." *Proc., 2011 GeoHunan International Conference - Pavements and Materials: Recent Advances in Design, Testing, and Construction, June 9, 2011 - June 11, 2011*, American Society of Civil Engineers (ASCE), 115-122.

Wang, H., and Li, G. "Numerical analysis on propagation and fatigue life of asphalt pavement surface crack." *Proc., 2011 International Conference on Manufacturing Science and Technology, ICMST 2011, September 16, 2011 - September 18, 2011*, Trans Tech Publications, 1658-1663.

Wang, L. B., Myers, L. A., Mohammad, L. N., and Fu, Y. R. "Micromechanics study on top-down cracking." National Research Council, 121-133.

Wen, H., and Bahia, H. (2009). "Characterizing fatigue of asphalt binders with viscoelastic continuum damage mechanics." *Transportation Research Record*(Compendex), 55-62.

Witczak, M., and Fonseca, O. (1996). "Revised predictive model for dynamic (complex) modulus of asphalt mixtures." *Transportation Research Record: Journal of the Transportation Research Board*, 1540(-1), 15-23.

Woo, W. J., Chowdhury, A., and Glover, C. J. (2008). "Field aging of unmodified asphalt binder in three texas long-term performance pavements." *Transportation Research Record*(2051), 15-22.

Woo, W. J., Chowdhury, A., and Glover, C. J. (2008). "Field aging of unmodified asphalt binder in three texas long-term performance pavements." *Transportation Research Record*(Compendex), 15-22.

Wu, W., Xu, Z., Tian, X., and Zhang, S. "Viscoelastic property of aging asphalt mixture and parameters determination method." *Proc., 2010 International Conference on Measuring Technology and Mechatronics Automation (ICMTMA 2010), 13-14 March 2010*, IEEE, 1083-1086.

Wu, X., and Luo, Y.-X. (2011). "Dynamic responses of a beam with functionally graded materials with timoshenko beam correction theory." *Zhendong yu Chongji/Journal of Vibration and Shock*, 30(10), 245-248.

Yan, X., Wang, W., Chu, X., Xie, L., and Ma, Y. "Methods and correlation of describing segment profile feature of asphalt pavement." *Proc., 2nd International Conference on Transportation Engineering, ICTE 2009, July 25, 2009 - July 27, 2009*, American Society of Civil Engineers, 3669-3674.

Yoda, M. (1980). "The j-integral fracture toughness for mode ii." *International Journal of Fracture*, 16(4), R175-R178.

Yong, Y., Xinhua, Y., and Chuanyao, C. (2009). "Experimental researches on visco-elastoplastic constitutive model of asphalt mastic." *Construction & Building Materials*, 23(10), 3161-3165.

You, Z., Adhikari, S., Masad, E., and Dai, Q. "Microstructural and micromechanical properties of field and lab-compacted asphalt mixtures." *Proc., Asphalt Paving Technology 2009, AAPT, March 15, 2009 - March 18, 2009*, Association of Asphalt Paving Technologist, 279-315.

Yu, X., and Du, Y. (2011). "Numerical simulation of reflective crack forming in semi-rigid asphalt pavement subjected to traffic load." *Key Engineering Materials*, 462-463, 599-604.

Yufeng, G., and Wanlin, G. (2006). "Self-healing properties of flaws in nanoscale materials: Effects of soft and hard molecular dynamics simulations and boundaries studied using a continuum mechanical model." *Physical Review B (Condensed Matter and Materials Physics)*, 73(Copyright 2006, The Institution of Engineering and Technology), 85411-85411.

Zhan, X.-l., Zhang, X.-n., Wang, D.-y., and Lu, L. (2009). "Microstructure of asphalt mastic using dynamic mechanical analysis." *Journal of Jilin University (Engineering and Technology Edition)*, 39(4), 916-920.

Zhang, D., Huang, X., and Zhao, Y. (2011). "Evaluation of the fracture resistance of asphalt mixtures based on bilinear cohesive zone model." *Journal of Testing and Evaluation*, 39(6).

Zhang, J.-p., Pei, J.-z., Xu, L., and Xing, X.-y. (2011). "Gyratory compaction characteristic of sbs warm mixed asphalt mixture." *Journal of Traffic and Transportation Engineering*, 11(1), 1-6.

Zhang, J., and Huang, X. (2010). "Viscoelastoplastic-damage mechanics model of permanent deformation in asphalt mixture." *Journal of Southeast University (Natural Science Edition)*, 40(Copyright 2010, The Institution of Engineering and Technology), 185-189.

Zhang, Z.-f., Zhang, C.-b., Feng, Z.-x., and Wang, J.-x. (2008). "Correlation analysis of the segregation and porosity of asphalt mixture." *Journal of Zhengzhou University Engineering Science*, 29(4), 73-76.

Zhao, Y., and Kim, Y. R. "Time-temperature superposition for asphalt mixtures with growing damage and permanent deformation in compression." National Research Council, 161-172.

Zhao, Y., Tan, Y., and Yu, X. (2010). "Stress-dependent mechanical behavior of asphalt mixtures." *Huazhong Keji Daxue Xuebao (Ziran Kexue Ban)/Journal of Huazhong University of Science and Technology (Natural Science Edition)*, 38(10), 124-127.

Zhao, Y., Wang, S., Zhou, C., and Tan, Y. (2010). "Analysis of top-down cracking of asphalt pavements based on fracture mechanics approach." *Tongji Daxue Xuebao/Journal of Tongji University*, 38(2), 218-222.

Zhao, Y., and Zhang, D. (2010). "Study of low temperature cracking of asphalt pavement based on cohesive zone model." *Journal of Highway and Transportation Research and Development*, 27(1), 11-16.

Zhong, Y., Zhu, X., Cao, K.-H., Zhou, Z.-Y., and Yang, Z.-P. (2008). "Influence of asphalt binder aging on mechanical performance of pavement functional layer." *Gongneng Cailiao/Journal of Functional Materials*, 39(1), 102-104+107.

Zhou, F., Hu, S., and Scullion, T. (2007). "Preliminary results of repeatability and sensitivity study on overlay tester for crack sealants." 20p.

Zhou, F., Hu, S., Scullion, T., Mikhail, M., and Walubita, L. F. (2007). "A balanced hma mix design procedure for overlays (with discussion)." Association of Asphalt Paving Technologists, pp 823-850.

Zhou, F., and Scullion, T. (2006). "Overlay tester: A simple and rapid screening test for characterizing crack resistance of hma mixes."Association of Asphalt Paving Technologies, pp 215-224.

Zhou, F., and Scullion, T. (2005). "Overlay tester: A simple performance test for thermal reflective cracking (with discussion and closure)." Association of Asphalt Paving Technologists, pp 443-484.

Zhou, F., and Scullion, T. (2003). "Upgraded overlay tester and its application to characterize reflection cracking resistance of asphalt mixtures." 44p.

Zhu, G., Wu, S., Liu, R., and Zhou, L. (2009). "Study on the fatigue property for aged asphalt mixtures by using four point bending tests." *6th International Forum on Advanced Material Science and Technology, IFAMST 2008, June 12, 2008 - June 14, 2008*, Trans Tech Publications Ltd, Hong Kong, China, 289-294.

Zou, J., and Roque, R. "Top-down cracking: Enhanced performance model and improved understanding of mechanisms." *Proc., Asphalt Paving Technology 2011, AAPT, March 27, 2011 - March 30, 2011*, Association of Asphalt Paving Technologist, 255-285.

Zou, W.-L., Wang, Z., and Yang, M. Z. (2004). "Gyratory compaction test for field compaction simulation of granular subgrade soils." *Yantu Lixue/Rock and Soil Mechanics*, 25(11), 1775-1778.

APPENDIX A

SUMMARY OF STATISTICAL ANALYSIS OF FIELD SPECIMEN AT 20 AND 30°

Table A-1. Statistical analysis summary of stiffness gradient at 20°C, year 1

Sample ID	Coring Location	Age	Test Temperature	n	k	Modulus at Surface	Modulus at Bottom
US-277-NBS-1-5	S	1.00	20C	5.30	1.75	1875.41	1070.96
US-277-RWP-1-2	W	1.00	20C	4.59	3.79	3708.88	977.33
US-277-RWP-1-5	W	1.00	20C	3.79	2.06	1722.83	837.02
μ				4.56	2.53	2435.71	961.77
б				0.76	1.10	1105.24	117.74
COV				16.62	43.48	45.38	12.24

Table A-2. Statistical analysis summary of stiffness gradient at 20°C, year 2

Sample ID	Coring Location	Age	Test Temperature	n	k	Modulus at Surface	Modulus at Bottom
US-277-NBS-2-3	S	2.00	20C	3.84	2.34	2529.66	1080.20
US-277-NBS-2-1	S	2.00	20C	5.30	1.55	2952.13	1905.44
US-277-RWP-2-1	W	2.00	20C	3.44	2.25	3316.67	1475.00
US-277-RWP-2-3	W	2.00	20C	3.87	2.04	2283.59	1119.02
μ				4.12	2.05	2770.52	1394.91
б				0.82	0.35	456.94	383.93
COV				19.83	17.29	16.49	27.52

Table A-3. Statistical analysis summary of stiffness gradient at 20°C, year 3

Sample ID	Coring Location	Age	Test Temperature	n	k	Modulus at Surface	Modulus at Bottom
US-277-NBS-3-1	S	3.00	20C	3.91	2.07	3625.26	1754.30
US-277-NBS-3-3	S	3.00	20C	3.93	2.48	4317.95	1738.10
US-277-RWP-3-1	W	3.00	20C	3.75	1.81	1996.14	1103.99
US-277-RWP-3-3	W	3.00	20C	3.78	2.02	3212.73	1594.28
μ				3.85	2.09	3288.02	1547.67
б				0.09	0.28	974.52	304.40
COV				2.37	13.54	29.64	19.67

Table A-4. Statistical analysis summary of stiffness gradient at 20°C, year 4

Sample ID	Coring Location	Age	Test Temperature	n	k	Modulus at Surface	Modulus at Bottom
US-277-NBS-4-2	S	4.00	20C	5.26	1.62	3077.33	1895.37
US-277-NBS-4-4	S	4.00	20C	3.73	2.24	3797.89	1695.42
US-277-RWP-4-1	W	4.00	20C	3.85	2.01	2326.04	1158.25
US-277-RWP-4-3	W	4.00	20C	3.90	2.09	3171.39	1514.50
μ				4.18	1.99	3093.16	1565.89
б				0.72	0.26	603.19	313.13
COV				17.15	13.22	19.50	20.00

Table A-5. Statistical analysis summary of stiffness gradient at 30°C, year 3

Sample ID	Coring Location	Age	Test Temperature	n	k	Modulus at Surface	Modulus at Bottom
US-277-NBS-3-1	S	3.00	30C	3.92	2.19	2351.75	1073.86
US-277-NBS-3-3	S	3.00	30C	3.80	2.40	1886.36	786.28
US-277-RWP-3-1	W	3.00	30C	3.74	2.19	2062.98	941.20
US-277-RWP-3-3	W	3.00	30C	3.82	2.08	1076.98	517.52
μ				3.82	2.22	1844.52	829.72
б				0.08	0.13	546.47	239.02
COV				1.96	6.00	29.63	28.81

Table A-6. Statistical analysis summary of stiffness gradient at 30°C, year 4

Sample ID	Coring Location	Age	Test Temperature	n	k	Modulus at Surface	Modulus at Bottom
US-277-NBS-4-2	S	4.00	30C	3.78	1.95	1965.97	1007.12
US-277-RWP-4-3	W	4.00	30C	3.79	2.06	1602.00	777.04
μ				3.79	2.01	1783.99	892.08
б				0.01	0.08	257.36	162.69
COV				0.31	3.86	14.43	18.24

APPENDIX B

ELASTIC UMAT SUBROUTINE

```
      SUBROUTINE UMAT(STRESS,STATEV,DDSDDE,SSE,SPD,SCD,
     1 RPL,DDSDDT,DRPLDE,DRPLDT,
     2 STRAN,DSTRAN,TIME,DTIME,TEMP,DTEMP,PREDEF,DPRED,CMNAME,
     3 NDI,NSHR,NTENS,NSTATV,PROPS,NPROPS,COORDS,DROT,PNEWDT,
     4 CELENT,DFGRD0,DFGRD1,NOEL,NPT,LAYER,KSPT,KSTEP,KINC)
C
C**********************************************************************
C
C      THIS SUBROUTINE CALCULATES NVE-VP USING EXPLICT ALGORITHM
C
C
C**********************************************************************

      INCLUDE 'ABA_PARAM.INC'
C
      CHARACTER*8 CMNAME
C
      DIMENSION STRESS(NTENS),STATEV(NSTATV),
     + DDSDDE(NTENS,NTENS),DDSDDT(NTENS),DRPLDE(NTENS),
     + STRAN(NTENS),DSTRAN(NTENS),TIME(2),PREDEF(1),DPRED(1),
     + PROPS(NPROPS),COORDS(3),DROT(3,3),DFGRD0(3,3),DFGRD1(3,3)
C
      DIMENSION STRESS_INCREMENT(NTENS)
      DIMENSION STIFFNESS(NTENS,NTENS)
C
      DATA ONE,TWO / 1.0D0,2.0D0 /

C
C --- PARAMETERS
C
      YOUNG = 500000.*COORDS(2)
      POISS= 0.3
      YOUNG = STATEV(1)
C
C --- CALCULATE ELASTIC STIFFNESS
C
      IF (NTENS.EQ.6) THEN
      DO K1=1,NTENS
      DO K2=1,NTENS
        STIFFNESS(K1,K2)=0.
      END DO
      END DO
      ALAM=POISS*YOUNG/((ONE+POISS)*(ONE-TWO*POISS))
      AMUE = YOUNG/(TWO*(ONE + POISS))
C
```

```
      STIFFNESS(1,1)=ALAM+TWO*AMUE
      STIFFNESS(1,2)=ALAM
      STIFFNESS(1,3)=STIFFNESS(1,2)
      STIFFNESS(2,1)=STIFFNESS(1,2)
      STIFFNESS(2,2)=STIFFNESS(1,1)
      STIFFNESS(2,3)=STIFFNESS(1,2)
      STIFFNESS(3,1)=STIFFNESS(1,2)
      STIFFNESS(3,2)=STIFFNESS(1,2)
      STIFFNESS(3,3)=STIFFNESS(1,1)
      STIFFNESS(4,4)=AMUE
      STIFFNESS(5,5)=AMUE
      STIFFNESS(6,6)=AMUE
      ELSE IF (NTENS.EQ.3) THEN
      DO K1=1,NTENS
      DO K2=1,NTENS
        STIFFNESS(K1,K2)=0.
      END DO
      END DO
      ALAM=POISS*YOUNG/((ONE+POISS)*(ONE-POISS))
      AMUE = YOUNG/(TWO*(ONE + POISS))
C
      STIFFNESS(1,1)=ALAM/POISS
      STIFFNESS(1,2)=ALAM
      STIFFNESS(2,1)=STIFFNESS(1,2)
      STIFFNESS(2,2)=STIFFNESS(1,1)
      STIFFNESS(3,3)=AMUE
      ENDIF
C
C --- CALCULATE STRESS INCREMENT
C
      DO K1=1,NTENS
        STRESS_INCREMENT(K1)=0.0
      END DO
C
      DO K1=1,NTENS
      DO K2=1,NTENS
        STRESS_INCREMENT(K1)=STRESS_INCREMENT(K1)+
     +  STIFFNESS(K1,K2)*DSTRAN(K2)
      END DO
      END DO
C
C --- UPDATE STRESS
C
      DO I1=1,NTENS
        STRESS(I1)= STRESS(I1)+STRESS_INCREMENT(I1)
      END DO
      YOUNG=STATVE(1)
C
C --- UPDATE JACOBIAN
C
        DO I=1,NTENS
        DO J=1,NTENS
          IF(J .GT. 3) THEN
```

```
            DDSDDE(I,J)=STIFFNESS(I,J)
          ELSE
            DDSDDE(I,J)=STIFFNESS(I,J)
          ENDIF
        END DO
        END DO
C
      RETURN
            END
```

APPENDIX C

MATLAB CODE TO FIND AREAS UNDER FRACTURE AND HEALING PORTIONS OF CURVE

```
function[cf_,gof]=damaged()
%Read data from excel file n=2
m2(:,1)=xlsread('damaged.xlsx','sheet2','K2:K251');
m2(:,2)=xlsread('damaged.xlsx','sheet2','N2:N251');
x2=m2(:,1);
y2=m2(:,2);
z2=polyarea(x2,y2);
xlswrite('damaged.xlsx',z2,'sheet2','Q17:Q17');
j=0;
for n=0:249
   if x2(n+1,1)>0
      j=j+1;
      x2plus(j,1)=x2(n+1,1)
   end
end
j=0;
for n=0:249
   if x2(n+1,1)>0
      j=j+1;
      y2plus(j,1)=y2(n+1,1)
   end
end
 z2plus=polyarea(x2plus,y2plus);
xlswrite('damaged.xlsx',z2plus,'sheet2','Q18:Q18');
%Read data from excel file n=3
m3(:,1)=xlsread('damaged.xlsx','sheet2','T2:T251');
m3(:,2)=xlsread('damaged.xlsx','sheet2','W2:W251');
x3=m3(:,1);
y3=m3(:,2);
z3=polyarea(x3,y3);
xlswrite('damaged.xlsx',z3,'sheet2','Z17:Z17');
j=0;
for n=0:249
   if x3(n+1,1)>0
      j=j+1;
      x3plus(j,1)=x3(n+1,1)
   end
end
j=0;
for n=0:249
   if x3(n+1,1)>0
```

```
      j=j+1;
      y3plus(j,1)=y3(n+1,1)
   end
end
 z3plus=polyarea(x3plus,y3plus);
xlswrite('damaged.xlsx',z3plus,'sheet2','Z18:Z18');
%Read data from excel file n=4
m4(:,1)=xlsread('damaged.xlsx','sheet2','AC2:AC251');
m4(:,2)=xlsread('damaged.xlsx','sheet2','AF2:AF251');
x4=m4(:,1);
y4=m4(:,2);
z4=polyarea(x4,y4);
xlswrite('damaged.xlsx',z4,'sheet2','AI17:AI17');
j=0;
for n=0:249
   if x4(n+1,1)>0
      j=j+1;
      x4plus(j,1)=x4(n+1,1)
   end
end
j=0;
for n=0:249
   if x4(n+1,1)>0
      j=j+1;
      y4plus(j,1)=y4(n+1,1)
   end
end
 z4plus=polyarea(x4plus,y4plus);
xlswrite('damaged.xlsx',z4plus,'sheet2','AI18:AI18');
%Read data from excel file n=5
m5(:,1)=xlsread('damaged.xlsx','sheet2','AL2:AL251');
m5(:,2)=xlsread('damaged.xlsx','sheet2','AO2:AO251');
x5=m5(:,1);
y5=m5(:,2);
z5=polyarea(x5,y5);
xlswrite('damaged.xlsx',z5,'sheet2','AR17:AR17');
j=0;
for n=0:249
   if x5(n+1,1)>0
      j=j+1;
      x5plus(j,1)=x5(n+1,1)
   end
end
j=0;
for n=0:249
   if x5(n+1,1)>0
      j=j+1;
      y5plus(j,1)=y5(n+1,1)
```

```
   end
end
 z5plus=polyarea(x5plus,y5plus);
xlswrite('damaged.xlsx',z5plus,'sheet2','AR18:AR18');
%Read data from excel file n=6
m6(:,1)=xlsread('damaged.xlsx','sheet2','AU2:AU251');
m6(:,2)=xlsread('damaged.xlsx','sheet2','AX2:AX251');
x6=m6(:,1);
y6=m6(:,2);
z6=polyarea(x6,y6);
xlswrite('damaged.xlsx',z6,'sheet2','BA17:BA17');
j=0;
for n=0:249
   if x6(n+1,1)>0
      j=j+1;
      x6plus(j,1)=x6(n+1,1)
   end
end
```